DISSERTATION

INNOVATIVE SAMPLING AND SURVEILLANCE METHODS IN THE AIR MICROBIOME

Submitted by

Peter Kessinger

Department of Environmental and Radiological Health Sciences

In partial fulfillment of the requirements

For the Degree of Doctor of Philosophy

Colorado State University

Fort Collins, Colorado

Summer 2026

Doctoral Committee:

Advisor: Sheryl Magzamen
Co-Advisor: Angela M. Bosco-Lauth

Joshua W. Schaeffer
Brad R. Borlee

ABSTRACT

INNOVATIVE SAMPLING AND SURVEILLANCE METHODS IN THE AIR MICROBIOME

The air microbiome is a growing community of increasing interest for both public health and One Health. Various types of particles, both organic and inorganic, can be transported in the air. Subsequently, this exposes humans, animals, and environments to these particles. This dissertation investigates the air microbiome, innovating novel sampling methods to sample in a vertical profile to investigate how altitude influences microbial distribution, as well as what different types of microbes are present. Additionally, this dissertation also implements a One Health framework to predict the location of pathogens of One Health interest that may either exist in or use the air microbiome for transport. This predictive work could help guide future sampling efforts for difficult to environmentally detect pathogens.

In Chapter 2, we used drones and a novel air sampler to improve both flight time and sample collection to aid future research efforts. Drone platforms are an emerging tool for scientific research, including air sampling. However, a challenge arises when the weight of air samplers impairs drone performance by approaching or exceeding payload capacity. This chapter addresses this limitation by comparing the SASS 3100 with a lightweight prototype designed for drone use across three experimental scenarios. The full-sized SASS 3100 and Light SASS prototype were compared across three environments: in a controlled chamber, outdoor ground level conditions, and elevated outdoors positions (boom lift for Full SASS, and quadcopter and hexacopter drone for the Light SASS). Samples were processed by extracting and quantifying the total DNA using

a Qubit 4.0 fluorometer, and assessment of microbial diversity via next-generation sequencing. Across most conditions, no significant differences were observed between samplers. An exception was observed in the elevated hexacopter trials, where differences in total DNA collected were detected, and in chamber experiments when comparing gene copies of *Pseudomonas syringae* recovered from aerosol. Diversity analyses showed there were no significant differences in the microbial diversity recovered from the filters on the different samplers used. Overall, these results indicate that the Full SASS and Light SASS samplers perform similarly under chamber, ground, and quadcopter-mounted conditions, but may differ when deployed on a hexacopter. Additional work is needed to better understand the influence the hexacopter operational field has on sampler bioaerosol recovery.

In Chapter 3, we expanded on the use of drones as an air surveillance platform. This chapter addresses the need for active microbial surveillance in the Planetary Boundary Layer (PBL) to mitigate risks to human, animal, and environmental health. While airborne transport of pathogens is well-documented, current research often lacks practical surveillance applications for real-time public health action. We demonstrate the utility of a drone-mounted air sampling system for conducting vertical microbial profiles within the PBL to bridge this gap. Conducted in Big Spring, Texas, we utilized a DJI Matrice 350 drone equipped with a SASS 3100 dry air sampler at altitudes of 100, 200, and 400 ft AGL, alongside ground-level controls. Microbial communities were characterized through 16S rRNA and ITS amplicon sequencing. Results from PERMANOVA and diversity analyses indicate that altitude and site location are primary drivers of microbial community variance. Significant differences in alpha and beta diversity were observed between ground-level and samples at altitude. Notably, several genera of One Health interest, including the human pathogen *Legionella*, showed significant enrichment at higher altitudes compared to ground

level. Fungal communities also exhibited distinct stratification, with specific taxa such as *Fusarium* showing enrichment with altitude. The findings validate the use of readily attainable drone technology to provide high-resolution data on aerosolized microbial communities. This approach equips public health officials with a scalable tool for monitoring pathogen transport, informing exposure assessments, and implementing timely communication strategies to protect vulnerable populations.

In Chapter 4, we used ecological niche modeling to predict where to deploy additional surveillance. Coccidioidomycosis (Valley Fever), caused by the soil-borne fungi *Coccidioides immitis* and *C. posadasii*, is an escalating public health threat in the Southwestern United States. Traditional environmental surveillance is hindered by the low reliability of soil sampling, while human case data are often confounded by long incubation times, resulting in spatial and temporal misalignment due to case reporting clustering in urban centers with exposure most likely occurring elsewhere. Other mammals, such as canines, also contract Valley Fever at comparable rates and symptoms to humans, making them ideal sentinels as they also live in close proximity with humans. Furthermore, canines do not travel as much as humans and are assumed to be more likely to have been exposed within their local areas. This chapter proposes a One Health framework to model *Coccidioides* spp. habitat suitability in Arizona (2004–2023) by utilizing both human surveillance data and simulated canine cases as proxy presence points for the pathogen. We integrated confirmed Valley Fever human case data from the Arizona Department of Health Services with canine cases simulated based on decennial census and veterinary survey data. Using an ensemble modeling approach incorporating Random Forest, Boosted Regression Trees, and Maximum Entropy, we combined both reported human case data and simulated canine case data with environmental and meteorological predictors, including soil moisture and temperature, air

temperature and humidity, soil pH, sand fraction, and land cover, to model relative habitat suitability for *Coccidioides spp*. Bias weighting and spatial thinning were applied to mitigate the influence of human population density. Human-only models demonstrated strong performance (AUC 0.7–0.9) but exhibited significant spatial bias toward urban centers (Phoenix and Tucson). Conversely, canine models, while yielding lower AUC scores (0.6–0.7), provided superior resolution in non-urban areas and identified suitable habitats away from human population hubs. Combined One Health models identified expanded suitability in Northern and Northeastern Arizona, aligning with recent increases in Valley Fever cases and environmental DNA detections. Integrating simulated canine Valley Fever sentinel data into fungal pathogen modeling addresses some limitations of human case reporting. This approach provides a more accurate representation of *Coccidioides* spp. distribution, offering a scalable framework to improve surveillance and public health risk communication in both endemic and emerging regions.

ACKNOWLEDGEMENTS

I would like to acknowledge my advisors, Dr. Sheryl Magzamen and Dr. Angela Bosco-Lauth, for being fantastic mentors and providing me with guidance during this process. I appreciate that you both were willing to work with me and find a way to combine infectious disease, One Health, and Environmental Health together to match the research I wanted to pursue as well as the career path I wanted to seek. You both pushed me to explore new methods and encouraged me to keep developing as a scientist. I will always be thankful and grateful for the time spent as your student.

I also want to thank Dr. Joshua Schaeffer for being on my committee, as well as for being part of my Environmental Health and research journey. You are a great mentor and teacher, and I enjoyed the time I had in your classes. I appreciate your continued support and mentorship. Thank you as well to Dr. Brad Borlee for taking the time to be on my committee and be a mentor during my time in BROADN. I am thankful for the discussions about the air microbiome, and appreciate your time spent providing thoughtful feedback on my research.

I also want to say thank you to Dr. Marina Nieto-Caballero, who has been so kind and patient teaching me how to navigate drone-based field work, as well as genomic lab work and data processing. I appreciate all your mentorship and guidance, and a large part of this dissertation was influenced by your teaching and advice.

Thank my friends in CSU Environmental Health and CSU Atmospheric Sciences. Beth and Kellin have been great friends since I started my Master's here at CSU, and have both suffered through classes and work with me, as well as fun times as CSU football games. Thank you as well to my new (in the grand scheme of things) friends at Atmospheric Sciences, including Emily,

Olivia, Andrey, Tyler, En, Andrew, Ivy and others! I appreciate the fun times we had when not working on our respective research.

Finally, I want to say thank you to my family for always being so supportive. I am lucky to have you all and appreciate the kindness and love from everyone that has supported me during this long process.

The following acknowledgements are adapted from Chapters 2-4. We gratefully acknowledge support from the NSF Biology Integration Institutes Program under Award # 2120117. We thank the CSU One Health Institute for contributions to and support of BROADN research, including the funding through the One Health Student Award (Kessinger, PI). We would also like to thank the Colorado State University Drone Center for providing expertise and support during this project, especially around the development and implementation of the sampler mounting systems. For Chapter four, we thank the Arizona State Department of Health Services for providing the human case data for this study.

TABLE OF CONTENTS

CHAPTER 1

INTRODUCTION[1]

This introduction provides a brief overview of concepts that will be further discussed in Chapters Two through Four. Initially, we will review the concept of One Health, as the One Health framework is the main motivation behind the work in Chapters Two through Four. I will discuss the air microbiome, and how it relates to the One Health concept. The air microbiome is also the target of the sampling and work done in chapters two and three, while playing a role in chapter four. After that, I will review the tools used, including sampling equipment, unmanned aircraft systems (UAS) (i.e., drones), and next generation sequencing to conduct surveillance. Finally, I will conclude by summarizing how ecological niche modeling can be beneficial in not only addressing One Health issues but serving as a guide for future work in the field.

1.1 Overview of One Health

One Health is a framework that considers the health of humans, animals, and the environment as an interconnected system (Mackenzie & Jeggo, 2019; *Microbes and Climate Change – Science, People & Impacts*, 2022; Tiedje et al., 2022). In this case, what occurs within one section of the One Health framework does not exist within a vacuum, and impacts the other two sections. Recently, more attention has been being given to incorporating microbes as not just the cause of a disease, but as a system that is connected to other communities within One Health. Changes to the health or functionality of one system may have consequences that influence the behavior and functionality of microbes themselves, such as a change in animal activity causing disturbances and a change in microbial distribution (*Microbes and Climate Change – Science,*

[1] Adapted from the introductions of the three articles in preparation presented in Chapters 2-4 of this dissertation. See individual chapters for full citations.

People & Impacts, 2022; Tiedje et al., 2022). Understanding the analysis of microbiomes can provide insights into the health of other One Health communities.

1.2 The Air Microbiome

The air microbiome consists of microbes that may be from long range transport, such as seen in dust transport from the Saharan desert, or could be lofted from local sources (Brodsky et al., 2023; Drautz-Moses et al., 2022; Finn et al., 2021; Rodríguez-Arias et al., 2023; D. J. Smith et al., 2018). These microbes are, at one point or another, part of the air microbiome. Climate conditions, meteorological variables, and human and animal activity can all contribute to disturbances and subsequent lofting of microbes into the atmosphere and Planetary Boundary Layer (PBL) (Brodsky et al., 2023; Drautz-Moses et al., 2022; Finn et al., 2021; Rodríguez-Arias et al., 2023). Microbes being lofted and aerosolized necessitates viewing the PBL and the movement of constituents of the PBL across space and time as a potential exposure pathway for humans, animals, and environments to different microbes, resulting in potential disease (Brodsky et al., 2023; Rodríguez-Arias et al., 2023; Tignat-Perrier et al., 2020). Examples include *Coccidioides immitis* and *posadasii*, *Fusarium oxysporum,* and downy mildew (Brodsky et al., 2023; Choudhury et al., 2017; Neufeld et al., 2018; Radosevich et al., 2025). Their transport can result in infection of humans and canines, as an example for *Coccidioides* spp., and different plants when it comes to *F. oxysporum* and downy mildew (Brodsky et al., 2023; Neufeld et al., 2018; Radosevich et al., 2025). The transport and potential exposure to these microbes can have direct health impacts on infected individuals, as well as economic impacts like agriculture and commerce. Due to this transport of potential pathogens within the PBL and atmosphere, it then becomes necessary to conduct sampling and surveillance to classify the air microbiome and alert to the presence of pathogenic organisms.

1.3 UAS and Air Sampling

Traditional methods for atmospheric air sampling, such as fixed towers, tethered balloons, and crewed aircraft, each possess inherent limitations regarding height, location flexibility, or operational costs. Unmanned aircraft systems (UAS), or drones, have emerged as a flexible and cost-effective alternative for conducting vertical profiles within the PBL. However, a significant technical hurdle is optimizing the weight-to-performance ratio of air sampling hardware for these platforms. Because drones operated under FAA Part 107 are restricted by weight, researchers often face a choice between lightweight, low-flow-rate samplers that allow for longer flight times and heavier, high-flow-rate samplers that improve collection efficiency but reduce endurance (Bangay et al., 2026; "Small Unmanned Aircraft Systems (UAS) Regulations (Part 107) | Federal Aviation Administration," n.d.). This study addresses this constraint by evaluating a lightweight prototype air sampler designed to maintain higher flow rate while improving the available sampling and flight time of drone-mounted sampling campaigns.

Once sampling hardware is optimized, drones can be deployed for active surveillance to characterize how pathogens move through the atmosphere. While many studies have described microbial movements in the PBL, few have implemented surveillance techniques that synthesize this information for immediate health action (Bangay et al., 2026; Brodsky et al., 2023; Crazzolara et al., 2019; Radosevich et al., 2025; D. J. Smith et al., 2018; Vélez-Rodríguez et al., 2020). By conducting stratified airborne sampling, drones can equip public health officials with real-time data regarding the exposure of human and animal populations and agricultural commodities to airborne contaminants. Such mobile surveillance allows for more informed decisions regarding when to communicate with industries and healthcare professionals to mitigate downstream health effects of humans, animals, and the environment.

1.4 Next Generation Sequencing

Next generation sequencing (NGS), especially amplicon sequencing, is a cost effective and efficient method for genus and even species level identification that can be used for surveillance and response by public health and healthcare providers (Bowers et al., 2019; Hoggard et al., 2018; Luhung et al., 2021; Mbareche et al., 2018). By extracting DNA from the collected samples, researchers can identify a range of microbes quickly and efficiently (Song et al., 2020). Furthermore, the use of NGS can improve detection not being constrained by cultureability, which is beneficial when very few of the collected microbes are viable for culturing (Chen et al., 2020; Damerum et al., 2023). Ultimately, the combination of an effective air sampler, a mobile platform, and powerful NGS, needs to be directed to provide meaningful data.

1.5 Ecological Niche Modeling

Ecological niche modeling can be beneficial in allowing researchers to target likely areas where field work is needed. Despite advances in sampling technology, some pathogens remain difficult to isolate directly from the environment. For example, *Coccidioides spp.*, the etiological agent of Valley Fever, is challenging to detect via traditional environmental sampling even in endemic areas (Morgan E. Gorris et al., 2019; Weaver et al., 2020). This gap in understanding exposure risk links directly with the One Health challenge that *Coccidioides spp.* represents.

Coccidioides spp. are soilborne pathogens that cause significant disease in animals and humans through environmental exposure (M. E. Gorris et al., 2018; Porter et al., 2024; Sykes et al., 2025). However, even though *Coccidioides spp.* are soilborne pathogens, the primary route of exposure and subsequent risk of infection of vulnerable hosts occur through inhalation (M. E. Gorris et al., 2018; Porter et al., 2024; Sykes et al., 2025). The aerosolization of *Coccidioides spp.* arthroconidia results in these arthroconidia becoming a part of the air microbiome, even if that

inclusion is temporary. This leads to a gap in knowledge about how *Coccidioides spp*. are transported in the air, such as how long the arthroconidia remain suspended, how far do they travel, and how this could influence host species exposure risks. However, the difficulty of successful environmental sampling necessitates the use of predictive modeling and sentinel species.

Canines may serve as ideal sentinels for Valley Fever because they are vulnerable to similar diseases, share human living environments, and have more localized travel patterns, which reduces bias in exposure reporting associated with human cases of communicable disease (Ferguson et al., 2024; Sykes et al., 2025). By combining human case data with canine sentinel data, we can create a more accurate representation of habitat suitability for pathogens like *Coccidioides spp*. This integrated modeling approach, moving from direct air sampling to the use of animal proxies, allows researchers to predict suitable habitats and target surveillance in regions where pathogens may be becoming endemic, ideally strengthening the One Health surveillance framework and guiding future field work.

1.6 Dissertation chapters and goals

The goal of this dissertation is to provide a One Health approach that combines research and public health practice to enhance surveillance in the air microbiome that affects humans, animals, and ecosystem health. Using innovative sampling by first validating a novel, drone-optimized air sampler, and then the deployment of the drone-optimized air sampler, identification of microbes through next generation sequencing, and guidance of a One Health habitat suitability model, we plan to demonstrate the utility of mobile sampling platforms and One Health frameworks to improve surveillance and help guide human, animal, and ecosystem health information collection and intervention.

Chapter two, with Appendix A as supplementary material, is in preparation for submission as:

Kessinger, P., Nieto-Caballero, M., Hill, T., Kraus, E., Hernandez, M., Magzamen, S., Bosco-Lauth, A., Kreidenweis, S., Performance Evaluation of Drone-Mounted Light SASS Sampler

Chapter three, with Appendix B as supplementary material, is in preparation for submission as:

Kessinger, P., Van Pelt, R., S., Bosco-Lauth, A., Magzamen, S., Drone-Mounted Air Sampling of the Planetary Boundary Layer for Microbial Surveillance

Chapter four, with Appendix C as supplementary material, is in preparation for submission as:

Kessinger, P., Bosco-Lauth, A., Magzamen, S., A One Health Approach to Model *Coccdioides* Species habitat in Arizona

Finally, Chapter five summarizes the work within this dissertation and discusses future work and direction.

CHAPTER 2

PERFORMANCE EVALUATION OF DRONE-MOUNTED LIGHT SASS SAMPLER[2]

2.1 INTRODUCTION

Planetary Boundary Layer air sampling, defined here as sampling above ground level, is an expanding field of environmental surveillance useful for microbial ecology. By sampling organisms at altitude, researchers can improve understanding of how biological particles or bioaerosols are transported from source to receptor. This framework is critical for public health, especially when considered through the lens of a One Health context (Barasona et al., 2014; Radosevich et al., 2025; B. Smith et al., 2015; Tirado & Cano, 2020), integrating human, animal, and environmental health. Many pathogens utilize the atmosphere as a means of transportation, allowing for exposure of host organisms through inhalation or deposition (Radosevich et al., 2025; Vélez-Rodríguez et al., 2020). An example that has been well documented is downy mildew, an opportunistic plant pathogen that significantly impacts crops, such as cucumbers, cantaloupe, and pumpkins (Neufeld et al., 2018; Ojiambo & Holmes, 2011a; Tör et al., 2023). There is strong evidence that downy mildew can be transported over long distances through atmospheric processes (Neufeld et al., 2018; Ojiambo & Holmes, 2011a). Other examples of long-range transport of bioaerosols include trans-Atlantic dust transport from Africa and regional wind-driven dispersal across the United States (Brodsky et al., 2023; Ojiambo & Holmes, 2011b; Savory et al., 2011). Variable altitude air sampling can provide a more comprehensive picture of how pathogens and other bioaerosols are transported through the atmosphere and expose potentially vulnerable

[2] Adapted from manuscript in prep: Kessinger, P., Nieto-Caballero, M., Hill, T., Kraus, E., Hernandez, M. T., Bosco-Lauth, A. M., Kreidenweis, S. M., Magzamen, S., (in prep). Performance Evaluation of Drone-Mounted Light SASS Sampler.

populations, including humans, animals, and crops (Radosevich et al., 2025; B. Smith et al., 2015; Tirado & Cano, 2020). By applying vertical sampling strategies, researchers and public health officials can improve their understanding of airborne transport pathways and, ultimately, better characterize the transmission mechanisms of airborne contaminants.

Currently, there are several approaches to conduct atmospheric air sampling, each with its own advantages and limitations. These include fixed towers, tethered balloons, and crewed aircraft, along with a range of compatible sampling instruments. Towers, such as those deployed by the National Ecological Observatory Network (NEON), are widely used to measure biological, hydrological, and meteorological processes. They provide stability and available infrastructure, allowing for the deployment and use of heavier and more complex sampling equipment (Zahn & Bou-Zeid, 2024). However, towers are limited in height due to structural constraints, and their fixed locations restrict flexibility for monitoring locations (Evans Ogden, 2026; Zahn & Bou-Zeid, 2024; Zhang et al., 2017). Tethered balloons offer greater vertical flexibility and portability than towers, but lack structural support, limiting the type of sampling equipment and weight that can be deployed (Zhang et al., 2017). Crewed aircraft offer the most flexibility, allowing for sampling over broad areas or targeted locations, depending on the type of aircraft (e.g., plane vs helicopter) deployed. However, aircraft-based sampling can be influenced by airflow disturbances and flight dynamics, which can introduce biases in the collected measurements or samples (Bieber et al., 2020; Zhang et al., 2017). Furthermore, aircraft operations are costly and require specialized and intense training in addition to logistical coordination to operate. Unmanned aircraft systems (UAS), or drones, are an emerging alternative that can improve airborne sampling flexibility while reducing aircraft logistical and administrative challenges.

Like other floating air sampling platforms, drones present a unique balance of advantages and limitations. They offer the operational flexibility of crewed aircraft while avoiding the associated costs and extensive training requirements. In the United States, researchers can obtain a Federal Aviation Administration (FAA) Part 107 Remote Pilot Certificate, which is the standard certification for commercial and research drone operations, allowing for independent deployment and operation (Bangay et al., 2026; "Small Unmanned Aircraft Systems (UAS) Regulations (Part 107) | Federal Aviation Administration," n.d., p. 107). This level of autonomy can increase deployment frequency while substantially reducing operational overhead. Furthermore, smaller drone platforms can reduce the impact of propeller wash on a proximal aerosol sampler, compared to the turbulence generated by larger, crewed aircraft (Bieber et al., 2020). To effectively collect biological air samples at higher altitudes, higher flow rate samplers are often required to compensate for the low concentration of biomass in the atmosphere (Bøifot et al., 2020). This presents a limitation, as drones operated under Part 107 are restricted to a total takeoff weight of less than 55 lbs (25 kg). Consequently, air sampler weight and payload capacity are critical constraints when using drone-based sampling strategies (Bangay et al., 2026; Bieber et al., 2020; Bøifot et al., 2020; Radosevich et al., 2025; "Small Unmanned Aircraft Systems (UAS) Regulations (Part 107) | Federal Aviation Administration," n.d.).

Because commercially available drones have relatively limited payload capacities, the weight of an air sampler can significantly reduce flight endurance and, consequently, total sampling time (Bieber et al., 2020). This often presents an exclusive choice between lightweight, low-flow-rate samplers that allow for longer flight times, but may collect insufficient biomass, or heavier, high-flow-rate samplers that can improve collection efficiency but constrain flight time and operational flexibility (Bieber et al., 2020; Bøifot et al., 2020). Furthermore, on smaller drone

platforms, heavier samplers are often mounted near the rotors, increasing the risk that the sampled air is influenced by propeller wash turbulence, potentially introducing bias or contamination (Bieber et al., 2020). Therefore, a significant technical hurdle remains: optimizing the weight-to-performance ratio of current air sampling hardware for drone-based applications.

The goal of this study is to compare two air samplers: the SASS 3100 dry air sampler, and a lightweight prototype SASS 3100 developed by Research International, Inc. Specifically, our goal was to evaluate whether reducing sampler weight could improve the longevity of drone-mounted air sampling campaigns while maintaining sampling performance.

To address this objective, this study is structured around two specific aims. Aim one evaluates whether the Full SASS and the Light SASS operate and collect comparable samples under identical conditions. Because the two samplers use the same active air sampling technology, we tested their performance in a controlled chamber by challenging each with a known tracer organism (*i.e.*, *Pseudomonas syringae*), followed by conducting side-by-side comparisons under outdoor ground-level conditions. Aim two assesses whether drone operation influences sampler recovery. This was tested by mounting the Light SASS on a drone platform and operating it alongside a boom lift equipped with the Full SASS in a field setting.

2.2 METHODS

2.2.1 Study Area

This study was conducted across three distinct locations: (1) a 10 m^3 environmentally controlled chamber at the University of Colorado at Boulder which has been previously described (Nieto-Caballero et al, 2023); (2) an outdoor ground-level site at Colorado State University's Foothills Campus; and (3) a field site at Colorado State University's Agricultural Research,

Development, and Education Center (ARDEC) (Nieto-Caballero et al., 2023). Both the Foothills Campus (40.5885, -105.148, Figure 1) and ARDEC (40.6463, -104.996, Figure 1) are located in Fort Collins, Colorado, and the chamber is located in the Aerobiology and Disinfection Laboratory in Boulder, Colorado. The indoor chamber is approximately 45 km southwest of the Fort Collins field sites.

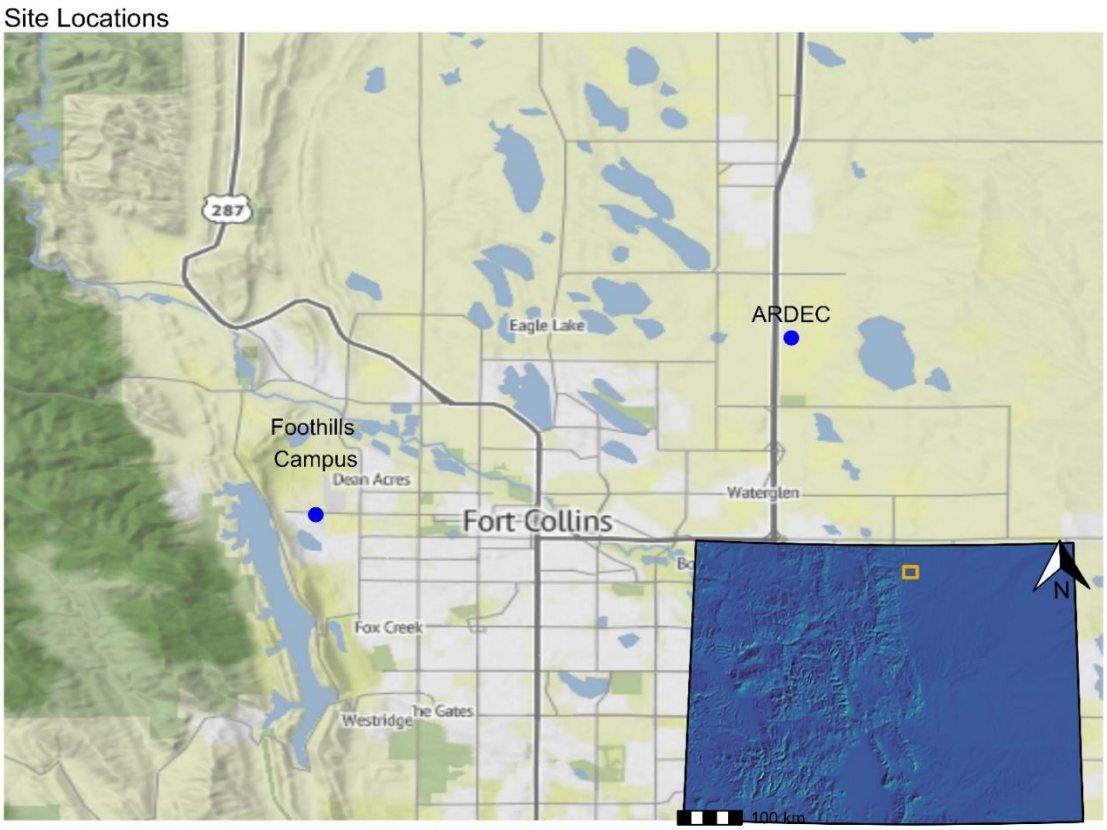

Figure 2.1 This map shows the study site locations, with Foothill Campus representing the Atmospheric Science Department at Colorado State University's Foothills Campus, and ARDEC representing Colorado State University's Agricultural Research, Development, and Education Center. The map in the bottom right corner represents a to-scale map with a box in the Northern region highlighting the approximate study area within the state of Colorado.

2.2.2 Sampling Design

For all experiments, the SASS 3100 dry air sampler (hereafter referred as "Full SASS", 3 kg) was set up alongside the lightweight prototype SASS 3100 (hereafter "Light SASS", 1 kg) (Research International, Inc, Monroe, WA). Both the Full SASS and Light SASS are capable of

sampling 300 liters per minute and use the same accessories, including filters and Bluetooth equipment. Both the Full SASS and Light SASS were received from Research International, Inc, calibrated for the designed flowrates. Flowrate is approximately within one percent from unit-to-unit. Additionally, the SASS system monitors rotations per minute (RPM) using a digital revolution sensor, and each flow setting corresponds to a particular RPM based on an empirical flow-vs-RPM curve fit (Research International, Inc, Monroe, WA). Flow rate is highly accurate between individual sampling units, though flow rate can fluctuate between filter lots by +/- 7%. This configuration allowed for direct side-by-side comparisons between the Full SASS and the Light SASS under identical sampling conditions. Both samplers were operated with standard EtO-sterilized polypropylene electret microfiber filters for all experiments (filter collection efficiency of 50% at 0.5 um, 12 mg/cm^2, P/N 7100-134-232-01, Research International, Inc, Monroe, WA) and equipped with a SASS specific rain cover that is used to protect the samplers in the field (Research Internation, Inc, Monroe, WA). Three distinct sampling setups were evaluated in this study: (1) chamber, (2) ground-level, and (3) elevated. Under all conditions, sampling was conducted at 300 liters per minute (LPM). Sampling time for the chamber study was 5 minutes per trial, for the ground it was 1 hour per trial, and for the elevated trials it was a median time of 23 minutes for the quadcopter and 27 minutes for the hexacopter. Elevated trial times differed due to being reliant upon drone flight times, which varied due to conditions and battery drain. All experiments were conducted in triplicate, with three samples collected per sampler type for each experiment.

2.2.3 Chamber Trials

The chamber trials were performed in a 10 m^3 controlled environment that allowed the aerosolization of a known tracer organism according to the methods previously described by

(Gomez et al., 2022). The chamber was equipped with internal fans for homogenous mixing, as well as HEPA filtration units to remove airborne particles in the chamber before and after trials. Liquid cultures of *Pseudomonas syringae* (optical density (OD) = 0.911 average for trials ± 0.135) were used as a tracer organism which was nebulized in a narrow particle size distribution. Before aerosolization of bacterial cultures, samplers were decontaminated using 70% isopropanol followed by DNA Away (Thermo Fisher Scientific, Waltham, MA) and then were co-located in the chamber on a metal shelf approximately 1.2 m above the chamber floor. Both samplers were equipped with Bluetooth antennas to allow for remote operation while the chamber remained sealed. The *P. syringae* culture was loaded into a 6-jet Collison nebulizer (CH Technologies, Westwood, New Jersey) in a biosafety cabinet. The nebulizer was attached to a compressed air cylinder that operated at 20 psi, and the bacterial culture was nebulized for 3.5 minutes. Both samplers ran at 300 L min^{-1} for 5 minutes. After each trial, both samplers were turned off and the chamber air was cleared with the HEPA filters. Once the chamber was clear of airborne particles, indicated by the Wideband Integrated Bioaerosol Sensor (Droplet envea Group, Longmont, CO) particle readout returning to baseline after HEPA filter activation, filters were removed from the samplers and placed into sterile Petri dishes inside the biosafety cabinet, sealed with Parafilm, and stored at -20 °C. Trials were repeated in triplicate, generating 3 samples per sampler. As parallel controls, two blank filters per sampler were collected to account for potential contamination associated with the samplers, the chamber environment, and/or filter handling. Blank filters were briefly placed on the samplers before immediately removing them and placing them in Petri dishes, sealing with parafilm, and stored at -20 °C for storage.

2.2.4 Field methods, elevated field trials

The elevated field trials were conducted at ARDEC. Two drones were acquired from the Colorado State University's Drone Center: a DJI Matrice 350 quadcopter (DJI, Shenzen, China) and an Aurelia X6 Pro V2 hexacopter (Aurelia Aerospace, Las Vegas, NV). The DJI Matrice 350 is capable of 55-minute flight times and can carry a max payload of 2.7 kg. The Aurelia X6 Pro V2 offers flight times of up to 70 minutes and a maximum payload of 6 kg. In addition, a rented boom lift with a basket was set to 12 meters above ground level. The boom lift and drone landing pad were set up in a barren field at ARDEC for ease of access and operation. A field workstation was set up under canopy tents using folding tables. Aluminum foil was secured on the surface of the table with tape and then cleaned with 70% isopropanol, followed by DNA away. Drone equipment was set up on a separate table and similarly decontaminated before deployment. The Light SASS was mounted on the DJI Matrice 350 for 3 replicate trials and then mounted on the Aurelia hexacopter for 3 additional replicate trials. Both the Light SASS and Full SASS were decontaminated with 70% isopropanol and DNA Away before each trial. The Full SASS was mounted on a tripod that was secured with zip-ties to the basket of the boom lift. Both the Light SASS and Full SASS were equipped with Bluetooth antennas and connected to a laptop to enable remote operation and covered with rain hats before starting the experiments. The boom lift was raised to 12 meters above ground level (AGL). Once the boom lift was in position, the drone was placed on a landing pad approximately 10 meters from the boom lift. The drone was then set to hover at the same sampling height of the boom lift (*i.e.*, 12 meters AGL). Once both instruments were in position, the laptops were used to start both samplers simultaneously via Bluetooth connection. Sampler duration was determined by safe drone flight limits, which depended on drone battery draw – also affected by ambient conditions. Before descending for landing, both samplers

were remotely turned off to prevent contamination related to descending and landing operations. Once the drone landed and the boom lift was lowered, filters were removed from the samplers and placed into sterile Petri dishes and sealed with Parafilm, working at the decontaminated foiled work surface underneath the tents. Samples were placed in a cooler with temperature packs cooled to -20° C. Trials for each drone type were conducted in triplicate. Samples were transported to the CSU Foothills Campus, where the filters were stored at -80° C until DNA extraction.

2.2.5 Sample extraction

DNA was extracted from all filters using the Qiagen DNeasy PowerSoil Pro Kit (Qiagen, Venlo, Netherlands). While originally intended for DNA extraction from soil samples, a modified protocol from Nieto-Caballero et al. (2025) was used for the SASS filters (Nieto-Caballero et al., 2025). All extractions were carried out in a laminar flow hood at the CSU Foothills Atmospheric Sciences Campus in the Kreidenweis Lab. When not in use, the laminar flow hood was sterilized with UV light and cleaned before and after every use with 10% bleach, 70 percent isopropanol, and DNA away. All equipment and surfaces were similarly decontaminated before and after use. The modified protocol involved cutting off a quarter of the filter and then cutting it into 6-8 smaller pieces to fit inside the bead-beating tube. After lysis, another modified step involved using a sterile syringe to recover any remaining liquid from the filter material before discarding the filter. DNA extraction was then conducted with the remaining fluid by using the Qiagen DNeasy PowerSoil Pro Kit protocol from the manufacturer (Qiagen, Venlo, Netherlands), starting with step 3. Once extractions were completed, samples were stored at -80ºC until ready for sequencing.

2.2.6 DNA quantification and amplicon sequencing

All DNA results were quality controlled using several control methods. As previously mentioned, blanks were taken for each trial and each sampler during chamber, ground, and field

trials. These blanks were extracted, quantified, and sequenced in the same way as the samples. Additionally, during DNA extraction, two extraction blanks were created for every six samples. These extraction blanks went through the entire extraction process without filters to ensure that there was either no contamination or that contamination from the extraction process and reagents could be quantified if observed. Finally, there were negative controls added to the next generation sequencing plate during amplification to ensure sample integrity.

Ground and elevated trial extracted DNA was quantified using a Qubit 4 Fluorometer and the associated high-sensitivity double-stranded DNA (HS-dsDNA) reagent kit (Invitrogen, Thermo Fisher Scientific, Waltham, MA). Under sterile conditions, DNA extracts were thawed. For each sample, 20 uL of extracted DNA was added to 180 uL of HS-dsDNA working solution. Two standards were prepared according to the manufacturer's protocol. Samples and standards were vortexed for 5 seconds and incubated for 2 minutes at room temperature. Standards were measured, followed by samples quantification (in ng/uL) with Qubit. Reported values were adjusted for eluted sample volume and air volume sampled to report ng/m^3 of air for results.

Chamber trial extracted DNA were sent for Quantitative Polymerase Chain Reaction (qPCR) at University of Colorado, Boulder. Gene copies of airborne *Pseudomonas syringae* were quantified via qPCR from purified DNA for the chamber trials. Amplification was facilitated using the specific primers Psy F (5'-ATG ATC GGA GCG GAC AAG-3') and Psy R (5'-GCT CTT GAG GCA AGC ACT-3') which target a 108 bp fragment found as a single-copy gene segment specific to *P. syringae* species (Guilbaud et al., 2016). Each 20 uL reaction was assembled using 18 uL of master mix and 2 uL of template DNA for standards and 2 uL of sample DNA for experimental trials. The final reaction concentrations consisted of 1X PowerUp SYBR Green Master Mix (Thermo Fisher Scientific, Waltham, MA), 0.2 uM of each primer, and 1.5 mM $MgCl_2$.

All reactions were conducted in triplicate, and quantification was determined via a standard curve generated from a dilution series ranging from 10^8 to 10^1 total copies. The standard sequence amplified was a custom 168bp gBlocks Gene Fragment (Integrated DNA Technologies, Coralville IA, USA) created from a *P. syringae* genome (GenBank: CP045799.1).

Sample DNA was quantified using the QuantStudio™ 3 System (Thermo Fisher Scientific, Waltham, MA). Thermal cycling was initiated with a two-step hold stage of 50°C for 2 minutes and 95°C for 3 minutes, followed by 40 cycles of denaturation at 95°C for 15 seconds, annealing at 60°C for 15 seconds, and extension at 72°C for 1 minute. To ensure amplicon specificity, a melt curve analysis was conducted immediately following the PCR stage, consisting of 95°C for 15 seconds, 60°C for 1 minute, and a final dissociation step reaching 95°.

Remaining ground and elevated trial sample DNA was sent for amplicon sequencing at Colorado State University's next-generation sequencing center for microbial community analysis. DNA was sequenced for bacteria and archaea community composition and was analyzed by amplifying the V4 region of the 16S rRNA gene following the Earth Microbiome Project protocols. PCR amplification was performed using the updated 515F (Parada et al., 2016) and 806R (Apprill et al., 2015) primer pair (515F: 5'-GTGYCAGCMGCCGCGGTAA-3'; 806R: 5'-GGACTACNVGGGTWTCTAAT-3'), which includes degeneracy to reduce bias against SAR11 and Thaumarchaeota lineages (Apprill et al., 2015; Parada et al., 2016). The forward primer contained a unique 12-bp Golay barcode to facilitate multiplexing.

Each sample was amplified in one 25-µL reaction and one 50-uL reaction containing 13.0 µL of PCR-grade water, 10.0 µL of 2x Platinum Hot Start PCR Master Mix (ThermoFisher Scientific, Waltham, MA), 0.5 µL (10 µM) of each primer, and 1.0 µL of template DNA, and 26.0 uL of PCR-grade water, 20.0 uL of 2x Platinum Hot Start PCR Master Mix, 1 uL (10 µM) of each

primer, and 2.0 uL of template DNA, respectively. Thermal cycling conditions consisted of an initial denaturation at 94°C for 3 min, followed by 35 cycles of 94°C for 45 s, 50°C for 60 s, and 72°C for 90 s, with a final extension at 72°C for 10 min.

Following amplification, reactions were pooled, and the presence of the target band (~300–350 bp) was confirmed via 1.5% agarose gel electrophoresis. Amplicons were quantified by plate using the Quant-iT PicoGreen dsDNA Assay Kit (ThermoFisher Scientific, Waltham, MA), and an equimolar pool was created by combining 240 ng of DNA from each sample. Each plate pool was cleaned using a magnetic bead clean up (AMPure beads, Beckman Coulter Life Sciences, Indianapolis, IN). Sequencing was performed on the Illumina MiSeq platform (Illumina, San Diego, CA). The library was spiked with 15% PhiX control DNA using an Illumina 2x250 kit (Illumina, San Diego, CA), and sequencing was conducted using custom Read 1, Read 2, and Index primers as described by (Caporaso et al., 2012).

2.2.7 Statistical analysis

We conducted all statistical analysis in R (4.5.1). Packages for data cleaning and statistical analysis included *tidyverse* (2.0.0), *rstatix* (0.7.3), *coin* (1.4-3), and *effsize* (0.8.1) (Hothorn et al., 2023; Kassambara, 2025; Torchiano, 2020; Wickham & RStudio, 2023). Packages for visualization included *ggplot2* (4.0.2), *ggextra* (0.11.0), *cowplot* (1.2.0), and *gridExtra* (2.3) (Attali & Baker, 2025; Auguie & Antonov, 2017; Wickham et al., 2026; Wilke, 2025). We used non-parametric statistical tests due to our small sample size (n=3 per sampler, n = 6 per group) and inability to determine normality. This included the Mann-Whitney U test and Cliff's Delta test to assess differences in sampled amounts by concentrations (Mann-Whitney U) and effect size (Cliff's Delta). 95% percent confidence intervals and effect size delta estimate were used to determine statistical relevance.

Alpha and beta diversity analyses were additionally used to assess whether the samplers produced comparable microbial community profiles. Amplicon sequence data were processed in *Qiime 2* (2024.2) for both diversity metrics. Alpha diversity metrics included Faith's Phylogenetic Diversity (Faith PD), Pielou's evenness, Shannon entropy, and observed features. Beta diversity analyses were generated to compare microbial community composition between sampler types. Last, Kruskal-Wallis tests were performed to assess pairwise comparisons between sampler types, and p-values were reported for each diversity metric.

2.3 RESULTS

Results are reported in three different categories: (1) chamber trials, (2) ground-level trials, and (3) elevated field trials. Chamber trial results are reported as qPCR copies m^{-3} of *Pseudomonas syringae*, whereas ground and elevated field trials are reported as total DNA concentrations normalized by sampled air volume (ng m^{-3}).

2.3.1 Chamber trial results

Chamber trial results are presented in Figure 5 and summarized in Table 1. The mean concentration of *P. syringae* detected by qPCR was 1.8×10^8 gene copies m^{-3} for the Full SASS and 2.4×10^7 gene copies m^{-3} for the Light SASS.

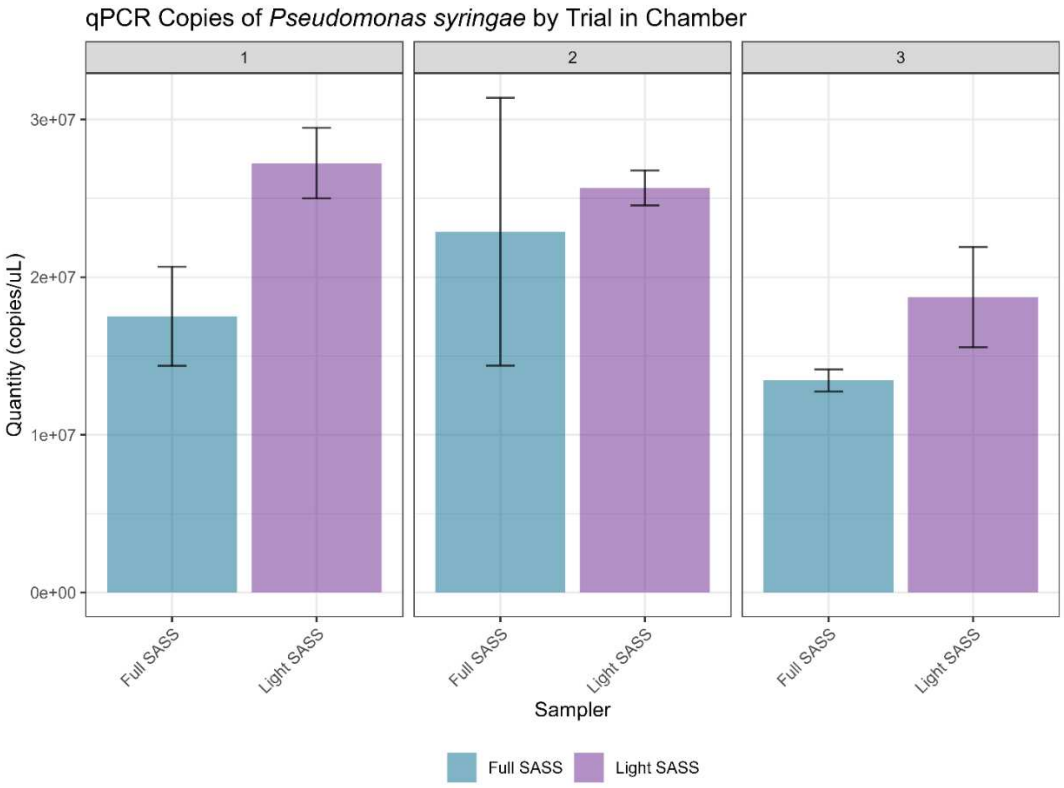

Figure 2.2: qPCR copies of *Pseudomonas syringae* for each trial by sampler. The light blue is the Full-sized SASS, and the purple is the Light SASS. Results are reported as a comparison of qPCR copies between samplers. Results for qPCR were conducted in triplicate to obtain error bars for each trial.

In all cases the Light SASS recovered a higher mean number of *Pseudomonas syringae* copies than the Full SASS during controlled bioaerosol chamber challenges. However, statistical comparisons of the genomic recovery between the samplers were not significant. This suggests that variability between replicate trials was sufficiently large so that no consistent performance difference between samplers could be confirmed. However, the negative Cliff's delta estimate (-0.78) suggested a trend toward greater recovery by the Light SASS under chamber conditions. Results for the chamber trials are summarized in Table 2.1.

Table 2.1: Results from Mann-Whitney U test and Cliff's Delta test for the chamber trials. The 95% confidence interval for the Mann-Whitney U test was [-20675617, 6224513] and included the null. The 95% confidence interval for Cliff's Delta test was [-0.98, 0.19] and included the null. The delta value was large (-0.78) and favored the Light SASS.

Experiment	Test	Estimate	95% Confidence Interval
Chamber	Mann-Whitney U	-7925153	[-20675617, 6224513]
Chamber	Cliff's Delta	-0.78	[-0.98, 0.19]

2.3.2 Ground-level field results

Ground-level field trials are presented in Figure 2.3 and summarized in Table 2.2. Mean total DNA concentrations for the Full SASS were 0.476 ng m^{-3} and 0.260 for the Light SASS. Although the Full SASS recovered a higher average DNA concentration than the Light SASS during ground-level sampling, statistical comparisons did not indicate a significant difference between samplers. The 95% confidence intervals for both the Mann–Whitney U (95% CI: [-0.05, 0.47]) and Cliff's delta (95% CI: [-0.61, 0.96]) analyses contained the null, suggesting that the observed differences were within the variability expected between replicate samples (Table 2.2). While the Cliff's delta estimate indicated a tendency toward greater DNA recovery by the Full SASS (Cliff's Delta estimate = 0.56, Table 2.2), the broad confidence intervals indicate substantial uncertainty in the magnitude of this difference.

2.3.3 Elevated field results

Elevated field trial results are shown in Figure 2.3 and summarized in Table 2. The quadcopter trials using the DJI Matrice 350 showed mean concentrations of 1.07 and 0.986 ng m^{-3} of sampled air for the Full SASS (boom lift) and Light SASS (drone), respectively (Figure 2.3). Mann-Whitney U confidence intervals contained the null (95% CI: [-0.14, 0.25]), indicating no statistically significant differences between samplers (Table 2.2).

The hexacopter trials using the Aurelia X6 Pro V2 trials showed mean DNA concentrations of 0.833 for the Full SASS mounted on the boom lift and 0.514 ng m^{-3} for the Light SASS when mounted on the hexacopter (Figure 2.3). In contrast to the quadcopter experiments, the Mann-Whitney U confidence interval did not overlap zero (95% CI: [0.07, 0.63]), indicating a statistically significant difference between samplers with hexacopter deployment (Table 2.2). DNA concentrations recovered from the Full SASS were consistently higher than those recovered from the Light SASS (Cliff's delta estimate =1, Table 2.2).

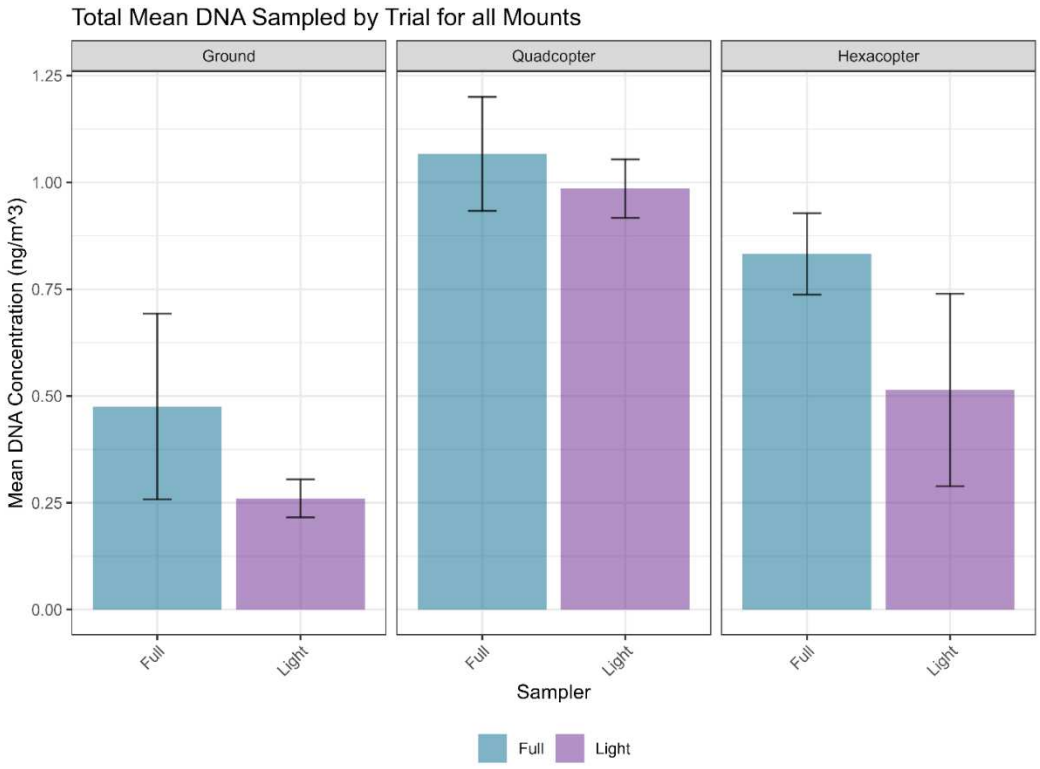

Figure 2.3: Total DNA concentration in ng/m^3 quantified using Qubit 4.0. The light blue is the Full-sized SASS, and the purple is the Light SASS. Results are reported as a comparison of ng/m^3 of DNA between samplers.

Table 2.2: Mann-Whitney U and Cliff's Delta test results by trial type with 95% confidence intervals. All confidence intervals were nonsignificant except for the elevated hexacopter trials. Significant confidence intervals are marked with an asterisk. Delta effect size estimates were large, medium, and large for ground, quadcopter, and hexacopter respectively.

Experiment	Test	Estimate	95% confidence interval
Ground	Mann-Whitney U	0.22	[-0.05, 0.47]
Elevated Quadcopter	Mann-Whitney U	0.13	[-0.14, 0.25]
Elevated Hexacopter	Mann-Whitney U	0.25	[0.07, 0.63]*
Ground	Cliff's Delta	0.56	[-0.61, 0.96]
Elevated Quadcopter	Cliff's Delta	0.33	[-0.81, 0.95]
Elevated Hexacopter	Cliff's Delta	1	[0.14, 1.00]*

2.3.4 Microbial diversity results

Alpha and beta diversity analyses were used for ground-level and elevated field trials to evaluate whether the sampler type had an influence on the recovery of the microbial community composition.

Alpha diversity comparisons for ground-level samples are presented in Figure 2.4. No statistically significant differences were observed between the Full SASS and Light SASS for Faith's Phylogenetic Diversity, Pielou's evenness, Shannon entropy, or observed features (p-values = 0.7, 1.0, 0.7, and 0.2, respectively).

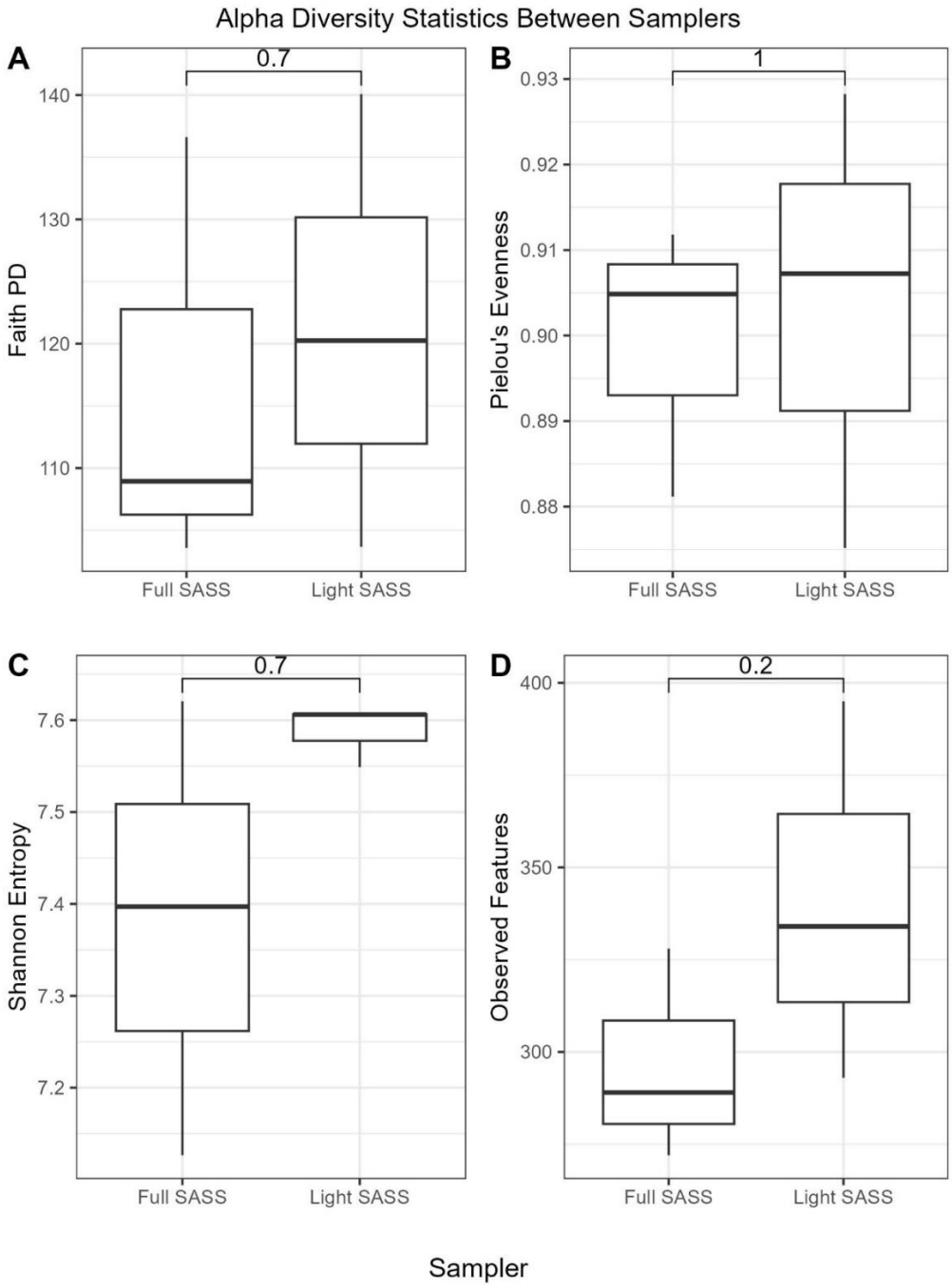

Figure 2.4: Alpha Diversity results at ground-level between the Full-sized SASS and Light SASS. P-values are all non-significant, indicating that there is not enough evidence to suggest a difference between the two samplers

Similarly, elevated field samples showed no statistically significant differences in alpha diversity metrics between samplers (Figure 2.5) with p-values of 0.7, 0.94, 0.82, and 0.94 for Faidh's PD, Pielou's evenness, Shannon entropy, and observed features, respectively.

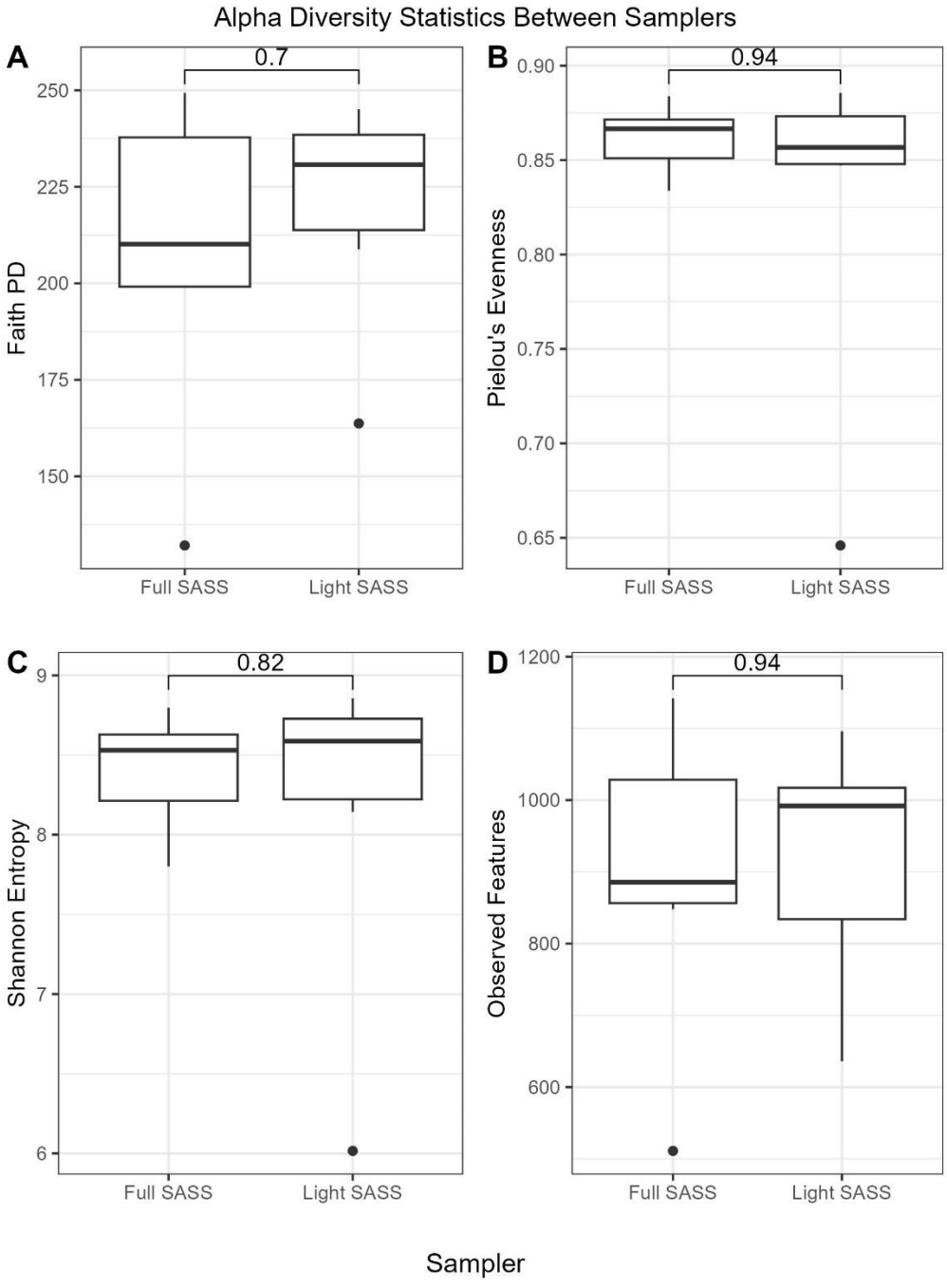

Figure 2.5: Alpha Diversity results at 12 meters between the Full-sized SASS and Light SASS, combining when mounted on both the DJI drone and Aurelia drone. P-values are all non-

significant, indicating that there is not enough evidence to suggest a difference between the two samplers

Beta diversity analyses also indicated similar microbial community compositions between samplers at elevation (Figure 2.6). Bray-Curtis, Jaccard, weighted UniFrac, and unweighted UniFrac comparisons were all non-significant (p-values = 0.902, 0.984, 0.954, and 0.951, respectively).

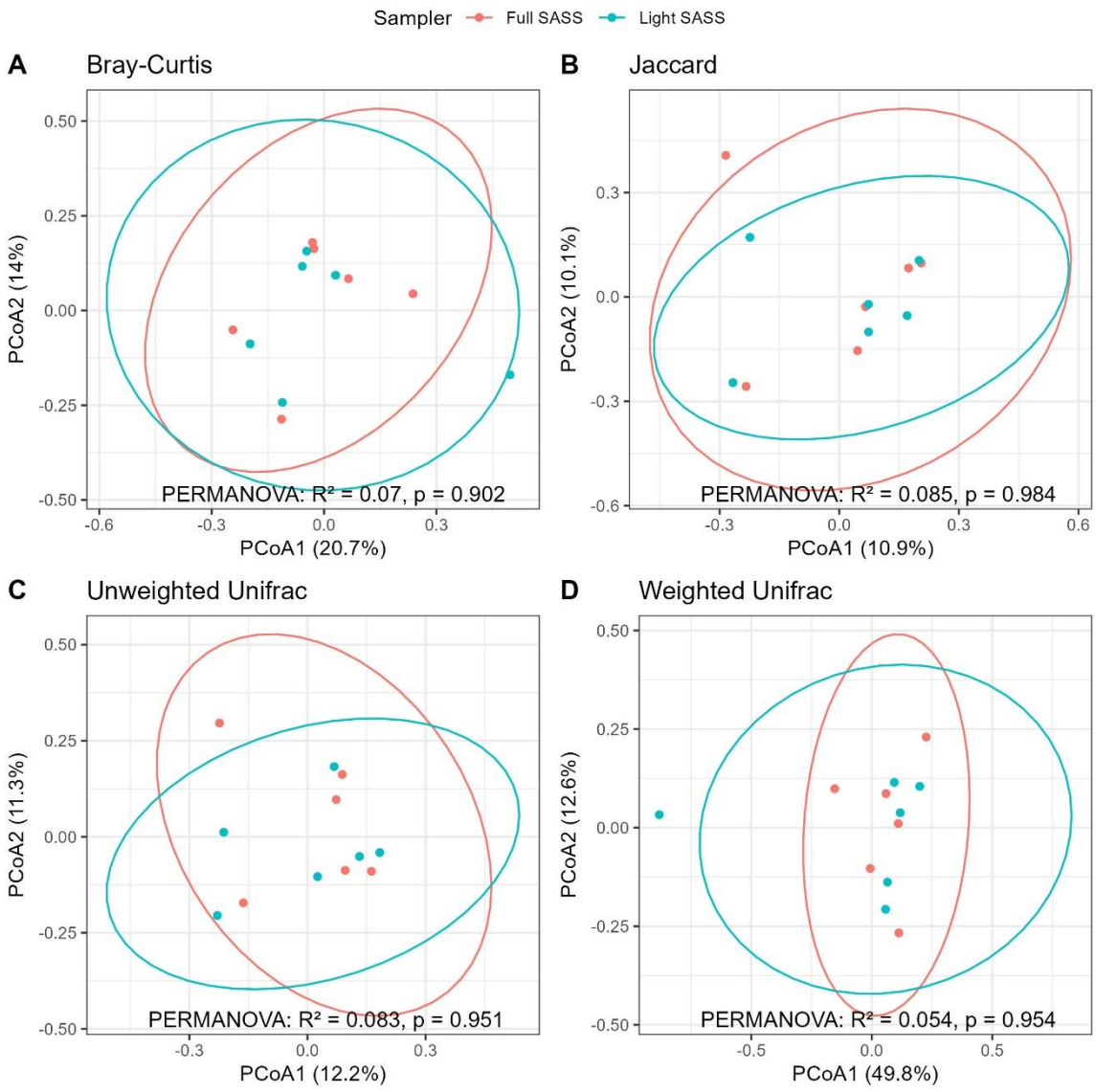

Figure 2.6: Beta Diversity results at 12 meters between the Full-sized SASS and Light SASS. P-values are all non-significant, indicating that there is not enough evidence to suggest a difference between the two samplers

Overall, diversity analyses suggest that the Full SASS and Light SASS recovered similar microbial community compositions across field deployments (i.e., at ground level and aloft).

2.4 CONCLUSIONS

The objective of this study was to evaluate whether a lightweight prototype version of the SASS 3100 (Light SASS) could provide comparable sampling performance to the widely used full-sized air sampler (Full SASS) (Ang et al., 2022; Bøifot et al., 2020; Mbareche et al., 2018) while reducing payload weight for drone-based bioaerosol sampling applications. The prototype sampler is a lightweight version of the SASS 3100 dry air sampler that maintained the same operational characteristics of the Full-sized SASS 3100 dry air sampler while reducing weight from approximately 3kg to 1kg through lighter housing materials, a significantly smaller casing size, and a smaller power system. Because payload capacity is a major limitation for drone-based applications, reducing sampler weight has the potential to improve flight endurance and operations during airborne sampling campaigns.

Overall, our findings show that the Light SASS performed comparably to the Full SASS across most experimental conditions. Chamber experiments, outdoor ground-level sampling, and elevated quadcopter deployments did not show statistically significant differences between samplers in DNA recovery or microbial diversity metrics. Our results showed that reducing sampler weight did not alter overall sampling performance under these conditions. On the other hand, elevated hexacopter trials showed a consistent separation between sampler DNA recovery, with the Full SASS recovering higher DNA concentrations than the Light SASS. Statistical analyses for the hexacopter trials aloft indicated significant differences between sampler recovery. A potential explanation is that the airflow dynamics specific to the Aurelia X6 Pro V2 influenced sampling efficiency. Drone-generated turbulence and prop wash have previously been identified

as important considerations in airborne sampling design (Bieber et al., 2020). In addition, drone vibration may have affected the Light SASS fan operation, effectively collecting lower air volumes, compared to the stationary Full SASS. This could potentially explain why significant differences were not observed between the hexacopter Light SASS and the Full SASS with respect to microbial diversity analyses. Additional experiments could potentially isolate whether these differences were caused by the propeller wash caused by using a hexacopter, or if they were specific to the Aurelia X6 Pro V2 platform and its intrinsic vibration, causing lower collection efficiency with the Light SASS.

Importantly, microbial diversity analyses demonstrated strong agreement between samplers across field deployments. Alpha and beta diversity analyses did not identify significant differences in microbial community composition between the bioaerosol recovered by Full SASS and the Light SASS. These findings suggest that drone deployment and reduced sampler weight did not bias the bioaerosols recovered. This is highly relevant for bioaerosol characterization applications, where multiple concerns exist, such as potential reduced air volume collected due to drone vibration or airflow disturbances, and their effects on microbial community composition.

A major strength of this study was the use of independent complementary deployment scenarios to assess sampler performance, including controlled chamber experiments, outdoor ground-level sampling, and elevated field deployments (*i.e.*, 12 m AGL). All scenarios were conducted in triplicate. Together, these experimental conditions allowed for method validation in a controlled and environmentally relevant sampling conditions. Additionally, incorporating microbial diversity analyses along with total DNA concentrations provided multiple independent metrics for comparison of sampler performance.

This study had some limitations. Experiments were performed under a limited set of drone deployment conditions. Expanding across a broader range of drone platforms could strengthen confidence in generalizing the findings from this study. Future work, assessing the influence of drone airflow dynamics and sampler placement, could improve the understanding of significant differences found in our study (see hexacopter total DNA results). Additionally, as mentioned in the methods, production variation between filter lots can influence flow rate of the SASS 3100, resulting in approximately a 7% variation of flow rate when set at 300 LPM. This could have influenced uncertainty in our measurements for total DNA collected.

In conclusion, our results indicate that the two samplers, the Full SASS and the Light SASS, provide comparable performance across most conditions tested, while substantially reducing payload weight. These findings support the use of the Light SASS in drone-based bioaerosol studies, particularly for low-biomass environments where maximizing flight duration and operational flexibility is critical. As drones continue to become a more prominent tool in the air sampling and scientific world, lightweight, high-flow bioaerosol samplers such as the Light SASS may become valuable tools for future airborne sampling campaigns.

2.5 ACKNOWLEDGEMENTS

We gratefully acknowledge support from the NSF Biology Integration Institutes Program under Award # 2120117. We thank the CSU One Health Institute for contributions to and support of BROADN research.

We would also like to thank the Colorado State University Drone Center for providing expertise and support during this project, especially around the development and implementation of the sampler mounting systems.

CHAPTER 3

DRONE-MOUNTED AIR SAMPLING OF THE PLANETARY BOUNDARY LAYER FOR MICROBIAL SURVEILLANCE [3]

3.1 INTRODUCTION

Airborne transport of organic and inorganic matter, including biological organisms, is a significant topic for human, animal, and environment health. Airborne transport of particulate matter can span hundreds or even thousands of miles, as seen with dust transport from the Saharan desert (Brodsky et al., 2023; Kellogg et al., 2004; Triadó-Margarit et al., 2022). This dust transports a variety of microbes, including those with pathogenic properties (Brodsky et al., 2023; Kellogg et al., 2004; Triadó-Margarit et al., 2022). Due to this dust transport phenomenon, humans, animals, and environments can be exposed to new contaminants, including those biological and pathogenic in nature (Bangay et al., 2026; Brodsky et al., 2023; Crazzolara et al., 2019; Triadó-Margarit et al., 2022). However, the initial disturbance and lofting of matter occurs closer to the ground (Crazzolara et al., 2019; D. J. Smith et al., 2011, 2018; Tignat-Perrier et al., 2020). The understanding of what particles are being disturbed and lofted into the air remains an important step for understanding exposure and potential downstream effects in communities.

There is a significant amount of aerosolization of microorganisms occurring in the planetary boundary layer (PBL) from disturbances and meteorological events (Crazzolara et al., 2019; D. J. Smith et al., 2018; Tignat-Perrier et al., 2020). The height of this layer can vary in altitude, typically from ground-level up to 2-3 km depending on location and time of day, but

[3] Adapted from a manuscript in preparation: Kessinger, P., Van Pelt, S. R., Bosco-Lauth, A. M., Magzamen, S., et al. (in prep). Drone-Mounted Air Sampling of the Planetary Boundary layer for Microbial Surveillance.

allows for mixing of aerosolized matter and biological organisms (D. J. Smith et al., 2018; Tignat-Perrier et al., 2020). This process results in the potential for lofting and long-range transport of said matter and biological organisms by eventually moving organisms into the free troposphere and beyond (D. J. Smith et al., 2018; Tignat-Perrier et al., 2020). As a result, populations and locations farther away from the point of emission can still become exposed to both local and long-range airborne transport (Brodsky et al., 2023; Crazzolara et al., 2019; D. J. Smith et al., 2018; Tignat-Perrier et al., 2020; Triadó-Margarit et al., 2022). The transport of biological organisms and contaminants can have negative impacts on human, animal, agriculture, and ecosystem health (Brodsky et al., 2023; Crazzolara et al., 2019). One such example is Fusarium Wilt (FW), caused by *Fursarium oxysorum* and its subtypes (Brodsky et al., 2023; Fones et al., 2020). *F. oxysorum*, while being a soil-borne pathogen, has demonstrated the capability of airborne transport, making it a significant pathogen of concern when it comes to agricultural health and subsequent economic impacts of crops like bananas (Brodsky et al., 2023; Crazzolara et al., 2019; Scarlett et al., 2015).

Prior literature quantifies and describes the microbial movements and compositions in the PBL, using methods such as cultivation, next generation sequencing, and qPCR (Bangay et al., 2026; Brodsky et al., 2023; Crazzolara et al., 2019; Radosevich et al., 2025; D. J. Smith et al., 2018; Triadó-Margarit et al., 2022; Vélez-Rodríguez et al., 2020). Next generation sequencing continues to advance, reducing costs and providing high quality microbial sequencing data (Caporaso et al., 2012; Kers & Saccenti, 2022). This has allowed researchers to learn more about characteristics and constituents of microbial communities and quantify microbial distributions (Bowers et al., 2019; Caporaso et al., 2012; Kers & Saccenti, 2022). However, there are fewer that work towards implementing surveillance techniques useful for public health, especially from a One Health perspective. The lack of integrated surveillance represents an underutilization of next

generation sequencing technology, as well as novel sampling methods, for One Health initiatives that could benefit public health surveillance, especially since previous work indicates the potential for One Health work in the air microbiome (Brodsky et al., 2023; Crazzolara et al., 2019; Triadó-Margarit et al., 2022).

To fill this gap, we propose the use of a readily attainable drone under the United States Part 107 license to demonstrate ease of use in a health surveillance capacity when outfitted with an air sampler optimized for drone operations. By doing so, we demonstrate the utility of using drone technologies to conduct vertical profiles within the PBL to equip public health officials with real-time data that is pertinent to exposure of vulnerable populations of animals, humans, and crops to airborne organisms. By working with improved information about aerosolized microbial communities, public health officials can make more informed decisions about when to conduct surveillance, as well as when to communicate with exposed populations, industries, and health care professionals to mitigate downstream health effects. Therefore, our objective is to demonstrate the drone and sampler utility by conducting stratified airborne sampling within the PBL, while describing the communities discovered and noting microbial genera of One Health interest.

3.2 METHODS

3.2.1 Study area

The study area for this work is in West Texas and included within the Plains region of the United States Department of Agriculture – Agriculture Research Service (USDA-ARS). The location was selected for proximity to USDA-ARS headquarters, a semi-arid environment with potential for dust events. Dust events in this location are important due to endemic soil-borne pathogens like *Coccidioides* spp. being present. There were three site locations, labeled as site one

(32.183, -101.45), two (32.280, -101.49), and three (32.422, -101.56). Sampling took place during August 6-8th of 2024 and August 12th-14th, 2024. The study biome is semi-arid desert, with temperatures during sampling ranging from 76-85 °F, humidity ranging from 36-67%, and wind speed ranging from 3-17 miles per hour.

3.2.2 Sampling design

For all locations, the SASS 3100 dry air sampler (hereafter referred as "Full SASS") served as the ground level air sampler. A lightweight prototype SASS 3100 (hereafter "Light SASS") served as the drone mounted sampler. The drone used for all drone work during this campaign was a quadcopter DJI Matrice 350 (M350) ((DJI, Shenzen, China)) from the Colorado State University Drone Center. The DJI Matrice 350 is capable of 55-minute flight times and can carry a max payload of 2.7 kg. Sampling design was previously described in Chapter Two. Briefly, both the Full SASS and Light SASS set to sample 300 liters per minute (LPM) and using the same accessories, including filters and Bluetooth equipment. Both samplers were equipped with standard EtO-sterilized polypropylene electret microfiber filters for all fieldwork (filter collection efficiency of 50% at 0.5 um, 12 mg/cm^2, P/N 7100-134-232-01, Research International, Inc, Monroe, WA) and equipped with a SASS specific rain cover that is used to protect the samplers in the field (Research International, Inc., Monroe, WA).

3.2.3 Field methods

Workstation set up followed similarly to Chapter One with some deviations. Aluminum foil was secured on the surface of the mid console of the work truck with tape and then cleaned with 70% isopropanol, followed by DNA away. Drone equipment was set up on the tailgate of the work truck and similarly decontaminated before deployment. The Light SASS was mounted on the DJI Matrice 350 and two Full SASS samplers were set up on tripods. Both the Light SASS and

Full SASS were decontaminated with 70% isopropanol and DNA Away before each elevation flight (e.g. decontaminated before 200 feet (ft) AGL, and then again before 400 feet AGL). The Light SASS was connected via Bluetooth antenna to a laptop and controlled using SASS 3100 software to enable remote operation, and the ground samplers were set to a 1-minute delay and operated manually, with the delay allowing researchers to clear the area before sampling began.

The two Full SASS samplers were placed approximately 1.5 meters off the ground to represent ground level. The ground level samplers were set approximately 25 ft away from center of the site location, 50 ft away from each other. The drone landing pad was set in between the two ground samplers, 25 ft away from each. The Light SASS was mounted on the drone for all flights. Selected altitudes above ground level (AGL) were 100 ft, 200 ft, and 400 ft. AGL selection was chosen based on increments between ground level and legal max flying altitude without a waiver (400 ft AGL). To maximize filter loading for samples at altitude, one filter was used for two flights of the same elevation. As an example, on August 6th, one filter was equipped on the drone for the 200 ft AGL flights. This filter was used for both flights, resulting in a combined sampling time for that elevation. The corresponding ground samples ran at the same time as the air samples with some overlap between battery changes. This resulted in median sampling times of 47 minutes for air and 55 minutes for ground. Number of flights was limited due to power availability to recharge drone batteries. At each site, there were 200 ft AGL flights each day, resulting in twelve 200 ft AGL flights. The first sampling week (August 6th-8th) also included two flights per day at 400 ft AGL, while the second sampling week (August 12th-14th) included two flights per day at 100 ft AGL. This resulted in a total of 36 flights and 36 samples total, air and ground. Flights included reaching the target altitude for that flight, hovering until battery limit warning was reached (15% battery remaining), and subsequent landing. Drone sampling only occurred during the hovering

portion of the flight at the target altitude. Once the drone landed and the ground samplers were off, filters were removed from the samplers and placed into sterile Petri dishes and sealed with Parafilm, working at the decontaminated foiled work surface in the work truck. Samples were placed in a cooler with temperature packs cooled to -0° C.

3.2.4 Sample preparation and transport

Once field work completed for that sampling day, samples were brought back to the USDA-ARS headquarters in Big Spring, Texas. Within a laboratory, samples were handled under aseptic technique. A counter space within the lab was cleaned with 70% isopropanol, followed by DNA away. Then aluminum foil was secured on the surface and similarly cleaned. Filters were then cut using lab scissors cleaned in 70% isopropanol, followed by DNA away and allowed to air dry before cutting. Scissors were cleaned between each filter. Filter halves were stored in Petri dishes wrapped in parafilm, bagged, and placed in 0° C freezers.

After conclusion of fieldwork, samples were placed with a portable cooler that was cleaned with 70% isopropanol and DNA away. Dry ice was then placed in the cooler and transported back to Colorado State University by car. Samples were then stored at -80° C until extraction.

3.2.5 Sample extraction

Before conducting DNA extraction, quality control steps were implemented similar to Chapter Two. Field blanks were obtained each day from each sampler and for each altitude sampled that day. These blanks were extracted and sequenced in the same way as samples to account for sampler, filter, and handling. Extraction controls were also used during the extraction process, with two extraction controls per six samples. These extraction controls were to account for the extraction process and handling and quantify any contamination if present. Finally, negative

controls were added to the amplification step of the next generation sequencing to ensure sample integrity.

DNA extraction follows the protocol as seen in chapter one. DNA was extracted from all filters using the Qiagen DNeasy PowerSoil Pro Kit (Qiagen, Venlo, Netherlands). While originally intended for DNA extraction from soil samples, a modified protocol from Nieto-Caballero et al. (2025) was used for the SASS filters (Nieto-Caballero et al., 2025). All extractions were carried out in a Biosafety cabinet at the CSU Foothills Animal Disease Laboratory. When not in use, the Biosafety Cabinet was sterilized with UV light and cleaned before and after every use with 10% bleach, 70 percent ethanol, and DNA away. All equipment and surfaces were similarly decontaminated before and after use. The modified protocol involved cutting off a quarter of the filter and then cutting it into 6-8 smaller pieces to fit inside the bead-beating tube. A modification from the Marina et al. 2025 protocol was the use of a Tissuelyser instead of a Fast-prep 24. Due to this modification, beads from the Qiagen bead-beating tube had to be transferred to a standard 2 mL sterile tube that fits within the Tissuelyser. After lysis, another modified step involved using a sterile syringe to recover any remaining liquid from the filter material before discarding the filter. DNA extraction was then conducted with the remaining fluid by using the Qiagen DNeasy PowerSoil Pro Kit protocol from the manufacturer (Qiagen, Venlo, Netherlands), starting with step 3. Once extractions were completed, samples were stored at -80^{o}C until ready for sequencing.

3.2.6 Amplicon sequencing

Amplicon sequencing follows the protocol as seen in chapter one. DNA was sequenced for bacteria and archaea community composition and was analyzed by amplifying the V4 region of the 16S rRNA gene following the Earth Microbiome Project protocols. PCR amplification was performed using the updated 515F (Parada et al., 2016) and 806R (Apprill et al., 2015) primer pair

(515F: 5'-GTGYCAGCMGCCGCGGTAA-3'; 806R: 5'-GGACTACNVGGGTWTCTAAT-3'), which includes degeneracy to reduce bias against SAR11 and Thaumarchaeota lineages (Apprill et al., 2015; Parada et al., 2016). The forward primer contained a unique 12-bp Golay barcode to facilitate multiplexing.

Each sample was amplified in one 25-µL reaction and one 50-uL reaction containing 13.0 µL of PCR-grade water, 10.0 µL of 2x Platinum Hot Start PCR Master Mix (ThermoFisher Scientific, Waltham, MA), 0.5 µL (10 µM) of each primer, and 1.0 µL of template DNA, and 26.0 uL of PCR-grade water, 20.0 uL of 2x Platinum Hot Start PCR Master Mix, 1 uL (10 µM) of each primer, and 2.0 uL of template DNA, respectively. Thermal cycling conditions consisted of an initial denaturation at 94°C for 3 min, followed by 35 cycles of 94°C for 45 s, 50°C for 60 s, and 72°C for 90 s, with a final extension at 72°C for 10 min.

Following amplification, reactions were pooled, and the presence of the target band (~300–350 bp) was confirmed via 1.5% agarose gel electrophoresis. Amplicons were quantified by plate using the Quant-iT PicoGreen dsDNA Assay Kit (ThermoFisher Scientific, Waltham, MA), and an equimolar pool was created by combining 240 ng of DNA from each sample. Each plate pool was cleaned using a magnetic bead clean up (AMPure beads, Beckman Coulter Life Sciences, Indianapolis, IN). Sequencing was performed on the Illumina MiSeq platform (Illumina, San Diego, CA). The library was spiked with 15% PhiX control DNA using an Illumina 2x250 kit (Illumina, San Diego, CA), and sequencing was conducted using custom Read 1, Read 2, and Index primers as described by (Caporaso et al., 2012).

While ITS amplicon sequencing and library preparation workflow for fungal communities followed the general framework of the 16S rRNA protocol, several modifications were implemented to address the specific requirements of the ITS1 region. Fungal-specific

amplification was achieved using the ITS1f–ITS2 primer pair (EMP.ITSkabir), with the 12-bp Golay barcode situated on the reverse primer (ITS2) rather than the forward primer (D. P. Smith & Peay, 2014). PCR kinetics were specifically adjusted for this marker, utilizing an annealing temperature of 52°C and an extension step at 68°C for 30 s. Unlike the uniform amplicons produced in 16S sequencing, the resulting ITS1 products exhibited characteristic biological length variation ranging from 250 to 600 bp (Bokulich & Mills, 2013; Hoggard et al., 2018). Furthermore, to stabilize sequencing on the Illumina platform, custom Read 1 and Read 2 sequencing primers were employed with extended 3′ bases (19 bp and 15 bp, respectively) to match the melting temperature of the Illumina adapters, a technical requirement distinct from the standard 16S protocol (Caporaso et al., 2012).

3.2.7 Statistical analysis

The statistical analysis follows similar to chapter one. We conducted all statistical analysis in Qiime 2 (2024.2) and R (4.5.1) (Bolyen et al., 2019; R Core Team, 2025). Packages for data cleaning and statistical analysis included *decontam* (1.28.0), *tidyverse* (2.0.0), and *vegan* (2.7-3) (Davis et al., 2018; Oksanen et al., 2026; Wickham & RStudio, 2023). Packages for visualization included *ggplot2* (4.0.2), *ggpubr* (0.6.3), *ggextra* (0.11.0), *scales* (1.4.0), *cowplot* (1.2.0), and *gridExtra* (2.3) (Attali & Baker, 2025; Auguie & Antonov, 2017; Kassambara et al., 2026; Wickham et al., 2025, 2026; Wilke, 2025).

Amplicon sequence data was processed in *Qiime 2* (2024.2) for both alpha and beta diversity metrics. All samples were rarefied to a depth of 7680 sequences to account for differences in sequences across samples. Alpha diversity metrics for 16S included Faith PD (phylogenetic diversity), Pielou's Evenness (species distribution), Shannon's Entropy (richness and distribution), and Observed features (richness), while alpha diversity for ITS included the same except Faith PD

due to not having a phylogenetic tree. Beta diversity for 16S analyses included Bray-Curtis (presence and abundance), Jaccards (presence/absence), Weighted Unifrac (abundance, phylogenetic), and Unweighted Unifrac (presence, phylogenetic), while ITS reported Jaccards, and Bray-Curtis due to lacking a phylogenetic tree. Diversity analysis included overall Kruskal-Wallis tests and pairwise Wilcoxon comparisons between altitudes, including ground-level, 100ft AGL, 200 ft AGL, and 400 ft AGL. P-values were reported for each diversity metric.

3.3 RESULTS

Results include a Permutational analysis of variance (PERMANOVA) and alpha and beta diversity metrics, including Faith PD, Pielou's Evenness, Shannon Entropy, and Observed Features for Alpha Diversity, and Bray-Curtis, Jaccard, Unweighted Unifrac, and Unifrac for Beta Diversity. Results are also summarized in a heatmap for top 40 genera at ground level and how it varies by altitude.

3.3.1 PERMANOVA

The PERMANOVA results indicated that meteorological variables played a role in the variance of microbial communities, with the R^2 value providing the percentage of variance accounted for by specific variables, but the altitude at which the sample was collected, as well as the site location, contributed the most to variance. For 16S, both altitude and location had p-values < 0.05, while the only meteorological variable of significance was temperature with a p-value of 0.01. Altitude explained the most variance, then location followed by temperature. Results are summarized in Table 3.1. Wind and humidity did play a role in some explanation of the variance, but not to the same extent as altitude, location, and temperature.

The results for ITS are also summarized in Table 3.1. Humidity, altitude, location, and temperature all had p-values < 0.05, with humidity and altitude contributing the most to

understanding variance within the microbial communities. Location and temperature were similar to each other but explained less variance than humidity and altitude. Wind was still important to explain some variance in the microbial communities, but was not as impactful as humidity, altitude, location, or temperature.

Table 3.1: PERMANOVA statistics using Margin effect for both 16S and ITS

Permanova Results for 16S		
Variable	**R^2**	**p-value**
Altitude	0.12	*0.0010
Wind	0.030	0.24
Humidity	0.030	0.081
Temperature	0.040	*0.014
Location	0.085	*0.0010
Permanova Results for ITS		
Variable	**R^2**	**p-value**
Altitude	0.095	*0.020
Wind	0.029	0.094
Humidity	0.097	*0.0030
Temperature	0.050	*0.017
Location	0.059	*0.046

3.3.2 Alpha diversity

The 16S results are presented with boxplots and include Kruskal-Wallis for overall comparisons covering multiple groups and Wilcoxon tests for pairwise comparisons and can be referenced in Figure 3.1. Alpha diversity metrics from the Kruskal-Wallis for Faith PD, Shannon's Entropy, and Observed Features were all significant, with p-values ranging from 0.00026 to 0.00055. This indicated that there was evidence that phylogenetic diversity, richness weighted by distribution, and overall richness were all affected by sampling altitude. Pielou's evenness had a non-significant p-value (0.58), suggesting that there is not enough evidence to show differences in community distribution by altitude.

For the Wilcoxon tests, differences between ground level (designated as 4 ft in the figures) and each altitude (100, 200, and 400 ft), were all significant for Faith PD (0.0062, 0.0065, 0.015), Shannon's Entropy (0.0062, 0.0024, 0.015), and Observed Features (0.0062, 0.0047, 0.015). However, Pielou's Evenness did not have significant p-values for pairwise altitude comparisons. Furthermore, Faith PD, Shannon's Entropy, and Observed Features did not have significant p-values in pairwise comparisons when comparing non-ground level altitudes (100 to 200, 200 to 400, and 100 to 400).

The ITS results follow the same set up as the 16S results, but without phylogenetic metrics and can be referenced in Figure 3.2. For the alpha diversity results, all metrics were nonsignificant except for observed features. The Kruskal-Wallis for observed features had a p-value of 0.0012, and pairwise comparisons for ground-level to different altitudes were significant (p-values of 0.012, 0.041, 0.0097, respectively). Furthermore, comparison between altitudes ranging from 100-400 ft included significant values when comparing 100 ft to 200 ft (p-value = 0.028), and 200 to 400 ft (p-value = 0.028).

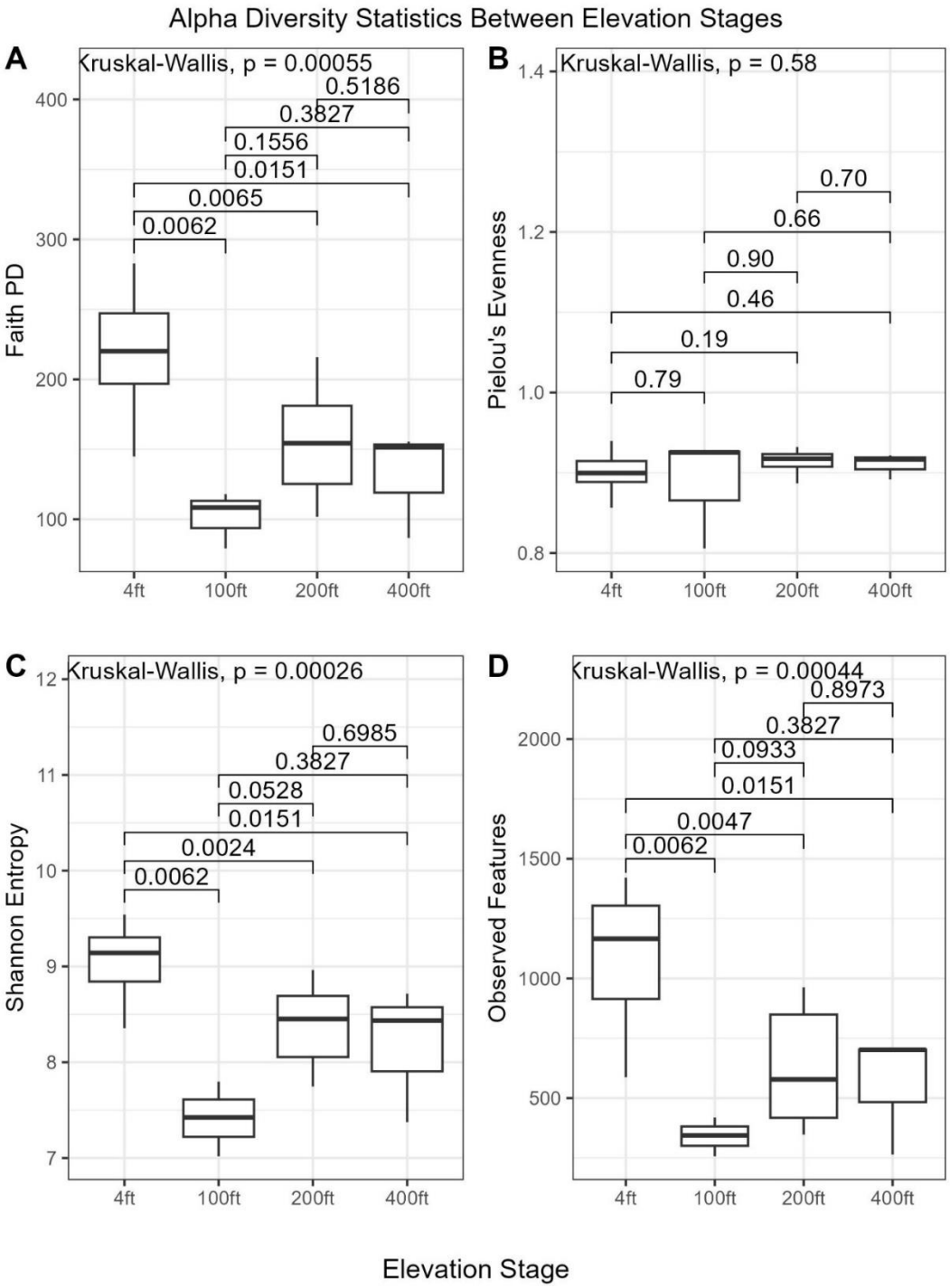

Figure 3.1: Alpha diversity results for 16S, including (A) Faith PD (phylogenetic diversity), (B) Pielou's Evenness (species distribution), (C) Shannon's Entropy (richness and distribution), and (D) Observed Features (richness). All metrics except Pielou's Evenness contained significant Kruskal-wallis p-values, and all altitudes as compared to ground-level (4ft) also included significant p-values. Comparisons between altitudes between 100-400 ft did not contain significant p-values.

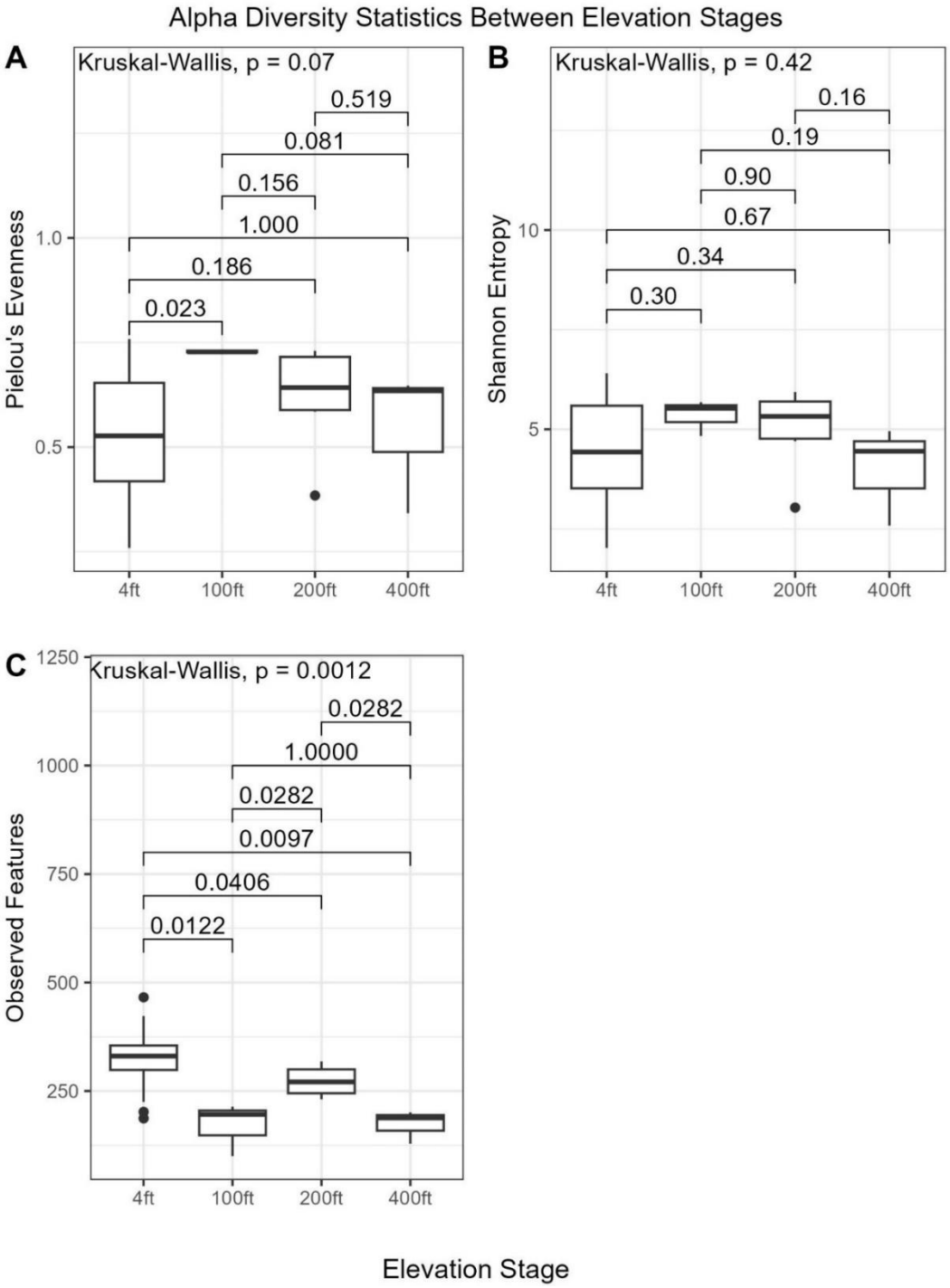

Figure 3.2: Alpha diversity results for ITS, including (A) Pielou's Evenness (species distribution), (B) Shannon's Entropy (richness and distribution), and (C) Observed Features (richness). There were no significant p-values for Kruskal-wallis tests, and only Observed Features had significant Wilcoxon p-values. All altitudes as compared to ground-level (4ft) included significant p-values. Altitude pairwise comparisons of 100 and 200 ft, as well as 200 and 400 ft, also had significant p-values.

3.3.3 Beta diversity

To evaluate the influence of altitude on 16S microbial community composition, we performed Principal Coordinates Analysis (PCoA) using four beta-diversity metrics (Figure 3.3). PERMANOVA analysis (as also seen in Table 3.1) revealed that altitude was a significant driver of community structure across all metrics tested ($p < 0.01$ in all metrics).

Variation in abundance-weighted community composition (Bray-Curtis; Fig 3.3A) and presence-absence patterns (Jaccard; Fig 3.3B) were significantly explained by altitude ($R^2 = 0.125$ and $R^2 = 0.109$, respectively). Incorporating phylogenetic information further confirmed these trends, with altitude having an $R^2 = 0.124$ in unweighted UniFrac (Fig 3.3C) and altitude having an $R^2 = 0.145$ in weighted UniFrac distances (Fig 3.3D).

The samples from 4ft (green) exhibited distinct clustering from the higher samples (100ft, 200ft, and 400ft), particularly along the first principal coordinate (PCoA1), which accounted for 21.9% of the variation in the weighted UniFrac model. While the higher samples showed higher degrees of overlap, the distinct positioning of the ground-level samples suggests a unique microbial signature at the ground-level as compared to the higher altitudes.

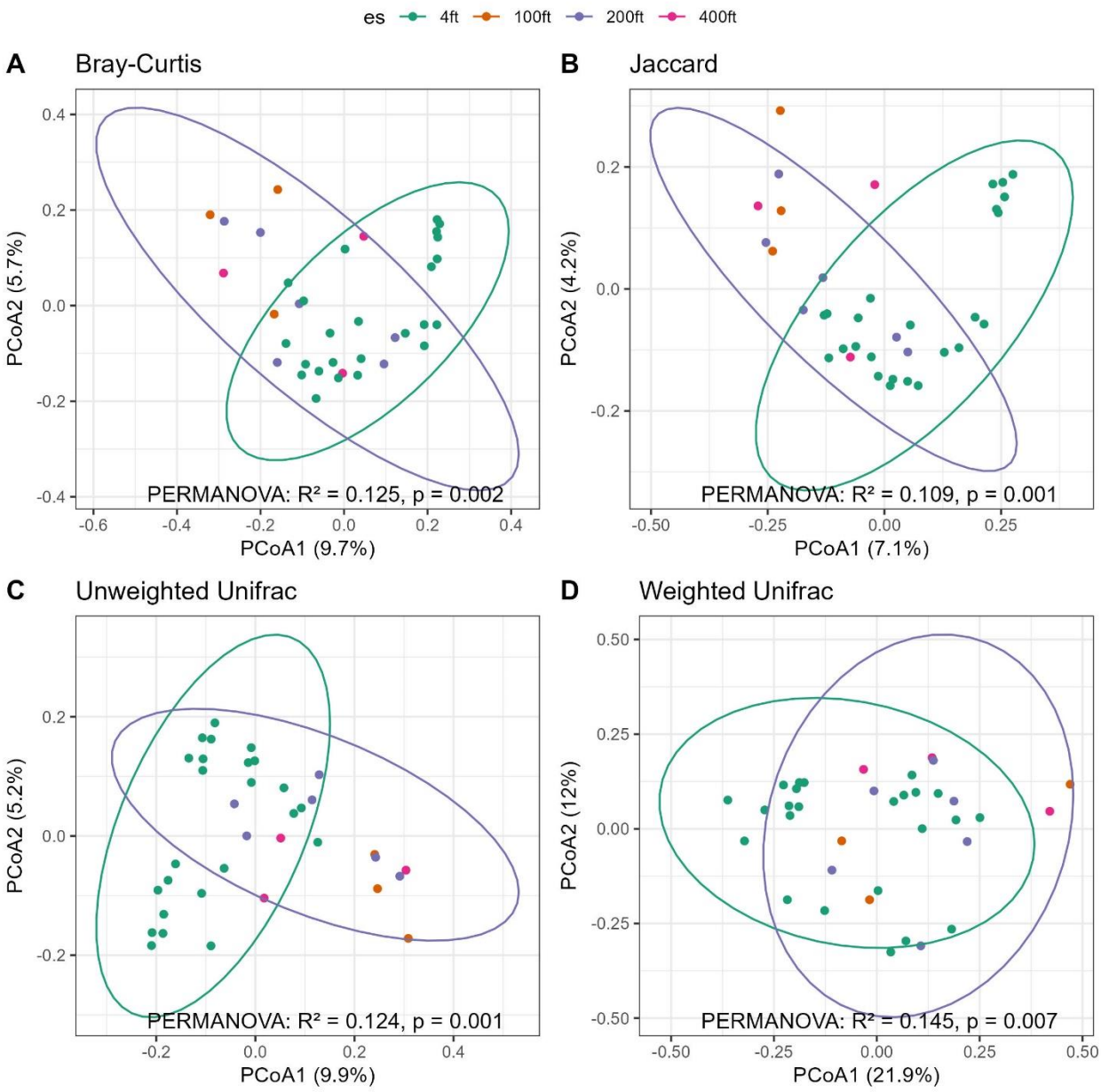

Figure 3.3: Beta diversity of 16S microbial communities across sampled altitudes. PCoA plots are based on (A) Bray-Curtis, (B) Jaccard, (C) Unweighted UniFrac, and (D) Weighted UniFrac distances. Samples are color-coded by altitude (4ft, 100ft, 200ft, and 400ft), and ellipses represent 95% confidence intervals. Statistical significance and the proportion of variance explained by altitude were determined via PERMANOVA.

Beta diversity analysis for ITS via PCoA revealed that altitude was still significantly influencing the fungal microbial community, although with more variation depending on the metric used (Figure 3.4). Altitude influence in abundance-weighted community composition (Bray-Curtis; Fig 3.4A) and presence-absence patterns (Jaccard; Fig 3.4B) were significantly

explained by altitude (R^2 = 0.154 and R^2 = 0.093, respectively). However, while the Bray-Curtis metric (Fig 3.4A) captured substantial 46.5% of the variance along the first principal coordinate, the clustering by altitude was less noticeable. This trend continued with the Jaccard's metric (Figure 3.4B). While still being statistically significant (p-value = 0.009), the 95% confidence ellipses also included significant overlap. This could suggest that while the altitude does play a role, differences in abundance of present species could be driving the changes seen in the Bray-Curtis metric (Figure 3.4A).

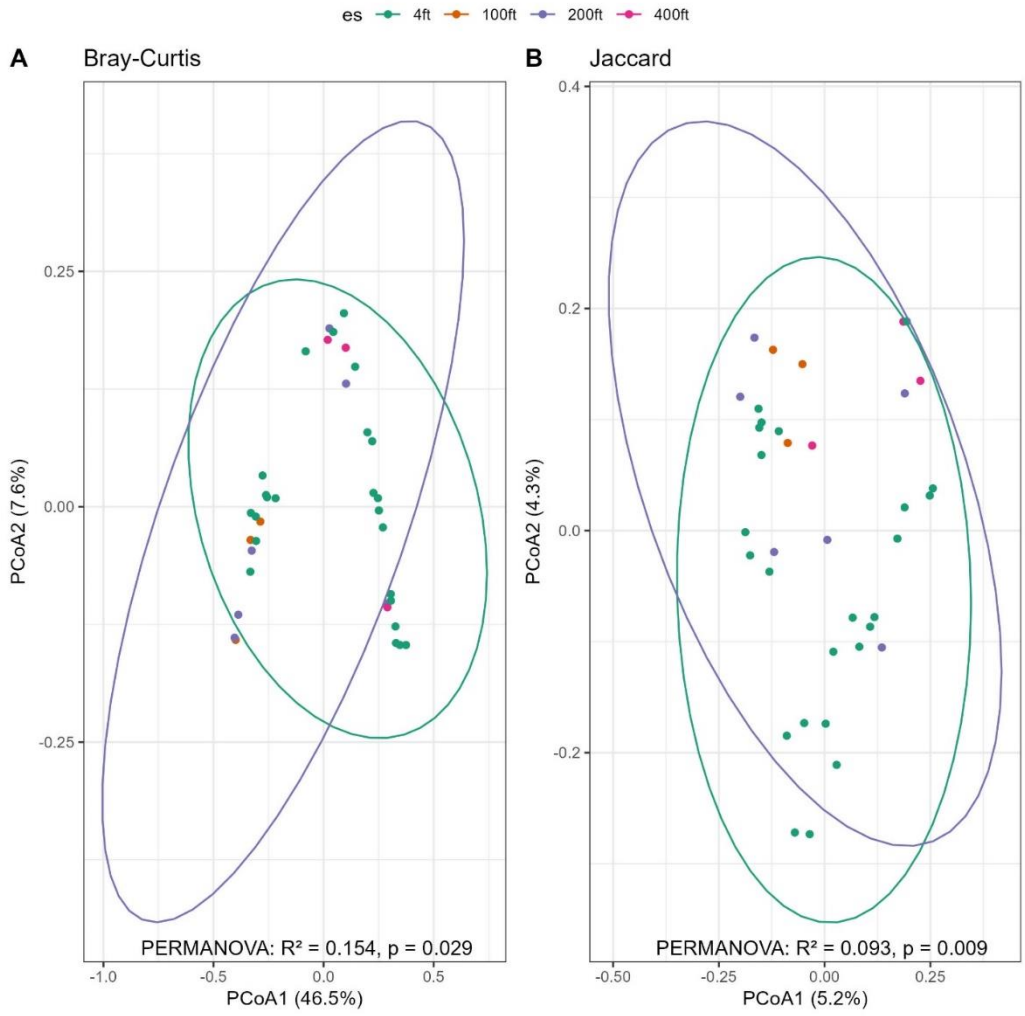

Figure 3.4: Beta diversity of ITS microbial communities across sampled altitudes. PCoA plots are based on (A) Bray-Curtis and (B) Jaccard. Samples are color-coded by altitude (4ft, 100ft, 200ft, and 400ft), and ellipses represent 95% confidence intervals. Statistical significance and the proportion of variance explained by altitude were determined via PERMANOVA.

3.3.4 Heatmaps

To evaluate the influence of altitude on 16S microbial communities, we calculated the $\log_2$ fold change in variance for identified genera at 100ft, 200ft, and 400ft relative to the ground-level baseline (4ft) (Figure 3.5). Hierarchical clustering revealed distinct patterns of taxonomic stratification, suggesting that atmospheric microbial composition is sensitive to vertical displacement from the terrestrial source.

Several genera exhibited a significant increase in variance at lower altitudes (100ft and 200ft) followed by a sharp decline at the highest sampling point. Genera within this category showed strong positive $\log_2$ fold changes (>2.0) at 100ft compared to the ground before transitioning to a negative $\log_2$ fold changes as altitude increased to 400ft. This includes the human pathogen *Legionella*, which is the causative agent of Legionnaires' disease, and the genus *Spiroplasma*, which contains arthropod endosymbionts and phytopathogens responsible for agricultural diseases such as citrus stubborn disease and corn stunt disease. The remaining members of this cluster comprise non-pathogenic environmental isolates, specifically the soil and aquatic bacterium *Sphingopyxis* and the marine-associated genus *Hahella*.

Conversely, a cluster of genera demonstrated an inverse relationship with altitude, showing depletion at 100ft but significant enrichment at 400ft. Taxa within this group included *Atopococcus*, *Chthonomonas*, *Aneurinibacillus*, and *Kibdelosporangium*. Notably, *Brevundimonas*, *Enterococcus*, and *Oligoflexus* exhibited the most extreme stratification; these genera were strongly underrepresented at 100ft (Log_2 fold change approximately -4.0) but transitioned to positive variance at the 400ft mark. This shift suggests the presence of a high-altitude microbial niche or long-range transport mechanisms that differ from local ground-level emissions. Functionally, this group includes the human and animal opportunistic pathogens

Enterococcus and *Brevundimonas*, alongside environmental spore-forming lineages characterized by endospore formation or complex filamentous structures, such as *Aneurinibacillus* and *Kibdelosporangium*. This cohort is completed by environmental isolates, including the animal-associated *Atopococcus*, the thermophilic environmental group *Chthonomonas*, and *Oligoflexus*.

A third group of microorganisms displayed a unique middle-ground type profile. These genera were significantly depleted at both the 100ft and 400ft levels but showed near-neutral or slightly positive variance at 200ft. This cohort was strictly defined by *Cystobacter*, *Melittangium*, and *Larkinella*, all of which are categorized as environmental, non-pathogenic organisms.

A final group of microorganisms maintained relatively stable, consistent variance across the 100ft and 200ft altitudes before undergoing a directional shift at the 400ft boundary. This pattern was exemplified by *Arthrobacter* and *Nitrosospira*. The 400ft sampling level served as the point of maximum variance divergence for the majority of the surveyed microbial community, yielding the most extreme positive or negative log2 fold change values recorded across the vertical profile. Biologically, this transitional cohort includes *Nitrosospira*, a genus of ammonia-oxidizing soil, and *Arthrobacter*, a globally distributed soil bacterium genus characterized by high metabolic

versatility and structural resistance to environmental starvation and desiccation, with rare strains documented as opportunistic pathogens.

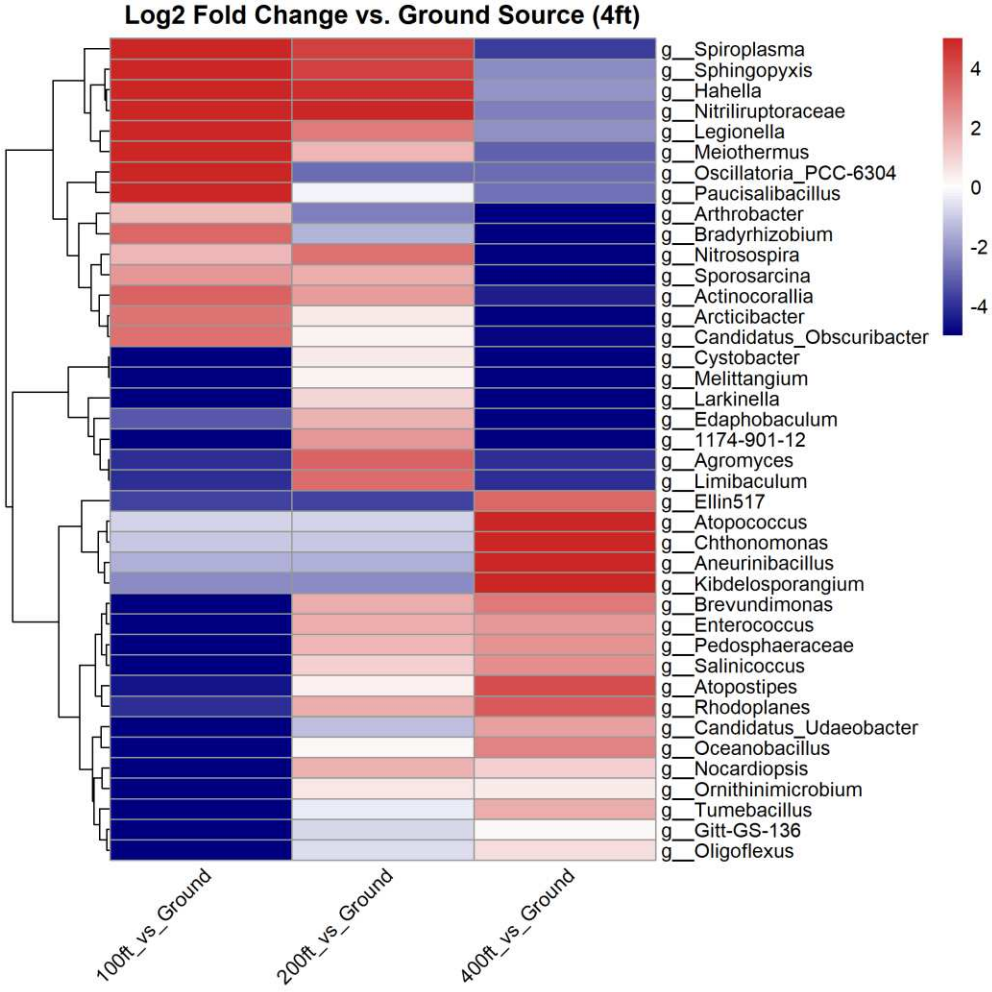

Figure 3.5: This figure shows Log 2-fold change in variance between 16S ground-level sampling (4 ft), and each altitude sampled (100, 200, and 400 ft). The red color indicates that this genus was enriched as compared to ground-level, the blue color indicates that this genus was depleted as compared to ground-level, and white indicates no real change. The dendrogram on the left used hierarchical clustering to identify patterns of distribution.

The same analysis was conducted for ITS microbial communities, looking at $\log_2$ fold change in variance for identified genera at 100ft, 200ft, and 400ft relative to the ground-level baseline (4ft) (Figure 3.6). Hierarchical clustering of $\log_2$ fold changes identified four primary patterns of distribution across the 100ft, 200ft, and 400ft sampling intervals.

A group of fungal genera exhibited maximum variance at the 100ft level, followed by a steady decline as altitude increased. The $\log_2$ fold change was strongly positive (>3.0) at 100ft but transitioned to neutral or negative values at 400ft. This group includes *Thanatephorus,* an agricultural pathogen responsible for root rot and damping-off in crops, and *Neophaeococcomyces*, a melanized black yeast recognized as an opportunistic subcutaneous tissue pathogen of humans. The remaining members of this cluster comprise non-pathogenic environmental isolates.

The 200ft altitude served as a peak variance point for a specific subset of the sampled fungal community, including *Blastobotrys*, *Myriangium*, and unidentified members of the orders Polyporales, Onygenales, and Hericiaceae. These taxa displayed strong negative variance at 100ft but significant positive enrichment at the 200ft tier. Biologically, this mid-altitude group includes *Blastobotrys*, an emerging opportunistic human yeast pathogen clinically notable for causing ear, eye, and respiratory tract infections and showing low susceptibility to standard azole antifungals. It also features *Myriangium*, an entomopathogenic genus that acts as a specialist parasite targeting scale insects on plant bark. The remainder of this cluster consists of environmental macrofungal and mold lineages.

At the 400ft threshold, a shift in fungal community composition occurred, with *Deniquelata*, *Solicoccozyma*, and *Ceriporia* exhibiting their highest positive log2 fold changes at this level. Concurrently, *Strelitziana* showed a pattern of progressive enrichment, with variance increasing linearly from 100ft to 400ft. This high-altitude group includes established agricultural plant pathogens, specifically *Strelitziana*, which causes "sooty blotch" disease on the skin of commercial fruit crops, and *Deniquelata*, a dark-spored genus documented to cause zonate leaf spots on tropical plant foliage. The remaining taxa are non-pathogenic environmental organisms.

In contrast to the higher altitude groups, a substantial number of fungal genera were significantly depleted at all sampled altitudes compared to the 4ft ground source. This ground-level group maintained negative log2 fold changes between -2.0 and -4.0 across the 100ft, 200ft, and 400ft thresholds and includes *Fusarium*, *Agaricus*, *Rhodosporidiobolus*, and *Stachybotrys*. Functionally, this highly depleted group includes severe plant and human pathogens. *Fusarium* is a global agricultural threat causing vascular wilt and head blight in crops while producing hazardous food-contaminating mycotoxins and acting as an opportunistic human tissue pathogen. *Stachybotrys* is a toxic mold that produces macrocyclic trichothecene mycotoxins responsible for severe respiratory inflammation and toxicoses in humans and animals. *Rhodosporidiobolus* is an emerging, hyper-virulent human yeast pathogen known to cause fatal fungemia and develop pan-drug resistance when incubated at human body temperature. Lastly, *Agaricus* serves as a non-pathogenic environmental organism.

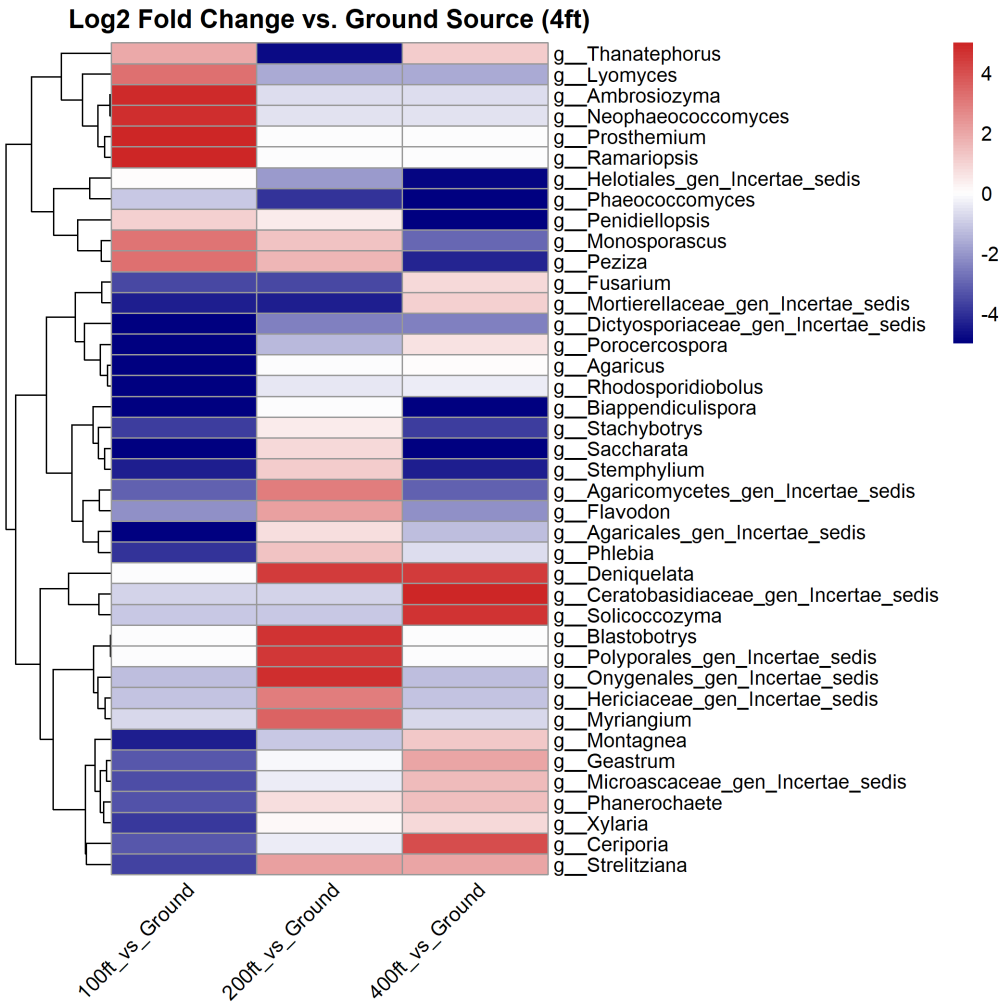

Figure 3.6: This figure shows Log 2-fold change in variance between ITS ground-level sampling (4 ft), and each altitude sampled (100, 200, and 400 ft). The red color indicates that this genus was enriched as compared to ground-level, the blue color indicates that this genus was depleted as compared to ground-level, and white indicates no real change. The dendrogram on the left used hierarchical clustering to identify patterns of distribution.

3.4 Conclusions

Airborne transport of microbes and microbial communities is a significant topic for human, animal, and environment health. This intersection of multiple groups results in a considerable One Health consideration, where long range transport of microbes and other particulates can impact different systems and result in disease. As such, there has been considerable work to quantify and describe both what matter and life exists in the air, as well as how this matter and life move in the

PBL and upper layers of the atmosphere. However, while there has been extensive research studying microbes, microbial communities, and the transport of microbes and microbial communities, the impacts and implications of airborne microbial transport for One Health remain relatively understudied. Our goal is to demonstrate how a system can be developed, deployed, and utilized to perform real time surveillance and convey important transport and potential exposure information to public health officials concerned with human, animal, and plant health. The information can then be disseminated to potentially exposed populations, industries, and communities. This would link surveillance with public knowledge and inform health practitioners to be aware of potential impacts on the communities they serve.

Our findings indicate that samples sequenced under 16S conditions for bacteria and archaea as well as samples sequenced under ITS conditions for fungal organisms did stratify by altitude at which samples were collected. Not only were there differences between samples collected at ground-level versus samples collected at altitude (100-400ft) for alpha and beta diversity metrics (Figures 1-4), but different genera were increased as compared to ground-level at different elevations (Figure 5-6). For example, the genus *Legionella,* a genera known to be a human pathogen, was enriched at 100 and 200 ft as compared to ground-level but was depleted at 400 ft (Figure 5). The enrichment at 100 and 200 ft suggests that it is being lofted but is not resilient enough to go higher in our samples. Additionally, the genera *Fusarium*, with some species implicated in crop diseases as discussed in the introduction, was detected in our ITS samples, with faint enrichment at 400 ft compared to ground level (Figure 6). This suggests that we were successful in sampling the air microbiome and maintaining distinct stratification between desired altitudes.

Our findings align well with previous work focused on characterization of the air microbiome (Kellogg et al., 2004; Song et al., 2020). Additionally, the use of the drone as an air sampling platform aligns with previous work demonstrating the use of drones and their capabilities to collect data in the air microbiome (Bangay et al., 2026; Crazzolara et al., 2019; Radosevich et al., 2025; Vélez-Rodríguez et al., 2020). Our findings include several genera that have implications for human, animal, and agricultural health, such as known human pathogens like *Legionella*, and *Enterococcus* within the 16S samples and *Fusarium* in the ITS samples. Additionally, there is an unidentified *Onygenales* within the ITS sample, which could have relation to pathogens of human concern such as *Coccidioides immitis* and *C. posadasii*. These genera add to the discussion of the health implications, especially within a One Health context (Bangay et al., 2026; Bowers et al., 2019; Brodsky et al., 2023; Crazzolara et al., 2019; Triadó-Margarit et al., 2022; Vélez-Rodríguez et al., 2020). However, it is worth noting that our findings did not align with Smith et al. 2018, which demonstrated a more homogeneous mixing of 16S sequenced samples (D. J. Smith et al., 2018). Though, Smith et al. 2018 noted that this could be due to contamination of hardware used for sampling, a significant engineering hurdle in their study (D. J. Smith et al., 2018). As such, our ability to remotely control our air sampler allowed us to accurately activate the sampler at the desired altitude, making our observations more specific to certain elevations above ground level. This could have led to stronger separations within the samples. However, it is worth noting that the up and down motion of the drone itself could have induced our own contamination as well, combined with the propeller wash upon landing, even with the sampler turned off. Furthermore, Bluetooth lost connection on two out of the 24 flights. This could have also led to contamination as drone position was adjusted to require the signal during those flights while the sampler was running. However, the sampler, in general, was able to collect at precise elevations.

Our work suggests that air sampling with a drone-mounted air sampler can provide genus level information within the PBL. This information could assist in surveillance and early warning systems for pathogens of human, animal, and agricultural concern. Future work, especially for One Health and public health surveillance, should attempt to use more specific and cost-effective methods for microbial detection and quantification in combination with drone and drone-mounted air sampling. For public health surveillance in specific areas or looking for specific pathogens, qPCR and tools like the CocciEnv qPCR assay could provide pathogen specific detection in a cost effective and efficient manner (Bowers et al., 2019; Radosevich et al., 2025). Otherwise, amplicon sequencing with low-biomass air samples can still provide results at reasonable cost and identification at the genus level, with the potential for some species level identification (Chen et al., 2020; Damerum et al., 2023; King et al., 2024; Song et al., 2020). This would provide quick surveillance for public health, and, if used routinely, could be used as an early detection system for potential pathogens that could disrupt human, animal, or environment (such as agriculture or forest) health.

Strengths of our work include the use of a validated drone and sampler method (Chapter Two), demonstrating that the lightweight sampler we are using is comparable with the ground sampler (Full SASS). This allowed for longer flight times and therefore more volume sampled, improving the amount of air and potentially increasing the amount of microbes collected. Another strength was the use of paired ground samples with each flight, creating a baseline to compare all samples at altitude against.

A limitation of our study was not conducting each airborne altitude (100-400 ft) in triplicate at each site during that sampling day. While each airborne altitude was collected in triplicate across the study period of six days, only altitude was in triplicate while day and site changed. This could

lead to unrealized relationships in the data or introduction of error. As a result, microbial communities at altitude might have reduced accuracy at each site due to not having enough replicate per site per altitude. This could miss the stochastic nature of the air microbiome. Additionally, at the field site, we did not have access to a -20°C or -80°C freezer for storage, relying on a 0°C freezer instead. While this gave us some preserving capabilities, it did not adhere to accepted long term storage expectations and could lead to premature degradation of samples, introducing missed taxa information and error.

In conclusion, our work managed to detect differences in microbial communities using a drone-mounted air sampler and stratifying by altitudes of ground-level (4ft), 100ft, 200ft, and 400ft. Furthermore, there were several genera of pathogenic interest, especially from a One Health perspective, that could have implications for human, animal, and environment (agriculture, forest) health. Examples of genera of interest included *Enterococcus*, *Legionella*, *Fusarium*. This lends importance to the demonstration that the implementation of real time airborne surveillance could be beneficial for public health services, public awareness, and health provider preparedness. Future work should increase sample sizes and use either more specifically targeted tests for certain pathogens, or species level next generation sequencing to promote the idea of cost effective and efficient implementation for public health capacities in the face of One Health challenges.

3.5 ACKNOWLEDGEMENTS

We gratefully acknowledge support from the NSF Biology Integration Institutes Program under Award # 2120117. We thank the CSU One Health Institute for contributions to and support of BROADN research.

We would also like to thank the Colorado State University Drone Center for providing expertise and support during this project, especially around the development and implementation of the sampler mounting systems.

CHAPTER 4

A ONE HEALTH APPROACH TO MODEL *COCCIDIOIDES* SPECIES HABITAT IN ARIZONA[4]

4.1 INTRODUCTION

Coccidioidomycosis, or Valley Fever, is a respiratory fungal disease prevalent in the Southwestern United States, parts of Southeastern Washington, Mexico, and parts of Central and South America (Chow et al., 2021; Donovan et al., 2019; M. E. Gorris et al., 2018). The etiological agents of Valley Fever are *Coccidioides immitis* and *Coccidioides posadasii* (Chow et al., 2021; Donovan et al., 2019; M. E. Gorris et al., 2018). Both *C. immitis* and *C. posadasii* cause identical disease but can have different geospatial ranges and differ genetically (Donovan et al., 2019; Mead et al., 2022). Valley Fever infection occurs when a susceptible host inhales Coccidioides arthroconidia, the spore form of *Coccidioides*. Only 40 percent of human cases develop symptoms, with the other 60 percent remaining asymptomatic (Donovan et al., 2019). When symptomatic, patients develop flu-like symptoms, with more serious forms of the disease developing respiratory complications (Donovan et al., 2019). Serious but rare forms of the disease can include fungal meningitis, which is fatal without supportive care (Donovan et al., 2019). Similarly, canines, (i.e., dogs), are also susceptible to Valley Fever. Canines develop similar disease as humans, presenting with pneumonia or flu-like symptoms (Sykes et al., 2025). Furthermore, canines are thought to be at higher risk of exposure due to activities such as digging and sniffing the ground (Sykes et al., 2025).

[4] Adapted from a manuscript in preparation: Kessinger, P., Bosco-Lauth, A. M., Magzamen, S., et al. (in prep): A One Health Approach to Model *Coccidioides* Species Habitat in Arizona.

Coccidioides spp. surveillance is a major challenge, with environmental matrix sampling unreliable in isolating *Coccidioides spp.* presence, even in endemic areas (Morgan E. Gorris et al., 2019; Weaver et al., 2020). Surveillance for *Coccidioides spp.* is also challenged due to its transmission cycle. The lack of a vector or clear animal interaction leads to the environment and climate variables being the primary drivers of exposure (Mead et al., 2022). Environmental factors such as increased temperatures and drier climates can facilitate an expansion of *Coccidioides* and further increase the amount of Valley Fever cases (M. E. Gorris et al., 2018; Li et al., 2025; Meisner et al., 2019; Weaver et al., 2020). Changing environmental dynamics can bring more immunologically naïve populations into contact with this pathogen and increase the present healthcare burden. Following, for prevention and treatment, it is necessary to expand the understanding of what in the environment promotes not only growth, but movement of *Coccidioides spp.* and therefore subsequent exposure of host populations to aerosolized arthroconidia, or spores.

While still important to overall surveillance, the low effectiveness of environmental sampling and lack of a vector leaves a major gap in understanding exposure risk. The unique infection dynamics of Valley Fever results in researchers developing methods to simultaneously model both the disease, Valley Fever, and the pathogen, *Coccidioides spp.* with limited data. Human Valley Fever incident cases have traditionally been the primary source of data for public health predictive modeling and research but could potentially discount environmental and ecological drivers of *Coccidioides spp.* and Valley Fever (Morgan E. Gorris et al., 2019; Shubitz et al., 2005; Sykes et al., 2025; Weaver et al., 2020). This is especially pertinent when trying to model *Coccidioides spp.* presence instead of Valley Fever due to the long incubation period of

Valley Fever and the movement of human populations, resulting in spatial and temporal misalignment of disease reporting locations versus actual area of exposure.

Canines may be of use for improved data resolution. Canines are vulnerable to similar disease as humans when infected with Valley Fever (Butkiewicz et al., 2025; Sykes et al., 2025). Canines are also prevalent in human homes and local activities, resulting in canines having similar exposures as humans (Butkiewicz et al., 2025; Shubitz et al., 2005; Sykes et al., 2025). The combination of similar disease status, living situations, and exposures, makes canines ideal sentinels for Valley Fever. Furthermore, a benefit to using canine cases is that canines do not travel as extensively as humans, with canines being more likely to be exposed when within their local area (Sykes et al., 2025). This makes reporting disease by location of residence or veterinarian less likely to incur as much bias as human cases, while maintaining generalizability to humans through activities that mimic high risk human exposure as well as mirroring day-to-day human travel.

Our goal for this analysis is to demonstrate that the use of Valley Fever case data, both human case data from the Arizona Department of Health Services and simulated canine cases, can be used as proxy locations for *Coccidioides spp.* presence in lieu of collection of environmental samples. While some analyses directly collect soil samples to confirm habitat suitability for *Coccidioides*, we used a blended model of reported human cases, simulated animal sentinel cases, and secondary data on meteorological and ecological conditions to combine human and animal sentinel cases to create a surface of habitat suitability for *Coccidioides spp.* This resulted in a combined aim of using characterized Valley Fever cases (canine and human) to create a One Health database with environmental predictors that are hypothesized to drive *Coccidioides spp.* growth and spread. Once created, this database was then used to predict suitable habitat for

Coccidioides spp. in Arizona to demonstrate that a combined modeling approach can use Valley Fever case data as a proxy for presence points of *Coccidioides spp.* and model areas that could increase an individual's exposure to *Coccidioides spp*. This could then indicate an increase in an individual's risk of developing Valley Fever. This modeling framework, trained and developed in endemic areas, can then be applied to other regions that do not have required reporting or are new to reporting Coccidioidomycosis cases, and allow researchers to target predicted areas to see if *Coccidioides spp.* are becoming endemic to new regions.

4.2 METHODS

4.2.1 Study area

The study area for our data is the state of Arizona in the United States. Twenty years of Valley Fever case data from 2004-2023 were available from the Arizona Department of Health Services. *Coccidioides spp.* are highly endemic in the state of Arizona, allowing for comparison of our work to known data and literature on *Coccidioides* presence in the state.

4.2.1.1 Study population

Our study populations are human Valley Fever cases in Arizona from 2004-2023 and simulated Valley Fever cases in canines. Human Valley Fever cases were defined and reported according to the Council of State and Territorial Epidemiologists' laboratory case definition (Sophia E. Kruger et al., 2026). Laboratory evidence for *Coccidioides spp*. was stratified into confirmatory and presumptive categories. Confirmatory evidence was defined as the isolation of *Coccidioides* spp. via culture, histopathological or cytopathological identification in clinical specimens, or detection via validated molecular assays including polymerase chain reaction (PCR) and matrix-assisted laser desorption ionization-time of flight (MALDI-TOF). Serological confirmation included the presence of coccidioidal antibodies in cerebrospinal fluid (CSF) or

specific serum markers, such as positive immunodiffusion, tube precipitin, concurrent IgM and IgG detection via enzyme immunoassay (EIA), or complement fixation (CF) titers >1:2. Presumptive evidence comprised CF titers of 1:2, lateral flow assays, latex agglutination, isolated IgM or IgG detection by EIA, or the detection of *Coccidioides* antigen in body fluids ("Coccidioidomycosis / Valley Fever (Coccidioides spp.) 2023 Case Definition | CDC," 2024). Human cases were geocoded to the census tract level. In addition to the human Valley Fever cases, modeled Valley Fever canine cases are by year from 2004-2023. There is no mandatory reporting for canine Valley Fever cases in Arizona; as such, we created a simulated state-wide canine population for this analysis. These simulated canine cases were modeled using Decennial census data from 2000-2020, American Veterinary Medical Association (AVMA) survey data, and serologic prevalence in canines from Sykes et al. 2025("FINAL_AVMA_PetDemographics102218-compressed.pdf," n.d.; Rowan, 2018; Sykes et al., 2025).

In addition to case data, population density data was downloaded from the Gridded Population of the World v4 dataset (GPWv4), at intervals of 2005, 2010, 2015, and 2020("Gridded Population of the World, Version 4 (GPWv4)," n.d.). Population density data served as a denominator to account for sampling bias due to clustered case reports by location of residence that was most likely not representative of actual exposure location.

4.2.2 Environmental Data

Environmental and meteorological data was selected using previous peer-reviewed literature that demonstrated association with *Coccidioides spp.* presence. Data source, variable, and resolution are recorded in Table 4.1. This included environmental and meteorological data from the North American Land Data Assimilation System phase 2 (NLDAS-2), the International

Soil Reference and Information Centre (ISRIC), and land cover from the Multi-Resolution Land Characteristics Consortium (MRLC)(Cosgrove et al., 2003; "ISRIC — World Soil Information," n.d.; Jeffery et al., 2014; Mitchell et al., 2004; Xia et al., 2012). NLDAS-2 included both the FORA125 model for atmospheric drivers, such surface air temperature, and NOAH125 model for terrestrial hydrological variables, such as soil moisture. ISRIC data included soil fractional composition as well as pH content and MRLC included categorical land cover types.

Table 4.1: List of Predictors Used along with the original resolutions

Data Source	Variable	Resolution	Reference
NLDAS-2	Soil Moisture at 0-10cm (kg m^{-2})	0.125x0.125 degrees	(Li et al., 2025)
	Soil Temperature at 0-10cm (°C)	0.125x0.125 degrees	(Li et al., 2025)
	Surface Air temperature 2 m above ground level (°C)	0.125x0.125 degrees	(Meisner et al., 2019)
	Surface Specific Humidity 2 m above ground level (kg kg^{-1})	0.125x0.125 degrees	(Fisher et al., 2007)
	Wind speed from zonal 10 m above ground level (m s^{-1})	0.125x0.125 degrees	(Li et al., 2025)
	Wind speed from Meridional 10 m above ground level (m s^{-1})	0.125x0.125 degrees	(Li et al., 2025)
ISRIC	Mean Sand content 5-15cm (%)	250 meters	(Meisner et al., 2019)
	Mean silt content 5-15cm (%)	250 meters	(Meisner et al., 2019)
	Mean clay content 5-15cm (%)	250 meters	(Meisner et al., 2019)
	Mean soc content 5-15cm (%)	250 meters	(Meisner et al., 2019)
	Mean phh2o content 5-15cm (0-14)	250 meters	(Meisner et al., 2019)
MRLC	Land Cover Types	30x30 meters	(Weaver et al., 2020)
GPWv4	Human Population Density	30 arc-second resolution	(Barber et al., 2022)

4.2.3 Data workflow and management

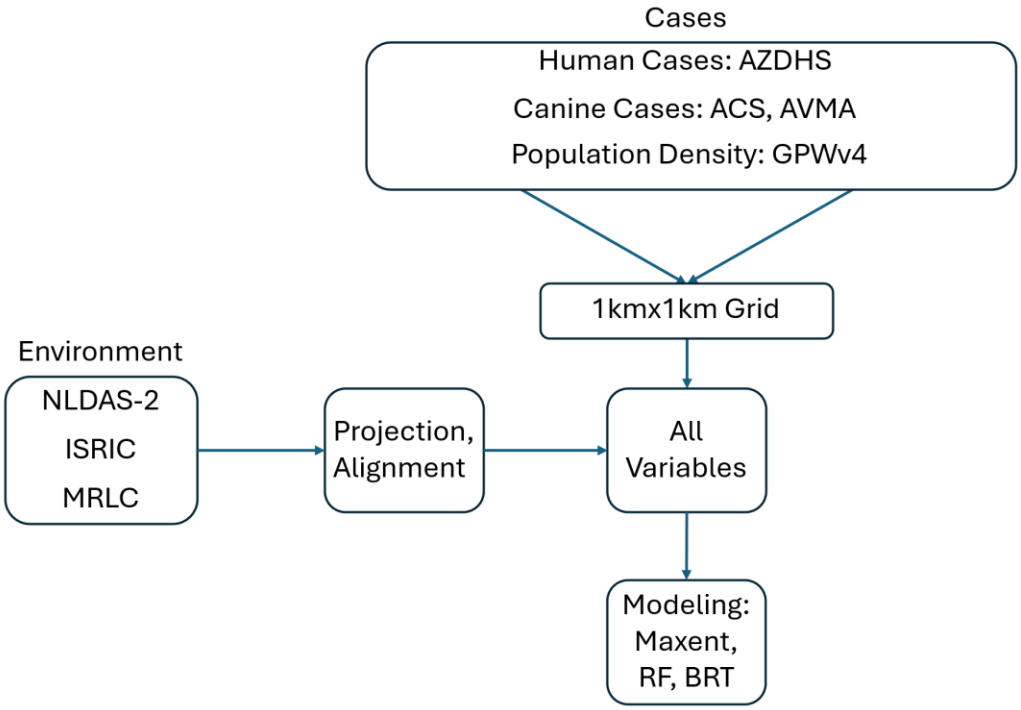

Figure 4.1: Data workflow to prepare for Modeling. Environmental data was source from NLDAS-2, ISRIC, and MRLC. Human cases were sourced from the Arizona Department of Health Services, while canine cases were simulated from American Community survey housing data and American Veterinary Medical Association pet ownership survey data.

Human data were read in first via housing totals per census tract via the United States Census for Decennial surveys via tidycensus (version 1.7.5) in R (version 4.5.1)("R: The R Project for Statistical Computing," n.d.; Walker et al., 2026). Housing totals were used to allow for approximation of canine populations, which utilized number of households to estimate canine population. The census data provided the shapefiles necessary to join the human Valley Fever cases to each census tract. Due to the timeframe, three shapefiles were downloaded to match census tracts in the Arizona during the study period: Decennial census 2000, 2010, and 2020. Valley Fever cases from 2004-2009 were joined to the Decennial shapefile from 2000, 2010-2019 cases joined to the Decennial shapefile 2010, and Valley Fever cases from 2020-2023 joined to the shapefile

from Decennial census 2020. Cases were matched to the appropriate census tract during the appropriate year.

Canine population estimate, as well as canine Valley Fever case estimates, were based on an AVMA survey data as well as total households per census tract in Arizona. The AVMA survey had canine percentage for Arizona by household at 43%, as well as average canines per household at 1.8 (Rowan, 2018). Furthermore, the AVMA has a scaling formula for canine count: 0.8857*year-1709.9. This formula, in combination with a baseline of 65 million canines, the average canines per household of 1.8, and the Arizona households with canines percentage of 43%, allowed for the estimation of canines per census tract per year. This value was then multiplied by the probability of serologic prevalence in canines from Sykes et al. 2025. Overall serologic prevalence of Valley Fever in canines was reported out as 37.6 percent (Sykes et al., 2025). Therefore, estimated canine counts were multiplied by 0.376 to result in estimated canine Valley Fever cases per year per census tract in Arizona.

To more accurately portray variables such as land cover type beyond proportions per census tract, cases were interpolated to a 1km X 1km grid for both humans and canines in Albers Equal Area (EPSG: 5070) using a combination of sf (version 1.1-0) and terra (version 1.9-1) packages in R (Hijmans et al., 2026; Pebesma et al., 2026).

After cases were interpolated on a 1 km X by 1 km grid, all NLDAS, ISRIC, MRLC, and GPWv4 data were aligned and joined to the case cells. The Terra package in R was used to align the environmental, land cover, and population density rasters to the case grids. Each variable was then joined to form annual spatial datasets from 2004-2023.

After the formation of the annual spatial datasets, cases (human and canine), population density, NLDAS, ISRIC, and MRLC data were extracted by year to form point data for presence

and absences. Presences were separated from absences to create presence dataframes for Maximum Entropy modeling by taking any cases of 0.5 or greater and labeling them as a binary 1 for presence. To correct spatial autocorrelation and clustering, cases were also thinned from 1 km to 10 km between unique presence points.

4.2.4 Variable selection

Using a combination of biological plausibility and correlation matrices from corrplot in R (version 0.95), variables were thinned from the original stack to a non-correlated group (Wei et al., 2024). Values of greater than the absolute value of 0.75 were removed from the modeling formula, with preference of variable selection driven by literature and biological plausibility for variables that influenced *Coccidioides spp.* growth and spread. The resulting formula is as follows:

Presence ~ Soil Temperature + Soil Moisture + Specific Humidity + Soil pH + Soil Sand Content + Land Cover Type

4.2.5 Ecological Niche Modeling

Models were built in the SDM R package (version 1.2-59) and modeling methods followed similar to Kessinger et al. 2025 (Kessinger et al., 2025; Naimi & Araújo, 2016). Three model types were selected: Boosted Regression Trees (BRT), Random Forest (RF), and Maximum Entropy (Maxent). These models were selected due to strong performance within habitat suitability and species distribution modeling frameworks (Barber et al., 2022; Cuéllar et al., 2020; Kessinger et al., 2025; Zeimes et al., 2015). The data was split 80% for training and 20% for testing for each year. Each model type had 10 iterations per study period year using cross-fold validation for a total of 10 BRT, 10 RF, and 10 Maxent models per year, 30 models total per year. Models were then ensembled using weighted mean. Cases were thinned to 10 kilometers for unique presence points for all models to prevent spatial autocorrelation. The models also used bias weights that were

calculated by taking the log of population density plus 1. Population density was sourced from GPWv4 population density rasters, and the weights were used to encourage more background points to be near clustered samples to adjust for cases being initially reported by place of residence. The average area under the curve (AUC) value is then reported for each year, Model performance was tracked using AUC values and plotted for each year per the weighted ensemble of the 10 iterations.

4.2.6 Prediction

Using the R package terra, the modeled ensemble output for each year is then used to predict the suitable habitat for *Coccidioides spp.* in Arizona. This resulted in predictions for each year in the study period for humans and canines. These annual predictions were then normalized by minimum-maximum scaling across years to ensure a constant relative scale for comparability and used to create a relative suitability index for *Coccidioides spp*. These were then used to create sentinel difference maps (annual canine ensembled map – annual human ensembled map) and maximum, mean, and minimum ensembled maps (with maximum, mean, and minimum value? between the annual canine ensemble map and the annual human ensemble map for *Coccidioides spp.* relative habitat suitability).

4.3 RESULTS

We conducted annual modeling for 2003-2024 and reported out annual habitat suitability for both human and canine predictions, as well as binary presence and sentinel difference. Final case counts, or proxy presence points, thinned to 10 km are tabulated in Table 4.2.

Table 4.2: Observed human cases and simulated canine case counts per year when case counts were thinned to 10km to reduce spatial autocorrelation

Year	Human Case Count	Canine Case Count
2004	46	525
2005	42	526
2006	49	526

2007	47	541
2008	44	541
2009	48	541
2010	93	590
2011	98	595
2012	92	609
2013	81	609
2014	77	617
2015	87	617
2016	84	618
2017	86	651
2018	89	652
2019	103	672
2020	127	616
2021	130	616
2022	124	617
2023	134	629

4.3.1 Variable selection

Variables were selected using a Pearson correlation matrix with results visible in Figure 4.2. Highly correlated variables (greater than 0.75) were considered for removal. Strong collinearity is notably present between temperature variables (r = 0.99 for air temperature and soil temperature) and between certain soil physical properties (sand, silt, and clay). Additionally, both specific humidity (Qair) and soil moisture (SoilM) were correlated with temperature. Removed variables included mean silt at 5-15 cm, mean clay at 5-15 cm, mean soc at 5-15 cm, and surface air temperature (Tair). Even though soil temperature and soil moisture correlation above 0.75, both were kept due to the previous literature and biological plausibility of being important for *Coccidioides* spp. growth. Specific humidity (Qair) was also kept even though it correlated with soil temperature due to also being thought to be biologically important for *Coccidioides spp.* presence.

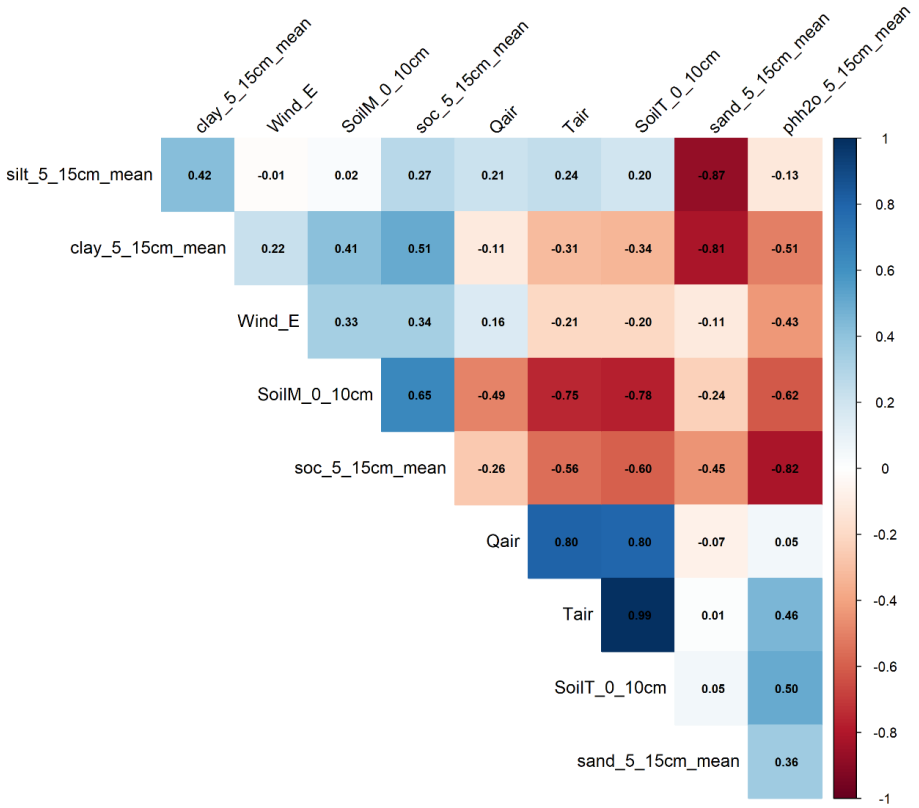

Figure 4.2: Pearson correlation matrix heatmap of environmental, atmospheric, and soil variables. Values within the cells represent Pearson correlation coefficients (r), with the color intensity mapped according to the scale bar on the right. Blue hues indicate positive correlations (up to +1.0), red hues indicate negative correlations (down to -1.0), and white indicates near-zero correlation.

4.3.2 Model performance

Model performance is reported with AUC scores over the study period in Figure 4.3. Human model performance ranked higher than canine model performance for both model types. Human models were mostly in the good category (0.7-0.9 AUC) with a few models making it into the excellent category (>0.9 AUC) for Maxent, while Random Forest human models stayed in the excellent category. Towards the end of the study period, human models began to dip towards AUC

values of 0.75 for Maxent. Canine values for AUC were lower, staying in the fair performance region (0.6-0.7) for Maxent, but still in the excellent range for Random Forest.

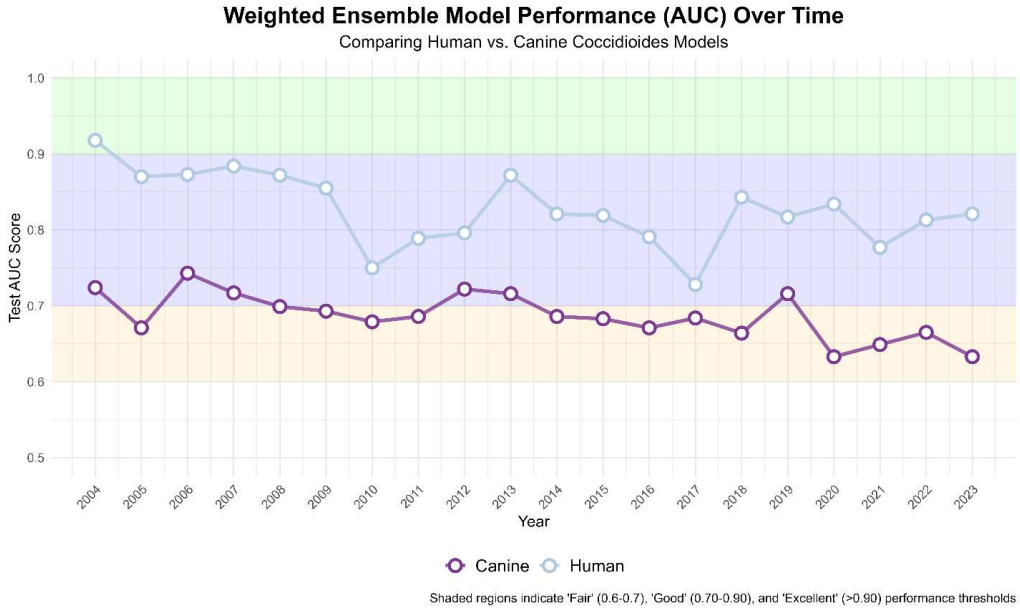

Figure 4.3: Ensembled model performance by AUC value. Humans are blue and canines are purple. The orange zone represents a fair model performance (0.6-0.7), blue a good performance (0.7-0.9), and green and excellent performance (>0.9).

Variable importance for the 2023 model year is included in Figure 4.4 (humans) and Figure 4.5 (canines). For humans, landcover and soil temperature were the largest contributors to response, with landcover contributing 0.38 response and soil temperature contributing 0.23.

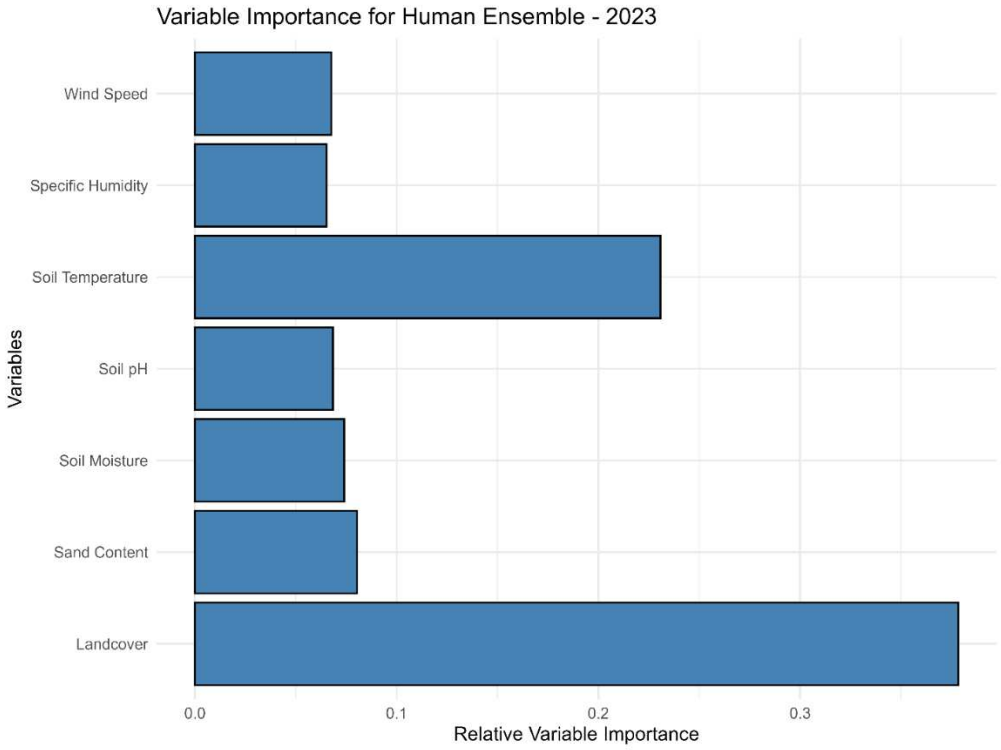

Figure 4.4: Relative variable importance for the human ensemble model (2023). The plot illustrates the ranking and relative weights of the seven predictor variables used in the model. Individual metrics, including Soil pH, Specific Humidity, Soil Temperature, Soil Moisture, Wind Speed, Sand Content, and Landcover, are evaluated based on their contribution to the overall ensemble model. The x-axis denotes the normalized relative importance scale ranging from 0.0 to 0.40.

Variable importance for canines was less defined in Figure 4.5, with more contributions for response spread out among the variables. However, soil pH and specific humidity were the highest contributors to relative response, 0.34 and 0.27 respectively. Soil temperature, wind speed, and soil moisture followed with sand content and landcover contributing the least.

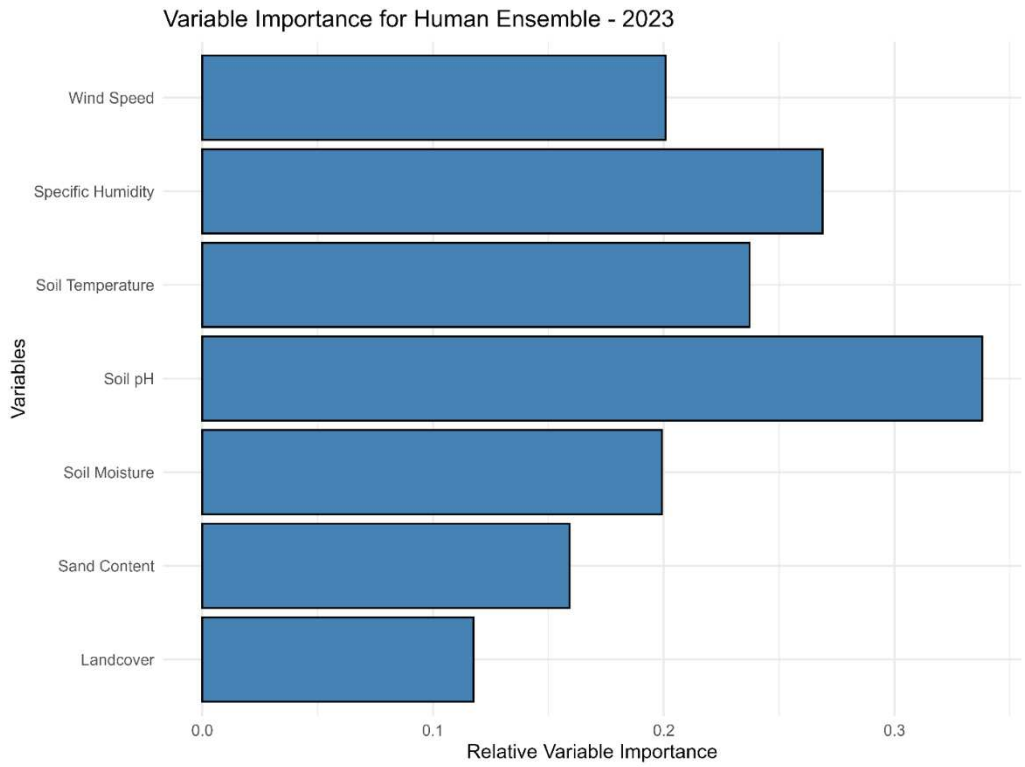

Figure 4.5: Relative variable importance for the canine ensemble model (2023). The plot illustrates the ranking and relative weights of the seven predictor variables used in the model. Individual metrics, including Soil pH, Specific Humidity, Soil Temperature, Soil Moisture, Wind Speed, Sand Content, and Landcover, are evaluated based on their contribution to the overall ensemble model. The x-axis denotes the normalized relative importance scale ranging from 0.0 to 0.35.

4.3.3 Habitat Suitability

Habitat suitability was predicted for the study area to demonstrate areas that the model predicted as suitable for *Coccidioides spp.* in the endemic region. The human ensemble model, displayed on the left of Figure 4.6, showed suitable habitat in the southwestern region of Arizona, clustering around population areas like Phoenix and Tucson. The canine model showed suitable habitat in parts of the Southwest and an increase in central and Northwest portions of Arizona, with a weaker signal as the map moves North.

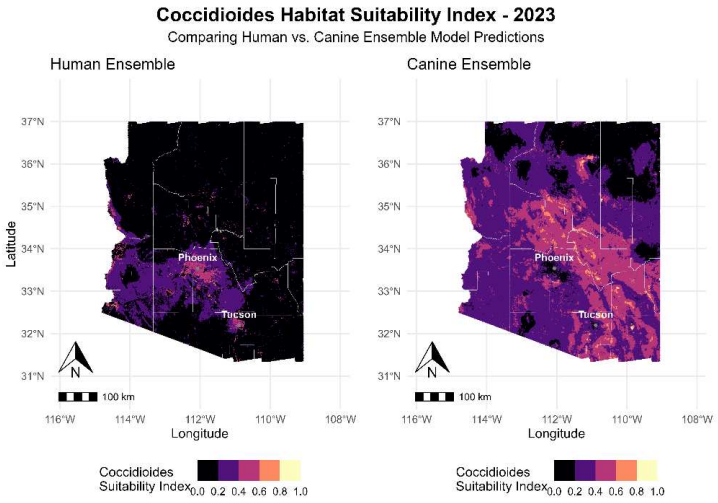

Figure 4.6: Ensemble Coccidioides spp. relative habitat suitability prediction for Arizona in 2023, with human and canine performance compared side by side using AUC scores.

When aggregating the canine and human models together using the maximum values, the mean values, and the minimum values, the trend remained similar for both maximum and mean (Figure 4.6). However, minimum performance dropped significantly and only showed suitability in the Southwest of Arizona (Figure 4.7).

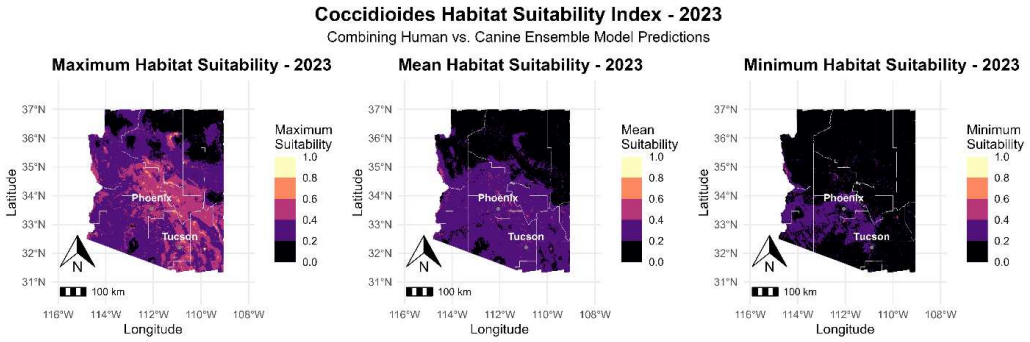

Figure 4.7: Combined model performance when aggregating canine and human models together. From left to right, models were aggregated using maximum values, mean values, and minimum values to show strongest, middle, and weakest performance for that year.

Sentinel mapping, or comparing suitability as predicted by canine models versus human models, resulted in canines driving prediction outside of and away from urban centers, and human models driving suitability in and near urban centers (Figure 4.8). On the scale, purple indicates that canines are driving suitability predictions more than humans, and orange is indicating that the human models are driving suitability predictions more than the sentinel species. White indicates that both species are predicting suitability evenly in that area.

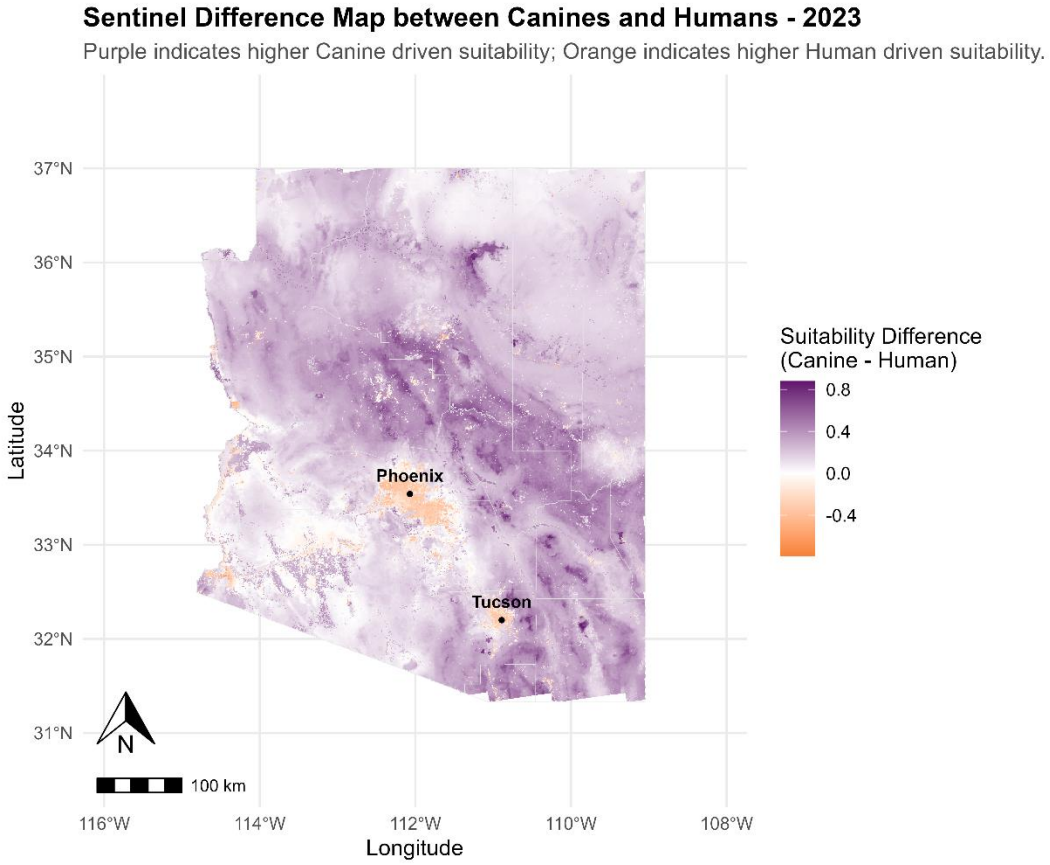

Figure 4.8: Sentinel comparison between canines and humans. If the color is purple, the canine models are driving suitability prediction, and if the color is orange, the human models are driving suitability. White means both models are predicting suitability evenly. The human models tended to predict more for and near urban centers, while the canine models tended to predict more for non-urban areas.

4.4 CONCLUSIONS

The objective of this study was to demonstrate that the use of Valley Fever case data, both human case data from the Arizona Department of Health Services and simulated canine cases, can be used as proxy points for *Coccidioides spp.* presence in the environment. This utility of using a one health framework to fill in data gaps provides a way to model pathogen organism habitat suitability (*Coccidioides spp.*) when working with disease case data (Valley Fever). By incorporating a sentinel species in combination with human cases, we sought to bypass the limitations of difficult environmental sampling and model *Coccidioides spp.* distribution and infer potential areas that may be used to guide and improve sampling and inform public and health providers of exposure risks.

Model performance from the ensemble of BRT, RF, and Maxent models produced AUC values from fair to excellent. However, the model performance must be scrutinized. The ensemble models performed well, with human models in the "good" category, and canine models in the "fair" category. However, human models, as demonstrated on the maps like Figure 4.6, show that urban centers still play a large role. In essence, there is concern that, even with spatial thinning and bias weighting with population density, the human model remains biased towards cases clustered in urban centers due to case reports geocoded by address of residence. This means that the model may be predicting some habitat suitability for *Coccidioides spp.*, but it may also be predicting where cases are likely to be diagnosed instead of where it would be likely to find *Coccidioides spp.* presence. However, the canine model, even though it had a lower AUC performance in the "fair" category, showed improved performance at isolating the urban signal while not eliminating urban influence. Combining the outputs of both the human ensemble model and canine ensemble model by maximum, mean, and minimum, resulted in a composite of relative

habitat suitability for *Coccidioides spp.* Specifically, in Figure 4.7. the mean and minimum ensemble demonstrated most suitable areas in the South and Southwestern region of Arizona, with focuses on urban centers like Phoenix and Tucson.

Relating to Gorris et al. 2019, our work also utilized human health data, focusing on human case data at the census tract level that was then interpolated in a 1km x 1km grid (M. E. Gorris et al., 2018; Morgan E. Gorris et al., 2019). Gorris et al. 2019 used county level incidence data in combination with temperature and precipitation to predict Valley Fever endemicity (Morgan E. Gorris et al., 2019). In general, our work aligned with findings in Gorris et al. 2019, with Gorris finding all of Arizona counties to be potentially suitable for endemicity in their model (Morgan E. Gorris et al., 2019). This matches our findings, especially with those of the canine ensemble model and the combined maximum canine and human ensemble predictions, which show *Coccidioides spp*. relative habitat suitability to be present in each county (Figure 4.6 and 4.7). This can also be seen in the mean model in Figure 4.7, with each Arizona county still having relative habitat suitability but with a more conservative combination of canine and human model predictions. For differences, our model is narrower in scope, only depicting Arizona instead of the lower 48 states of the United States. Furthermore, our model has a higher spatial resolution, focusing on census tract level instead of county level. This could have contributed to the fact that while our model agrees with Gorris et al. 2019 that all Arizona counties have the potential for endemicity, there are gaps within the state itself.

Our findings are in agreement with Weaver et al. 2020, which modeled Valley Fever using random generated presence points based on cases and incidence per 100,000 (Weaver et al., 2020). Both our model and the model in Weaver et al. 2020 found higher potential distributions or relative habitat suitability in the southwestern part of Arizona, especially when using the human ensemble

and minimum combined canine and human models (Figure 4.6 and 4.7) (Weaver et al., 2020). However, Weaver et al. included more of the western and southwestern United States, while our model only included Arizona (Weaver et al., 2020). Furthermore, while Weaver et al. 2020 used randomly generated points per case per 100,000, our simulated data was focused on canine cases in combination with real-world human cases of Valley Fever to create our overall presence points(Weaver et al., 2020). This could have resulted in our model having more relative habitat suitability and higher resolution in the Northern parts of Arizona, both to the West and East.

Finally, we also compared our work to Dobos et al. 2021, which used soil data from the National Soil Information System, Soil Survey Geographic Database, and the State Soil Geographic Database to create a habitat suitability index for *Coccidioides* spp. (Dobos et al., 2021). This was a model driven by environmental and climatic variables thought suitable for *Coccidioides* spp. presence, as determined by areas of high endemicity and previous literature (Dobos et al., 2021). In the focused area of Arizona, Dobos et al. 2021 had similar findings to our human model in central and Southwestern portion of the state, while the Dobos et al. 2021 model also had agreement with our canine ensemble model and maximum ensemble model in the Northern parts of the state, including both eastern and western regions. However, Dobos et al. 2021 did have regions that did not have published data, including the region just to the Northwest of Phoenix, where our model had higher levels of relative habitat suitability.

Overall, our results aligned with previously completed work involving *Coccidioides* spp. and Valley Fever in Arizona. In addition, we combined approaches by incorporating real-world human case data with simulated canine case data to create our presence points and then used that to extract environmental variables identified from previous literature that are thought to be beneficial to *Coccidioides* spp. habitat. This combined approach allowed us to incorporate a One

Health framework that built upon the individual approaches taken before in Gorris et al. 2019, Weaver et al. 2020, and Dobos et al. 2021 (Dobos et al., 2021; Morgan E. Gorris et al., 2019; Weaver et al., 2020).

This One Health framework where we included both simulated sentinel species in combination with real-world human health and environmental data instead of only human health data or only environmental variables could have strengthened our model and aided in providing better resolution of predicting relative habitat suitability for *Coccidioides* spp. in Arizona. While the simulation of canine cases could be seen as adding "noise" to our model that could obscure real relationships, our use of a simulated species for modeling use has precedent, having seen use in frameworks like (Kessinger et al., 2025), (Patyk et al., 2020), and (Burdett et al., 2015) for simulated livestock. This could indicate that our work could be potentially capturing more information due to the implementation of simulated canine data without just artificially inflating counts and creating noise.

Additionally, our findings align with recent work regarding Coccidioides dynamics in Arizona, especially Northern Arizona. Mead et al. 2022 found increasing cases in Northern Arizona during 2019, and succeeded in detecting *Coccidioides* DNA in the soil of Northern Arizona (Mead et al., 2022). This matches with the maximum and mean model showing relative suitability in parts of Northern Arizona, and aligns with habitat suitability modeled in Dobos et al 2021 (Dobos et al., 2021). This also follows the pattern of *Coccidioides* expansion, as discussed in Gorris et al. 2019 and Mead et al. 2022 (Morgan E. Gorris et al., 2019; Mead et al., 2022). This could indicate changing disease dynamics as *Coccidioides* expands from heavily endemic areas to less endemic areas and bring more individuals not previously exposed into contact with *Coccidioides*.

Our analysis indicates that the use of a sentinel species along with human case data can improve modeling capabilities in data sparse environments. Sentinel species can provide additional information, especially when the disease mechanics of exposure, infection, and clinical manifestation are as similar as with canines and humans regarding Valley Fever. By combining both real human Valley Fever cases with simulated canine cases, our models aligned with previous work, as well as matched ground level observations as seen in Mead et al. 2022 in less endemic areas as compared to the South and Southwest of Arizona (Mead et al., 2022). Through a One Health approach, researchers and public health officials can improve disease modeling and mapping, allowing for improved forecasts, surveillance, and communication. Timely public communication is critical for notifying populations and health practitioners about potential exposure or increased exposure, especially with an underreported and often misdiagnosed disease such as Valley Fever.

Strengths and Limitations: Our models had a large dataset, spanning from 2004-2023 with high resolution data for human cases of Valley Fever (census tract level) and a thorough use of data sources to simulate our canine Valley Fever cases (AVMA survey data, Sykes et al. 2025 canine serologic prevalence data). We incorporated variables linked to *Coccidioides spp.* presence, such as soil moisture and temperature, land use, and soil characteristics like pH and soil content. With these combined, we had a strong, spatially and temporarily available dataset to produce our models. Furthermore, we combined multiple types of models (MaxEnt, RF, and BRT) to produce ensembled approaches to try and capture the habitat suitability of *Coccidioides spp.* using case data as proxy presence points.

However, our simulation of canine cases made several assumptions, including simulating canine counts and cases using survey data from both the American Census Survey and the

American Veterinary Medical Association. This could introduce error and cause our assumed canine case counts to vary. Additionally, we spatially interpolated our cases to extract variables at a 1-kilometer resolution. This could have resulted in the loss of some cases due to spreading them over entire census tracts and only taking grid cells with a 0.5 or greater as a case.

For human cases, some of the laboratories that Arizona used for Valley Fever testing switched to a less strict definition in 2009, resulting in a spike in cases. This persisted until 2012, and may have inflated case counts from 2009-2013, making generalizability to those years difficult (Sophia E. Kruger et al., 2026).

Another issue was that by restricting our work to the state of Arizona, we may have edge effects due to distortions around the edges of the state, which could induce bias in measurements near the state borders.

Finally, we reduced our environmental and case datasets to annual, which removed some temporality and seasonality that could have improved our resolution and predictions.

Overall, we successfully demonstrated that there is potential to use a One Health framework to predict pathogen suitability when using cases as proxy presence points. By combining canines and humans together, we were able to create habitat suitability maps that focused on expected habitat areas, while reducing the clustering around urban interfaces where suitable habitat is not as plentiful.

This could help improve surveillance efforts, as well as steer future prediction efforts in suspected or non-endemic areas. Implementation of a sentinel species with both human and sentinel species case data could improve resolution of disease dynamics. Particularly around zoonotic diseases that have strong animal and human components. Future work should focus on incorporating both animal and human data, including moving beyond a simulated dataset and

incorporating reported canine cases with reported human cases. Both the veterinary world and human healthcare world could benefit from additional synergy, especially when discussing the realm of zoonotic diseases.

4.5 ACKNOWLEDGEMENTS

We thank the Arizona State Department of Health Services for providing the human case data for this study.

We gratefully acknowledge support from the NSF Biology Integration Institutes Program under Award # 2120117. We thank the CSU One Health Institute for contributions to and support of BROADN research, including the funding through the One Health Student Award (Kessinger, PI).

CHAPTER 5

SUMMARY, CONCLUSIONS, AND FUTURE WORK

5.1 SUMMARY AND CONCLUSIONS

This dissertation explores the intersection of environmental microbiology, drone technology, and public health through a One Health perspective. The following summary synthesizes the three core chapters provided: Chapter Two presents the technical validation of a lightweight bioaerosol sampler, Chapter Three presents the application of the lightweight bioaerosol sampler in characterizing atmospheric microbial communities, and Chapter Four presents the predictive modeling of soil-borne pathogens using sentinel species to guide future work.

In Chapter Two, we validated a lightweight prototype air sampler (Light SASS) from Research International Inc against the gold standard of the Full SASS 3100, also from Research International Inc, to determine suitability of the Light SASS for drone-based environmental airborne surveillance. Light SASS performance was tested across three environments: a controlled 10 m^3 chamber using *Pseudomonas syringae* as a tracer, outdoor ground-level sites, and elevated field trials at 12 meters above ground level (AGL). We then used DNA extraction, qPCR, and amplicon sequencing to determine that the Light SASS performed comparably to the Full SASS in both chamber and ground-level conditions with no statistically significant differences in DNA recovery or microbial diversity. However, when combined with the drone platform, the quadcopter (DJI Matrice 350) trials showed no significant difference but the hexacopter (Aurelia X6 Pro V2) trials revealed lower DNA recovery for the Light SASS, potentially due to platform-specific

airflow dynamics or vibration. Therefore, our work in chapter two concluded that the Light SASS effectively optimizes the weight-to-performance ratio, enabling longer flight endurance for atmospheric sampling without compromising data quality under most conditions.

Chapter Three is built upon the method validation of Chapter Two. We applied the drone-mounted system to conduct stratified airborne sampling in Big Spring, Texas, to investigate microbial transport and potential public health risks. Utilizing a DJI Matrice 350, researchers performed vertical profiles within the PBL to characterize microbial communities at various altitudes (ground level, 100, 200, and 400 ft). The analysis identified several genera with significant implications for human, animal, and agricultural health, including *Legionella*, *Enterococcus*, and *Fusarium*. It also detected *Onygenales*, an order containing virulent pathogens like *Coccidioides*. Statistical analysis showed that phylogenetic diversity and richness were significantly affected by sampling altitude. The ability to activate the sampler remotely allowed for precise elevation-specific observations, though drone-induced turbulence remained a minor consideration for potential contamination. This work demonstrates that drone-mounted samplers can provide high-resolution, genus-level data that is critical for developing early warning systems for airborne pathogens.

Finally, in Chapter Four, we shifted our work from direct atmospheric sampling to predictive modeling, using a One Health framework to map the relative habitat suitability of *Coccidioides spp.* (the causative agent of Valley Fever) in Arizona. The study utilized a novel approach by combining human case data from health departments with simulated canine case data to serve as proxy indicators for environmental pathogen presence. Using an ensemble of Boosted

Regression Trees, Random Forest, and Maxent models, the research found that human models were often biased toward urban centers where cases are reported. In contrast, canine models were more effective at isolating the urban signal and identifying suitability in non-urban areas. Composite models identified hotspots in Southern and Southwestern Arizona, aligning with known endemic regions, but also predicted suitable habitats in parts of Northern Arizona, which has seen increasing case reports recently. This chapter highlights the utility of sentinel species in filling data gaps, allowing for more accurate risk assessment and targeted environmental sampling in regions where pathogens may be emerging.

Together, these chapters form a comprehensive workflow for environmental surveillance. The dissertation moves from method validation (proving that lightweight samplers and drones can accurately sample the air) to field application (identifying specific pathogens of concern in the atmosphere) and finally to predictive modeling (using both human and animal health data to forecast where those pathogens reside in the environment). Collectively, the studies provide a framework for public health officials to monitor and mitigate the risks posed by airborne biological contaminants utilizing a One Health approach.

5.2 FUTURE WORK

This section focuses on specific directions future work can go to build upon the presented research in this dissertation.

5.2.1 Drone compatibility with lightweight air samplers

Future work should include additional drone-mounted trials, especially when considering the hexacopter style drone used in chapter two. Our hypothesis of why the hexacopter style drone

had discrepancies between Light SASS and Full SASS performance, as compared to the more comparable performance between the Light SASS and Full SASS when the Light SASS was mounted on the DJI Matrice 350 quadcopter drone, is that the hexacopter configuration induced potential mechanical bias. This could be due to the configuration of the rotors themselves causing too much propeller wash that prevented even sampling by the Light SASS or could be a mechanical interference such as vibration from the drone influencing the fan of the Light SASS itself. Future work should attempt to quantify the influence of different drone configurations, focusing on propeller wash influence and sampler performance under flight conditions.

5.2.2 Drone surveillance and utilization

Like the future work for Chapter Two, future work for chapter three needs to focus on stronger characterization of the vertical profile. To accomplish this, instead of spreading resources too thin over multiple sites, only one site will be selected. Site selection will focus on endemic regions for *Coccidioides* spp., using inspiration from chapter four, as well as the results in chapter three including *Onygenales*, the order that includes *Coccidioides* spp. Site selection should use previous literature that has successfully identified soil samples positive for *Coccidioides* spp. presence and then confirm positive presence before air sampling. This may not be the *Coccidioides* spp. that is collected though air sampling, but should confirm that aerosolized *Coccidioides* spp. should be possible within that area. By starting in a location that previous literature has successfully identified *Coccidioides* spp. from a soil sample, we would hope to bypass, or at least mitigate, the difficulty of successful environmental sampling for *Coccidioides* spp.

Once confirmed, air sampling should focus on daily air sampling missions with additional equipment. A limitation of our study was the low number of drone batteries and lack of ability to charge the drone batteries quickly in the field. This resulted in us only having the capability for four flights before running out of charge. Therefore, future studies should include an enhanced field site that includes a generator to provide consistent and fast charging for drone batteries. Additional batteries should also be included to allow for continuous flying should conditions allow. Samples should be taken at similar stratifications (ground level, 100 ft, 200 ft, and 400 ft), but with additional trials per day. Previous work into *Coccidioides* spp. and Valley Fever incidence indicates that wetter conditions followed by dry seasons typically result in more growth and more subsequent arthroconidia availability for aerosolization, respectively (M. E. Gorris et al., 2018; Morgan E. Gorris et al., 2019; Radosevich et al., 2025; Weaver et al., 2020). Therefore, sampling should occur during the summer and fall, as hotter conditions in endemic areas may be conducive to aerosolization (M. E. Gorris et al., 2018).

In addition to this improved sampling campaign, future work should also consider including NGS using ITS2 primers for *Coccidiodes* spp. detection. ITS2 primers could potentially be more applicable for *Ascomycota*, the division in which *Coccidioides* spp. resides (Bowers et al., 2019; Hoggard et al., 2018; Yang et al., 2018). ITS2 primers might also increase accuracy when it comes to fungal classification, but fungal sequencing is difficult due to the highly variable nature of ITS (Taylor et al., 2016; Winand et al., 2025; Yang et al., 2018). Future work should also include specific qPCR tests for Valley Fever, to demonstrate disease specific surveillance capabilities (Bowers et al., 2019; Radosevich et al., 2025).

5.2.3 One Health synergy with human and animal reported cases

Future work for *Coccidioides* habitat suitability modeling should continue to pursue a One Health framework. Our model demonstrated that inclusion of a sentinel species, especially in the case where data availability is scarce or skewed by reporting bias, is beneficial. However, the matter remains that our sentinel species data was simulated, and not actual reported cases.

Therefore, future work should attempt to work with local veterinarians and public health departments to create a composite database for Valley Fever cases. Valley Fever in humans is required to be reported in Arizona, but it is not the same case for canines (M. E. Gorris et al., 2018). However, canines, being a strong sentinel species for Valley Fever, should be incorporated as observed data points instead of simulated to help enhance our understanding of the ecological niche that *Coccidioides* spp. inhabits (Sykes et al., 2025). A transdisciplinary team including researchers, public health officials including state level veterinarians from the Arizona Department of Health Services and Department of Agriculture, and veterinary clinics could work together to improve monitoring for Valley Fever and create the combined database needed for future modeling projects.

This is continuing with the understanding that *Coccidioides* spp. presence points are difficult to ascertain from environmental sampling, and Valley Fever cases could continue to serve as proxy presence points for *Coccidioides* spp. presence. Expanding upon that, it is important to continue to pursue an understanding of *Coccidioides* spp. presence in the environment rather than only incidence and case prediction, as this could move health response from reactionary to preventative. Understanding where ecological hotspots are could help with how to best

communicate that to the public and healthcare professionals to reduce exposure and ultimately reduce cases.

5.3 Final thoughts

This dissertation establishes a One Health framework for environmental surveillance by integrating lightweight drone technology with next-generation microbial sequencing analysis and predictive modeling. The research successfully navigates a workflow from the method validation of lightweight air samplers to field application in potentially identifying significant human and agricultural pathogens across stratified atmospheric altitudes. By bridging these technical capabilities with predictive modeling, the work demonstrates how sentinel species can fill critical data gaps, identifying emerging disease hotspots and mitigating the reporting biases in areas with limited data availability. Ultimately, these findings advocate for a transdisciplinary approach that shifts public health efforts from reactionary measures to preventative strategies, utilizing high-resolution environmental data to monitor and mitigate the risks of airborne biological pathogens.

REFERENCES

Apprill, A., McNally, S., Parsons, R., & Weber, L. (2015). Minor revision to V4 region SSU rRNA 806R gene primer greatly increases detection of SAR11 bacterioplankton. *Aquatic Microbial Ecology*, *75*, 129–137. https://doi.org/10.3354/ame01753

Attali, D., & Baker, C. (2025, September 1). ggExtra: Add Marginal Histograms to "ggplot2", and More "ggplot2" Enhancements (Version 0.11.0). Retrieved from https://cran.r-project.org/web/packages/ggExtra/index.html

Auguie, B., & Antonov, A. (2017, September 9). gridExtra: Miscellaneous Functions for "Grid" Graphics (Version 2.3). Retrieved from https://cran.r-project.org/web/packages/gridExtra/index.html

Bangay, R., Matsuki, A., & Tuno, N. (2026). Drones and fungal spores: comparisons of low-cost sampling methods. *Aerobiologia*, *42*(1), 24. https://doi.org/10.1007/s10453-026-09912-1

Barasona, J. A., Mulero-Pázmány, M., Acevedo, P., Negro, J. J., Torres, M. J., Gortázar, C., & Vicente, J. (2014). Unmanned Aircraft Systems for Studying Spatial Abundance of Ungulates: Relevance to Spatial Epidemiology. *PLOS ONE*, *9*(12), e115608. https://doi.org/10.1371/journal.pone.0115608

Barber, R. A., Ball, S. G., Morris, R. K. A., & Gilbert, F. (2022). Target-group backgrounds prove effective at correcting sampling bias in Maxent models. *Diversity and Distributions*, *28*(1), 128–141. https://doi.org/10.1111/ddi.13442

Bieber, P., Seifried, T. M., Burkart, J., Gratzl, J., Kasper-Giebl, A., Schmale, D. G., & Grothe, H. (2020). A Drone-Based Bioaerosol Sampling System to Monitor Ice Nucleation Particles

in the Lower Atmosphere. *Remote Sensing*, *12*(3), 552. https://doi.org/10.3390/rs12030552

Bøifot, K. O., Gohli, J., Skogan, G., & Dybwad, M. (2020). Performance evaluation of high-volume electret filter air samplers in aerosol microbiome research. *Environmental Microbiome*, *15*(1), 14. https://doi.org/10.1186/s40793-020-00362-x

Bokulich, N. A., & Mills, D. A. (2013). Improved Selection of Internal Transcribed Spacer-Specific Primers Enables Quantitative, Ultra-High-Throughput Profiling of Fungal Communities. *Applied and Environmental Microbiology*, *79*(8), 2519–2526. https://doi.org/10.1128/AEM.03870-12

Bolyen, E., Rideout, J. R., Dillon, M. R., Bokulich, N. A., Abnet, C. C., Al-Ghalith, G. A., et al. (2019). Reproducible, interactive, scalable and extensible microbiome data science using QIIME 2. *Nature Biotechnology*, *37*(8), 852–857. https://doi.org/10.1038/s41587-019-0209-9

Bowers, J. R., Parise, K. L., Kelley, E. J., Lemmer, D., Schupp, J. M., Driebe, E. M., et al. (2019). Direct detection of Coccidioides from Arizona soils using CocciENV, a highly sensitive and specific real-time PCR assay. *Medical Mycology*, *57*(2), 246–255. https://doi.org/10.1093/MMY/MYY007

Brodsky, H. K., Calderón, R., Hamilton, D. S., Li, L., Miles, A., Pavlick, R., et al. (2023). Assessing long-distance atmospheric transport of soilborne plant pathogens. *Environmental Research Letters*, *18*(10), 104021. https://doi.org/10.1088/1748-9326/acf50c

Burdett, C. L., Kraus, B. R., Garza, S. J., Miller, R. S., & Bjork, K. E. (2015). Simulating the Distribution of Individual Livestock Farms and Their Populations in the United States: An Example Using Domestic Swine (Sus scrofa domesticus) Farms. *PLOS ONE*, *10*(11), e0140338. https://doi.org/10.1371/JOURNAL.PONE.0140338

Butkiewicz, C. D., Sykes, J. E., Camponuri, S. K., Weaver, A. K., & Shubitz, L. F. (2025). The costs of the diagnosis and treatment of canine coccidioidomycosis in endemic regions, USA, 2022. *Preventive Veterinary Medicine*, *245*, 106660. https://doi.org/10.1016/j.prevetmed.2025.106660

Caporaso, J. G., Lauber, C. L., Walters, W. A., Berg-Lyons, D., Huntley, J., Fierer, N., et al. (2012). Ultra-high-throughput microbial community analysis on the Illumina HiSeq and MiSeq platforms. *The ISME Journal*, *6*(8), 1621–1624. https://doi.org/10.1038/ismej.2012.8

CDC. (2025, June 5). Respiratory Virus Hospitalization Surveillance Network (RESP-NET). Retrieved July 23, 2025, from https://www.cdc.gov/resp-net/dashboard/index.html

Chen, P., Sun, W., & He, Y. (2020). Comparison of the next-generation sequencing (NGS) technology with culture methods in the diagnosis of bacterial and fungal infections. *Journal of Thoracic Disease*, *12*(9). https://doi.org/10.21037/jtd-20-930

Choudhury, R. A., Koike, S. T., Fox, A. D., Anchieta, A., Subbarao, K. V., Klosterman, S. J., & McRoberts, N. (2017). Spatiotemporal Patterns in the Airborne Dispersal of Spinach Downy Mildew. *Phytopathology®*, *107*(1), 50–58. https://doi.org/10.1094/PHYTO-04-16-0162-R

Chow, N. A., Kangiser, D., Gade, L., McCotter, O. Z., Hurst, S., Salamone, A., et al. (2021). Factors Influencing Distribution of Coccidioides immitis in Soil, Washington State, 2016. *mSphere*, *6*(6), e00598-21. https://doi.org/10.1128/mSphere.00598-21

Coccidioidomycosis / Valley Fever (Coccidioides spp.) 2023 Case Definition | CDC. (2024, May 30). Retrieved May 1, 2026, from https://ndc.services.cdc.gov/case-definitions/coccidioidomycosis-2023/

Cosgrove, B. A., Lohmann, D., Mitchell, K. E., Houser, P. R., Wood, E. F., Schaake, J. C., et al. (2003). Real-time and retrospective forcing in the North American Land Data Assimilation System (NLDAS) project. *Journal of Geophysical Research: Atmospheres*, *108*(D22), 2002JD003118. https://doi.org/10.1029/2002JD003118

Crazzolara, C., Ebner, M., Platis, A., Miranda, T., Bange, J., & Junginger, A. (2019). A new multicopter-based unmanned aerial system for pollen and spores collection in the atmospheric boundary layer. *Atmospheric Measurement Techniques*, *12*(3), 1581–1598. https://doi.org/10.5194/amt-12-1581-2019

Cuéllar, A. C., Kjær, L. J., Baum, A., Stockmarr, A., Skovgard, H., Nielsen, S. A., et al. (2020). Modelling the monthly abundance of Culicoides biting midges in nine European countries using Random Forests machine learning. *Parasites and Vectors*, *13*(1). https://doi.org/10.1186/s13071-020-04053-x

Damerum, A., Malka, S., Lofgren, N., Vecere, G., & Krumbeck, J. A. (2023). Next-generation DNA sequencing offers diagnostic advantages over traditional culture testing. *American Journal of Veterinary Research*, *84*(8). https://doi.org/10.2460/ajvr.23.03.0054

Davis, N. M., Proctor, D. M., Holmes, S. P., Relman, D. A., & Callahan, B. J. (2018). Simple statistical identification and removal of contaminant sequences in marker-gene and metagenomics data. *Microbiome*, *6*(1), 226. https://doi.org/10.1186/s40168-018-0605-2

Dobos, R. R., Benedict, K., Jackson, B. R., & McCotter, O. Z. (2021). Using soil survey data to model potential Coccidioides soil habitat and inform Valley fever epidemiology. *PLOS ONE*, *16*(2), e0247263. https://doi.org/10.1371/journal.pone.0247263

Donovan, F. M., Shubitz, L., Powell, D., Orbach, M., Frelinger, J., & Galgiani, J. N. (2019). Early Events in Coccidioidomycosis. *Clinical Microbiology Reviews*, *33*(1), e00112-19. https://doi.org/10.1128/CMR.00112-19

Drautz-Moses, D. I., Luhung, I., Gusareva, E. S., Kee, C., Gaultier, N. E., Premkrishnan, B. N. V., et al. (2022). Vertical stratification of the air microbiome in the lower troposphere. *Proceedings of the National Academy of Sciences*, *119*(7), e2117293119. https://doi.org/10.1073/pnas.2117293119

Evans Ogden, L. (2026). The national ecological observatory network: past, present, and future. *BioScience*, *76*(4), 317–322. https://doi.org/10.1093/biosci/biaf107

Ferguson, A. J., Thompson, G. R., Bruyette, D., & Sykes, J. E. (2024). The dog as a sentinel and animal model for coccidioidomycosis. *Medical Mycology*, *62*(1), myad139. https://doi.org/10.1093/mmy/myad139

FINAL_AVMA_PetDemographics102218-compressed.pdf. (n.d.). Retrieved from https://murrowcourses.com/graphics/wp-content/uploads/2021/05/FINAL_AVMA_PetDemographics102218-compressed.pdf

Finn, D. R., Maldonado, J., De Martini, F., Yu, J., Penton, R., Fontenele, R. S., et al. (2021). Agricultural practices drive biological loads, seasonal patterns and potential pathogens in the aerobiome of a mixed-land-use dryland. *Science of the Total Environment*, *798*, 149239. https://doi.org/10.1016/j.scitotenv.2021.149239

Fisher, F. S., Bultman, M. W., Johnson, S. M., Pappagianis, D., & Zaborsky, E. (2007). Coccidioides Niches and Habitat Parameters in the Southwestern United States. *Annals of the New York Academy of Sciences*, *1111*(1), 47–72. https://doi.org/10.1196/annals.1406.031

Fones, H. N., Bebber, D. P., Chaloner, T. M., Kay, W. T., Steinberg, G., & Gurr, S. J. (2020). Threats to global food security from emerging fungal and oomycete crop pathogens. *Nature Food*, *1*(6), 332–342. https://doi.org/10.1038/s43016-020-0075-0

Gomez, O., McCabe, K. M., Biesiada, E., Volbers, B., Kraus, E., Nieto-Caballero, M., & Hernandez, M. (2022). Airborne murine coronavirus response to low levels of hypochlorous acid, hydrogen peroxide and glycol vapors. *Aerosol Science and Technology*, *56*(11), 1047–1057. https://doi.org/10.1080/02786826.2022.2120794

Gorris, M. E., Cat, L. A., Zender, C. S., Treseder, K. K., & Randerson, J. T. (2018). Coccidioidomycosis Dynamics in Relation to Climate in the Southwestern United States. *GeoHealth*, *2*(1), 6–24. https://doi.org/10.1002/2017GH000095

Gorris, Morgan E., Treseder, K. K., Zender, C. S., & Randerson, J. T. (2019). Expansion of Coccidioidomycosis Endemic Regions in the United States in Response to Climate Change. *GeoHealth*, *3*(10), 308–327. https://doi.org/10.1029/2019GH000209

Gridded Population of the World, Version 4 (GPWv4): Population Density Adjusted to Match 2015 Revision UN WPP Country Totals, Revision 11. (n.d.). Retrieved March 26, 2026, from https://search.earthdata.nasa.gov/search/granules?p=C3540929692-ESDIS

Guilbaud, C., Morris, C. E., Barakat, M., Ortet, P., & Berge, O. (2016). Isolation and identification of Pseudomonas syringae facilitated by a PCR targeting the whole P. syringae group. *FEMS Microbiology Ecology*, *92*(1), fiv146. https://doi.org/10.1093/femsec/fiv146

Hijmans, R. J., Brown, A., Barbosa, M., Bivand, R., Chirico, M., Cordano, E., et al. (2026, March 26). terra: Spatial Data Analysis (Version 1.9-11). Retrieved from https://cran.r-project.org/web/packages/terra/index.html

Hoggard, M., Vesty, A., Wong, G., Montgomery, J. M., Fourie, C., Douglas, R. G., et al. (2018). Characterizing the Human Mycobiota: A Comparison of Small Subunit rRNA, ITS1, ITS2, and Large Subunit rRNA Genomic Targets. *Frontiers in Microbiology*, *9*. https://doi.org/10.3389/fmicb.2018.02208

Hothorn, T., Winell, H., Hornik, K., Wiel, M. A. van de, & Zeileis, A. (2023, September 27). coin: Conditional Inference Procedures in a Permutation Test Framework (Version 1.4-3). Retrieved from https://cran.r-project.org/web/packages/coin/index.html

ISRIC — World Soil Information. (n.d.). Retrieved July 8, 2024, from https://www.isric.org

Jeffery, C., Ozonoff, A., & Pagano, M. (2014). The effect of spatial aggregation on performance when mapping a risk of disease. *International Journal of Health Geographics*, *13*(1), 9. https://doi.org/10.1186/1476-072X-13-9

Kassambara, A. (2025, October 18). rstatix: Pipe-Friendly Framework for Basic Statistical Tests (Version 0.7.3). Retrieved from https://cran.r-project.org/web/packages/rstatix/index.html

Kassambara, A., Business, L. E. (Faculty of E. and, Debrecen, U. of, & Hungary). (2026, February 24). ggpubr: "ggplot2" Based Publication Ready Plots (Version 0.6.3). Retrieved from https://cran.r-project.org/web/packages/ggpubr/index.html

Kellogg, C. A., Griffin, D. W., Garrison, V. H., Peak, K. K., Royall, N., Smith, R. R., & Shinn, E. A. (2004). Characterization of Aerosolized Bacteria and Fungi From Desert Dust Events in Mali, West Africa. *Aerobiologia*, *20*(2), 99–110. https://doi.org/10.1023/B:AERO.0000032947.88335.bb

Kers, J. G., & Saccenti, E. (2022). The Power of Microbiome Studies: Some Considerations on Which Alpha and Beta Metrics to Use and How to Report Results. *Frontiers in Microbiology*, *12*. https://doi.org/10.3389/fmicb.2021.796025

Kessinger, P., James, A. M., Patyk, K. A., Vigil, S. L., Ruder, M. G., & Magzamen, S. (2025). A habitat suitability analysis for three Culicoides species implicated in bluetongue virus transmission in the Southeastern United States. *Medical and Veterinary Entomology*, *39*(2), 373–384. https://doi.org/10.1111/mve.12786

King, K. M., Canning, G. G. M., & West, J. S. (2024). MinION Sequencing of Fungi in Sub-Saharan African Air and a Novel LAMP Assay for Rapid Detection of the Tropical Phytopathogenic Genus Lasiodiplodia. *Pathogens*, *13*(4), 330. https://doi.org/10.3390/pathogens13040330

Li, Q., Zhang, B., Wang, R., Li, H., Zhan, Y., Tong, D., & Bell, J. E. (2025). Effects of Soil Moisture and Soil Temperature on Coccidioidomycosis. *GeoHealth*, *9*(12), e2025GH001574. https://doi.org/10.1029/2025GH001574

Luhung, I., Uchida, A., Lim, S. B. Y., Gaultier, N. E., Kee, C., Lau, K. J. X., et al. (2021). Experimental parameters defining ultra-low biomass bioaerosol analysis. *Npj Biofilms and Microbiomes*, *7*(1), 1–11. https://doi.org/10.1038/s41522-021-00209-4

Mackenzie, J. S., & Jeggo, M. (2019). The One Health Approach—Why Is It So Important? *Tropical Medicine and Infectious Disease*, *4*(2), 88. https://doi.org/10.3390/tropicalmed4020088

Mbareche, H., Veillette, M., Bilodeau, G. J., & Duchaine, C. (2018). Bioaerosol Sampler Choice Should Consider Efficiency and Ability of Samplers To Cover Microbial Diversity. *Applied and Environmental Microbiology*, *84*(23), e01589-18. https://doi.org/10.1128/AEM.01589-18

Mead, H. L., Kollath, D. R., Teixeira, M. de M., Roe, C. C., Plude, C., Nandurkar, N., et al. (2022). Coccidioidomycosis in Northern Arizona: an Investigation of the Host, Pathogen, and Environment Using a Disease Triangle Approach. *mSphere*, *7*(5), e00352-22. https://doi.org/10.1128/msphere.00352-22

Meisner, J., Clifford, W. R., Wohrle, R. D., Kangiser, D., & Rabinowitz, P. (2019). Soil and climactic predictors of canine coccidioidomycosis seroprevalence in Washington State: An ecological cross-sectional study. *Transboundary and Emerging Diseases*, *66*(5), 2134–2142. https://doi.org/10.1111/tbed.13265

Microbes and Climate Change – Science, People & Impacts: Report on an American Academy of Microbiology Virtual Colloquium held on November 5, 2021. (2022). Washington (DC): American Society for Microbiology. Retrieved from http://www.ncbi.nlm.nih.gov/books/NBK580166/

Mitchell, K. E., Lohmann, D., Houser, P. R., Wood, E. F., Schaake, J. C., Robock, A., et al. (2004). The multi-institution North American Land Data Assimilation System (NLDAS): Utilizing multiple GCIP products and partners in a continental distributed hydrological modeling system. *Journal of Geophysical Research: Atmospheres*, *109*(D7), 2003JD003823. https://doi.org/10.1029/2003JD003823

Naimi, B., & Araújo, M. B. (2016). sdm: a reproducible and extensible R platform for species distribution modelling. *Ecography*, *39*(4), 368–375. https://doi.org/10.1111/ECOG.01881

Neufeld, K. N., Keinath, A. P., Gugino, B. K., McGrath, M. T., Sikora, E. J., Miller, S. A., et al. (2018). Predicting the risk of cucurbit downy mildew in the eastern United States using an integrated aerobiological model. *International Journal of Biometeorology*, *62*(4), 655–668. https://doi.org/10.1007/s00484-017-1474-2

Nieto-Caballero, M., Davis, R. D., Fuques, E., Gomez, O. M., Huynh, E., Handorean, A., et al. (2023). Carbohydrate vitrification in aerosolized saliva is associated with the humidity-dependent infectious potential of airborne coronavirus. *PNAS Nexus*, *2*(2), pgac301. https://doi.org/10.1093/pnasnexus/pgac301

Nieto-Caballero, M., Barry, K. R., Hill, T. C. J., Douglas, T. A., DeMott, P. J., Kreidenweis, S. M., & Creamean, J. M. (2025). Airborne Bacteria over Thawing Permafrost Landscapes

in the Arctic. *Environmental Science & Technology*, *59*(18), 9027–9036. https://doi.org/10.1021/acs.est.4c11774

Ojiambo, P. S., & Holmes, G. J. (2011a). Spatiotemporal Spread of Cucurbit Downy Mildew in the Eastern United States. *Phytopathology®*, *101*(4), 451–461. https://doi.org/10.1094/PHYTO-09-10-0240

Ojiambo, P. S., & Holmes, G. J. (2011b). Spatiotemporal Spread of Cucurbit Downy Mildew in the Eastern United States. *Phytopathology®*, *101*(4), 451–461. https://doi.org/10.1094/PHYTO-09-10-0240

Oksanen, J., Simpson, G. L., Blanchet, F. G., Kindt, R., Legendre, P., Minchin, P. R., et al. (2026, March 4). vegan: Community Ecology Package (Version 2.7-3). Retrieved from https://cran.r-project.org/web/packages/vegan/index.html

Parada, A. E., Needham, D. M., & Fuhrman, J. A. (2016). Every base matters: assessing small subunit rRNA primers for marine microbiomes with mock communities, time series and global field samples. *Environmental Microbiology*, *18*(5), 1403–1414. https://doi.org/10.1111/1462-2920.13023

Patyk, K. A., McCool-Eye, M. J., South, D. D., Burdett, C. L., Maroney, S. A., Fox, A., et al. (2020). Modelling the domestic poultry population in the United States: A novel approach leveraging remote sensing and synthetic data methods. *Geospatial Health*, *15*(2). https://doi.org/10.4081/gh.2020.913

Pebesma, E., Bivand, R., Racine, E., Sumner, M., Cook, I., Keitt, T., et al. (2026, February 24). sf: Simple Features for R (Version 1.1-0). Retrieved from https://cran.r-project.org/web/packages/sf/index.html

Porter, W. T., Gade, L., Montfort, P., Mihaljevic, J. R., Bowers, J. R., Willman, A., et al. (2024). Understanding the exposure risk of aerosolized Coccidioides in a Valley fever endemic metropolis. *Scientific Reports*, *14*(1), 1311. https://doi.org/10.1038/s41598-024-51407-x

R Core Team. (2025). R: A language and environment for statistical computing.

R: The R Project for Statistical Computing. (n.d.). Retrieved March 31, 2026, from https://www.r-project.org/

Radosevich, M. T., Dobson, S., Weaver, A. K., Lampman, P., Kollath, D., Couper, L., et al. (2025). Detection of Airborne Coccidioides Spores Using Lightweight Portable Air Samplers Affixed to Uncrewed Aircraft Systems in California's Central Valley. *Environmental Science & Technology Letters*, *12*(5), 580–586. https://doi.org/10.1021/acs.estlett.4c01089

Rodríguez-Arias, R. M., Rojo, J., Fernández-González, F., & Pérez-Badia, R. (2023). Desert dust intrusions and their incidence on airborne biological content. Review and case study in the Iberian Peninsula. *Environmental Pollution*, *316*, 120464. https://doi.org/10.1016/j.envpol.2022.120464

Rowan, A. (2018). Companion Animal Statistics in the USA. *Demography and Statistics for Companion Animal Populations Collection*. Retrieved from https://www.wellbeingintlstudiesrepository.org/demscapop/7

Savory, E. A., Granke, L. L., Quesada-Ocampo, L. M., Varbanova, M., Hausbeck, M. K., & Day, B. (2011). The cucurbit downy mildew pathogen Pseudoperonospora cubensis. *Molecular Plant Pathology*, *12*(3), 217–226. https://doi.org/10.1111/j.1364-3703.2010.00670.x

Scarlett, K., Tesoriero, L., Daniel, R., Maffi, D., Faoro, F., & Guest, D. I. (2015). Airborne inoculum of Fusarium oxysporum f. sp. cucumerinum. *European Journal of Plant Pathology*, *141*(4), 779–787. https://doi.org/10.1007/s10658-014-0578-3

Shubitz, L. F., Butkiewicz, C. D., Dial, S. M., & Lindan, C. P. (2005). Incidence of Coccidioides infection among dogs residing in a region in which the organism is endemic. *Journal of the American Veterinary Medical Association*, *226*(11), 1846–1850. https://doi.org/10.2460/javma.2005.226.1846

Small Unmanned Aircraft Systems (UAS) Regulations (Part 107) | Federal Aviation Administration. (n.d.). Retrieved July 8, 2024, from https://www.faa.gov/newsroom/small-unmanned-aircraft-systems-uas-regulations-part-107

Smith, B., Beman, M., Gravano, D., & Chen, Y. (2015). Development and validation of a microbe detecting UAV payload. In *2015 Workshop on Research, Education and Development of Unmanned Aerial Systems (RED-UAS)* (pp. 258–264). https://doi.org/10.1109/RED-UAS.2015.7441015

Smith, D. J., Griffin, D. W., & Jaffe, D. A. (2011). The high life: Transport of microbes in the atmosphere. *Eos, Transactions American Geophysical Union*, *92*(30), 249–250. https://doi.org/10.1029/2011EO300001

Smith, D. J., Ravichandar, J. D., Jain, S., Griffin, D. W., Yu, H., Tan, Q., et al. (2018). Airborne Bacteria in Earth's Lower Stratosphere Resemble Taxa Detected in the Troposphere: Results From a New NASA Aircraft Bioaerosol Collector (ABC). *Frontiers in Microbiology*, *9*. https://doi.org/10.3389/fmicb.2018.01752

Smith, D. P., & Peay, K. G. (2014). Sequence Depth, Not PCR Replication, Improves Ecological Inference from Next Generation DNA Sequencing. *PLOS ONE*, *9*(2), e90234. https://doi.org/10.1371/journal.pone.0090234

Song, H., Crawford, I., Lloyd, J. R., Robinson, C. H., Boothman, C., Bower, K., et al. (2020). Airborne Bacterial and Eukaryotic Community Structure across the United Kingdom Revealed by High-Throughput Sequencing. *Atmosphere*, *11*(8), 802. https://doi.org/10.3390/atmos11080802

Sophia E. Kruger, M. P. H., Irene Ruberto, P., Thomas Williamson, M. P. H., Justin V. Remais, P., Alexandra K. Heaney, P., & Jennifer R. Head, P. (2026). Regional Increases in Incidence of Coccidioidomycosis (Valley Fever) — Arizona, 2005–2022. *MMWR. Morbidity and Mortality Weekly Report*, *75*. https://doi.org/10.15585/mmwr.mm7506a3

Sykes, J. E., Camponuri, S. K., Weaver, A. K., Thompson, G. R., & Remais, J. V. (2025). Use of Dog Serologic Data for Improved Understanding of Coccidioidomycosis: A One Health

Approach. *The Journal of Infectious Diseases*, *231*(5), e986–e995. https://doi.org/10.1093/infdis/jiaf184

Taylor, D. L., Walters, W. A., Lennon, N. J., Bochicchio, J., Krohn, A., Caporaso, J. G., & Pennanen, T. (2016). Accurate Estimation of Fungal Diversity and Abundance through Improved Lineage-Specific Primers Optimized for Illumina Amplicon Sequencing. *Applied and Environmental Microbiology*, *82*(24), 7217–7226. https://doi.org/10.1128/AEM.02576-16

Tiedje, J. M., Bruns, M. A., Casadevall, A., Criddle, C. S., Eloe-Fadrosh, E., Karl, D. M., et al. (2022). Microbes and Climate Change: a Research Prospectus for the Future. *mBio*, *13*(3), e00800-22. https://doi.org/10.1128/mbio.00800-22

Tignat-Perrier, R., Dommergue, A., Vogel, T. M., & Larose, C. (2020). Microbial Ecology of the Planetary Boundary Layer. *Atmosphere*, *11*(12), 1296. https://doi.org/10.3390/atmos11121296

Tirado, F., & Cano, P. T. (2020). Drones and epidemiology: A new anatomy for surveillance. *BioSocieties*, *15*(1), 115–133. https://doi.org/10.1057/s41292-019-00144-w

Tör, M., Wood, T., Webb, A., Göl, D., & McDowell, J. M. (2023). Recent developments in plant-downy mildew interactions. *Seminars in Cell & Developmental Biology*, *148–149*, 42–50. https://doi.org/10.1016/j.semcdb.2023.01.010

Torchiano, M. (2020, October 5). effsize: Efficient Effect Size Computation (Version 0.8.1). Retrieved from https://cran.r-project.org/web/packages/effsize/index.html

Triadó-Margarit, X., Cáliz, J., & Casamayor, E. O. (2022). A long-term atmospheric baseline for intercontinental exchange of airborne pathogens. *Environment International*, *158*, 106916. https://doi.org/10.1016/j.envint.2021.106916

Vélez-Rodríguez, Z., Torres-Pratts, H., & Maldonado-Ramírez, S. L. (2020). Use of Drones to Recover Fungal Spores and Pollen from the Lower Atmosphere. *Caribbean Journal of Science*, *50*(1), 159–170. https://doi.org/10.18475/cjos.v50i1.a16

Walker, K., Herman, M., & Eberwein, K. (2026, February 9). tidycensus: Load US Census Boundary and Attribute Data as "tidyverse" and 'sf'-Ready Data Frames (Version 1.7.5). Retrieved from https://cran.r-project.org/web/packages/tidycensus/index.html

Weaver, E., Kolivras, K. N., Thomas, R. Q., Thomas, V. A., & Abbas, K. M. (2020). Environmental factors affecting ecological niche of Coccidioides species and spatial dynamics of valley fever in the United States. *Spatial and Spatio-Temporal Epidemiology*, *32*, 100317. https://doi.org/10.1016/j.sste.2019.100317

Wei, T., Simko, V., Levy, M., Xie, Y., Jin, Y., Zemla, J., et al. (2024, October 14). corrplot: Visualization of a Correlation Matrix (Version 0.95). Retrieved from https://cran.r-project.org/web/packages/corrplot/index.html

Wickham, H., & RStudio. (2023, February 22). tidyverse: Easily Install and Load the "Tidyverse" (Version 2.0.0). Retrieved from https://cran.r-project.org/web/packages/tidyverse/index.html

Wickham, H., Pedersen, T. L., Seidel, D., Software, P., PBC [cph, & fnd. (2025, April 24). scales: Scale Functions for Visualization (Version 1.4.0). Retrieved from https://cran.r-project.org/web/packages/scales/index.html

Wickham, H., Chang, W., Henry, L., Pedersen, T. L., Takahashi, K., Wilke, C., et al. (2026, February 3). ggplot2: Create Elegant Data Visualisations Using the Grammar of Graphics (Version 4.0.2). Retrieved from https://cran.r-project.org/web/packages/ggplot2/index.html

Wilke, C. O. (2025, July 7). cowplot: Streamlined Plot Theme and Plot Annotations for "ggplot2" (Version 1.2.0). Retrieved from https://cran.r-project.org/web/packages/cowplot/index.html

Winand, R., D'hooge, E., Van Uffelen, A., Bogaerts, B., Van Braekel, J., Hoffman, S., et al. (2025). Investigating fungal diversity through metabarcoding for environmental samples: assessment of ITS1 and ITS2 Illumina sequencing using multiple defined mock communities with different classification methods and reference databases. *BMC Genomics*, *26*(1), 729. https://doi.org/10.1186/s12864-025-11917-y

Xia, Y., Mitchell, K., Ek, M., Sheffield, J., Cosgrove, B., Wood, E., et al. (2012). Continental-scale water and energy flux analysis and validation for the North American Land Data Assimilation System project phase 2 (NLDAS-2): 1. Intercomparison and application of model products. *Journal of Geophysical Research: Atmospheres*, *117*(D3). https://doi.org/10.1029/2011JD016048

Yang, R.-H., Su, J.-H., Shang, J.-J., Wu, Y.-Y., Li, Y., Bao, D.-P., & Yao, Y.-J. (2018). Evaluation of the ribosomal DNA internal transcribed spacer (ITS), specifically ITS1 and ITS2, for the analysis of fungal diversity by deep sequencing. *PLOS ONE*, *13*(10), e0206428. https://doi.org/10.1371/journal.pone.0206428

Zahn, E., & Bou-Zeid, E. (2024). Observational partitioning of water and CO_2 fluxes at National Ecological Observatory Network (NEON) sites: a 5-year dataset of soil and plant components for spatial and temporal analysis. *Earth System Science Data*, *16*(12), 5603–5624. https://doi.org/10.5194/essd-16-5603-2024

Zeimes, C. B., Quoilin, S., Henttonen, H., Lyytikäinen, O., Vapalahti, O., Reynes, J.-M., et al. (2015). Landscape and Regional Environmental Analysis of the Spatial Distribution of Hantavirus Human Cases in Europe. *Frontiers in Public Health*, *3*, 54. https://doi.org/10.3389/fpubh.2015.00054

Zhang, K., Wang, D., Bian, Q., Duan, Y., Zhao, M., Fei, D., et al. (2017). Tethered balloon-based particle number concentration, and size distribution vertical profiles within the lower troposphere of Shanghai. *Atmospheric Environment*, *154*, 141–150. https://doi.org/10.1016/j.atmosenv.2017.01.025

APPENDIX A1

SUPPLEMENTAL INFORMATION FOR CHAPTER 2

Introduction

This supplemental material describes the different sampling setups in detail, with images for the chamber trials (Figure A1.1), ground-level (Figure A1.2), and elevated field trials (Figures A1.3-A1.5). Finally, we included images of each drone used (The DJI Matrice 350 quadcopter and the Aurelia X6 Pro V2 hexacopter) for clarification of sampler set up (Figures A1.6-A1.7).

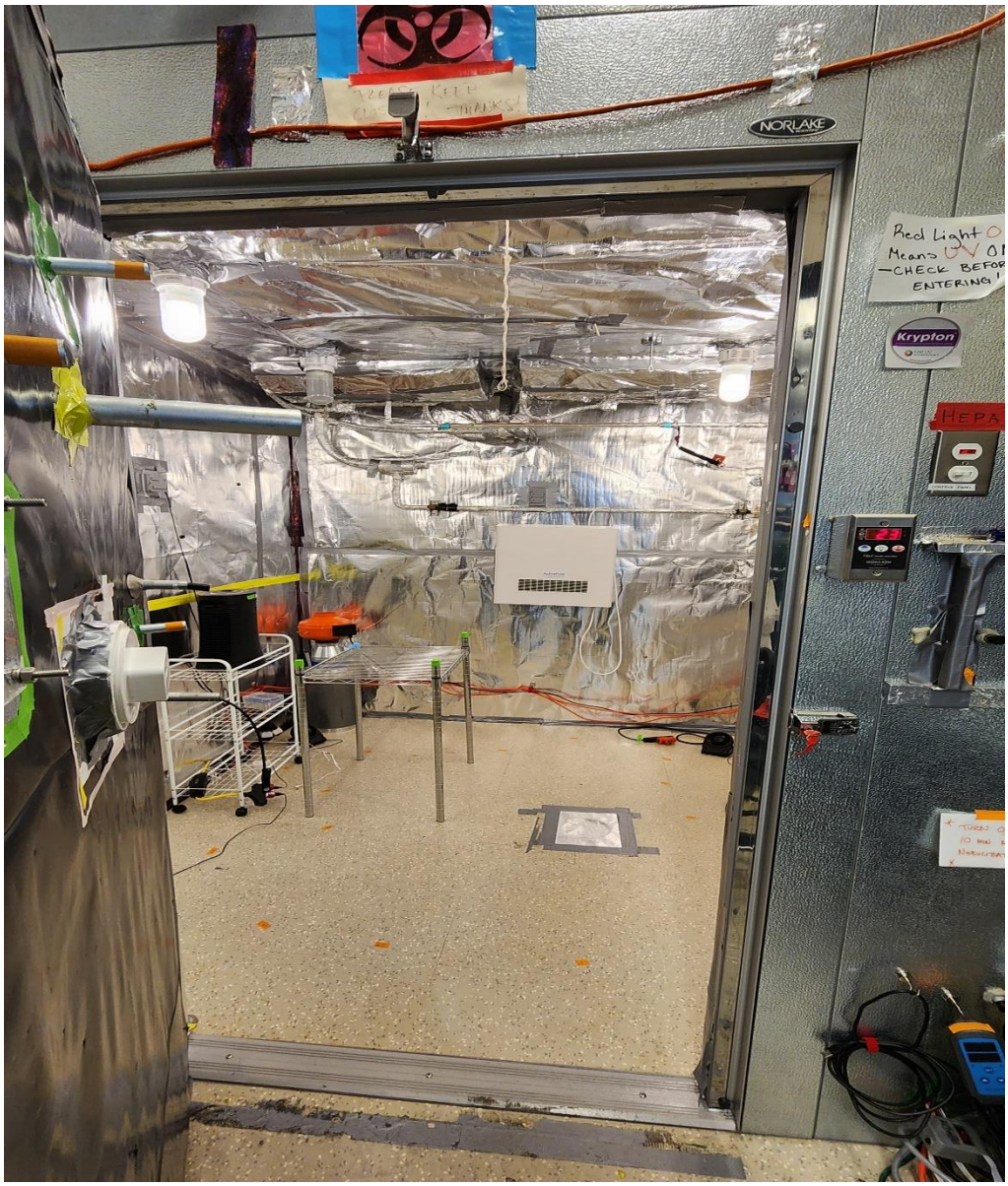

Figure A1.1. Sampling setup and demonstration of location for chamber trials used in chapter 2. The chamber is a sealed $10m^3$ location allowing for the nebulization of tracer organism in a controlled environment. Both the Full SASS and Light SASS were setup on the metal table to the left of center in the room.

Figure A1.2. Sampling setup and demonstration of location for ground-level trials used in chapter 2. Samplers were located at the Colorado State University Foothills Campus. Samplers were placed away from builds at the edge of a large field and approximately 4 feet off the ground and 2 feet apart.

Figure A1.3. Sampling setup and demonstration of location for elevated field trials used in chapter 2. Samplers were located at the Colorado State University Agricultural Research, Development, and Education Center (ARDEC). Samplers were placed in an agricultural area on the side of a empty field and gravel road. The Full SASS was placed on the boom lift and the Light SASS was placed on the drone (DJI Matrice 350 quadcopter pictured).

Figure A1.4. Sampling setup and demonstration of location for elevated field trials used in chapter 2. Samplers were located at the Colorado State University Agricultural Research, Development, and Education Center (ARDEC). Samplers were placed in an agricultural area on the side of a empty field and gravel road. The Full SASS was placed on the boom lift and the Light SASS was placed on the drone (Aurelia X6 Pro V2 hexacopter pictured).

Figure A1.5. Close up image of sampling setup and demonstration of location for elevated field trials used in chapter 2. The Full SASS was placed on the boom lift on the left side of the image and the Light SASS was placed on the drone on the right side of the image (DJI Matrice 350 quadcopter pictured).

Figure A1.6. Detailed image of Light SASS air sampler setup on the DJI Matrice 350 quadcopter drone. Both the drone and the sampler were thoroughly cleaned to reduce the chance of contamination.

Figure A1.7. Detailed image of Light SASS air sampler setup on the Aurelia X6 Pro V2 hexacopter drone. Both the drone and the sampler were thoroughly cleaned to reduce the chance of contamination.

APPENDIX A2

SUPPLEMENTAL INFORMATION FOR CHAPTER 3

Introduction

This supplemental material gives more information about the sampling site and weather conditions under which sampling occurred during field work for chapter 3. The appendix provides a table with weather conditions during sampling for each date that sampling occurred (Table A2.1). Finally, we included images of the sampling setup and an example of a the sampling location (Figures 2A.1-2A.2).

Table A2.1: Weather conditions recorded during sampling. Average temperature, humidity, and wind speed in degrees Fahrenheit, percent, and miles per hour (mph) were recorded, respectively.

Sample Date	Average Temperature (°F)	Average Humidity (%)	Average Wind Speed (mph)
08/06/2024	85	41	6
08/07/2024	86	36	3
08/08/2024	76	47	5
08/12/2024	81	60	17
08/13/2024	79	67	12
08/14/2024	79	62	11

Figure A2.1. Sampling setup and demonstration of location during field sampling. Ground-level samplers were set up 25 feet away from the drone landing pad, seen in the center. The ground-level tripods were equipped with the Full SASS 3100, while the drone was equipped with the Light SASS prototype. Sight conditions were arid to semi-arid, with dry soil and sparse vegetation.

APPENDIX A3

SUPPLEMENTAL INFORMATION FOR CHAPTER 4

Introduction

This appendix provides more context for Chapter 4. We added a model performance time series, breaking down the ensemble model performance into each individual model type: random forest, maximum entropy, and boosted regression trees (Figure A3.1). We also provided additional years of predicted *Coccidioides spp.* distribution including 2004, 2008, 2012, 2016, and 2020 comparing the prediction when using human Valley Fever cases as presence points as compared to simulated canine Valley Fever cases as pressure points (Figures A3.2-3.6). We also included the maximum, mean, and minimum predictions of *Coccidioides spp.* relative habitat suitability during the same years as figures A3.2-A3.6 (Figures A3.7-A3.11). Finally, we included the sentinel species comparison map for years 2004, 2008, 2012, 2016, and 2020 (Figure A3.12-A3.16).

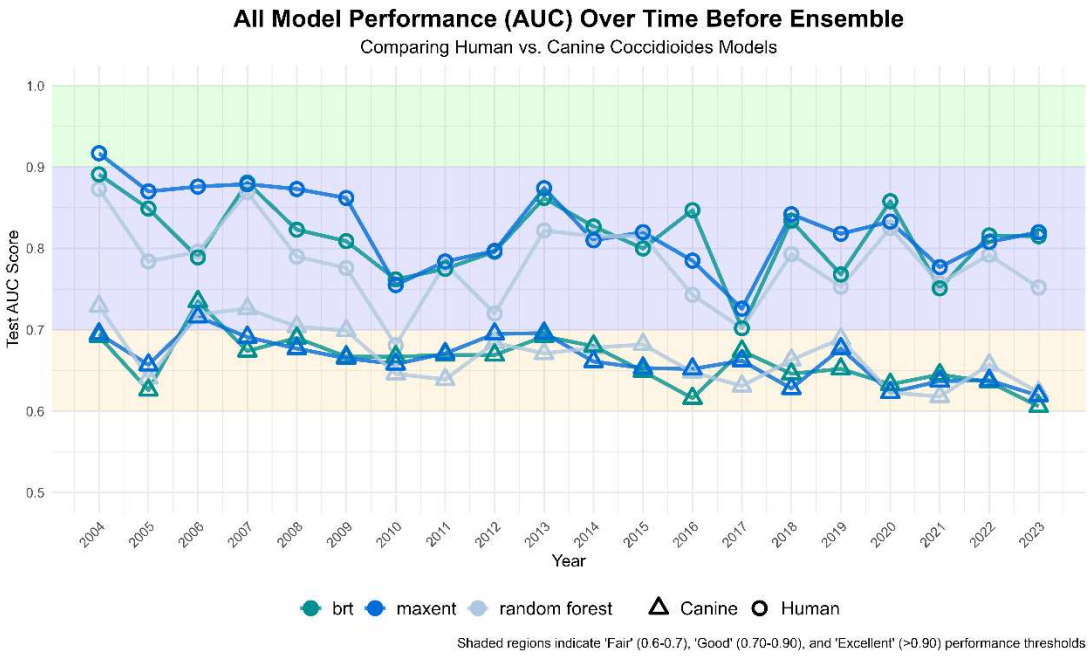

Figure A3.1: Individual model type performance by AUC value, including boosted regression trees (brt, green), maximum entropy (maxent, blue), and random forest (light blue). Humans are circles and canines are triangles. The orange zone represents a fair model performance (0.6-0.7), blue a good performance (0.7-0.9), and green and excellent performance (>0.9).

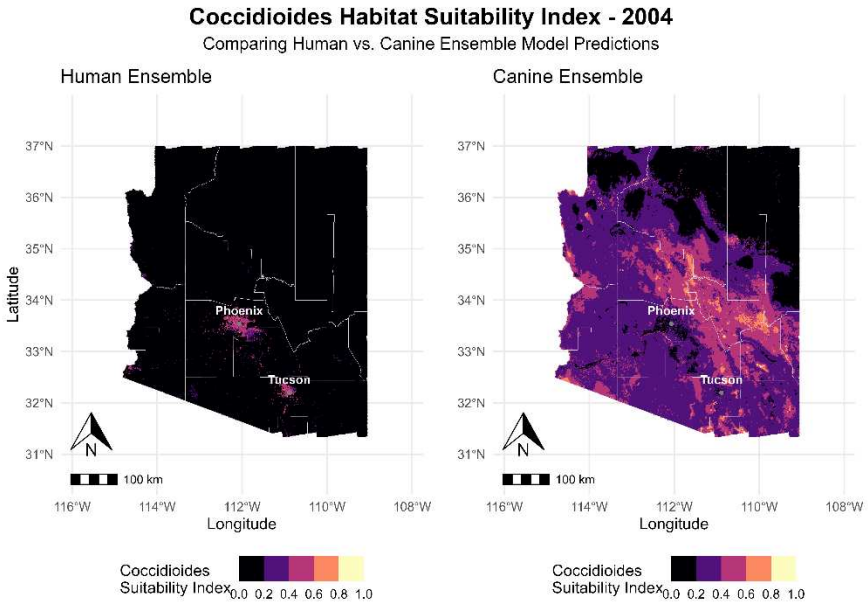

Figure A3.7: Ensemble Coccidioides spp. relative habitat suitability prediction for Arizona in 2004, with human and canine performance compared side by side using AUC scores.

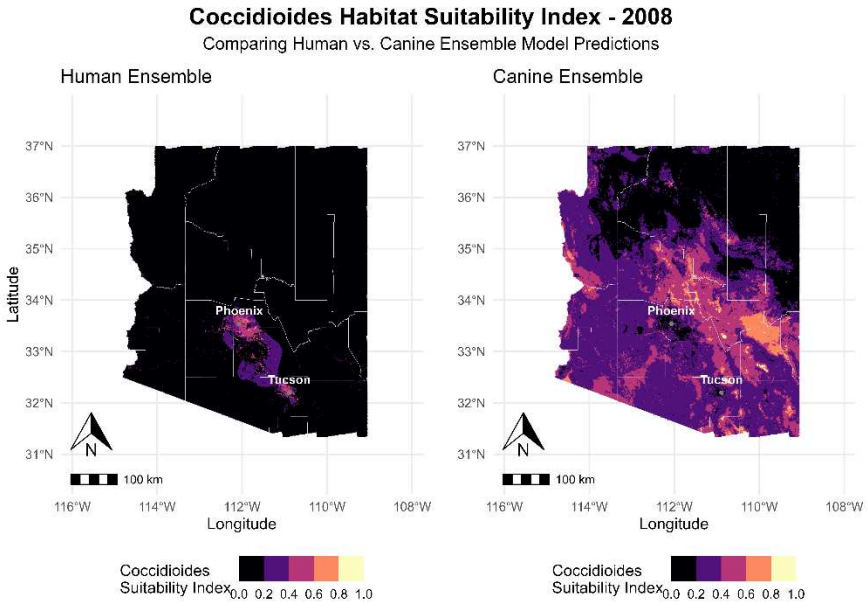

Figure A3.3: Ensemble Coccidioides spp. relative habitat suitability prediction for Arizona in 2008, with human and canine performance compared side by side using AUC scores.

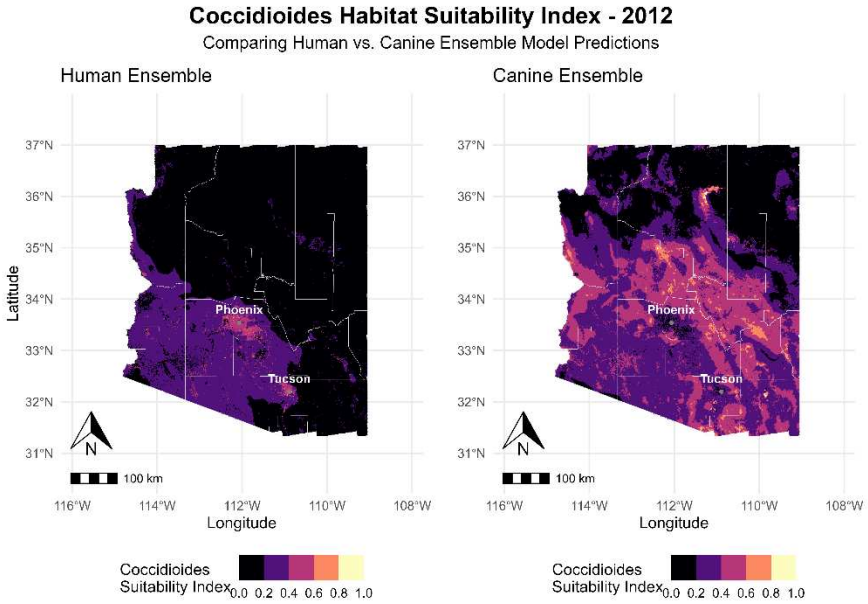

Figure A3.4: Ensemble Coccidioides spp. relative habitat suitability prediction for Arizona in 2012, with human and canine performance compared side by side using AUC scores.

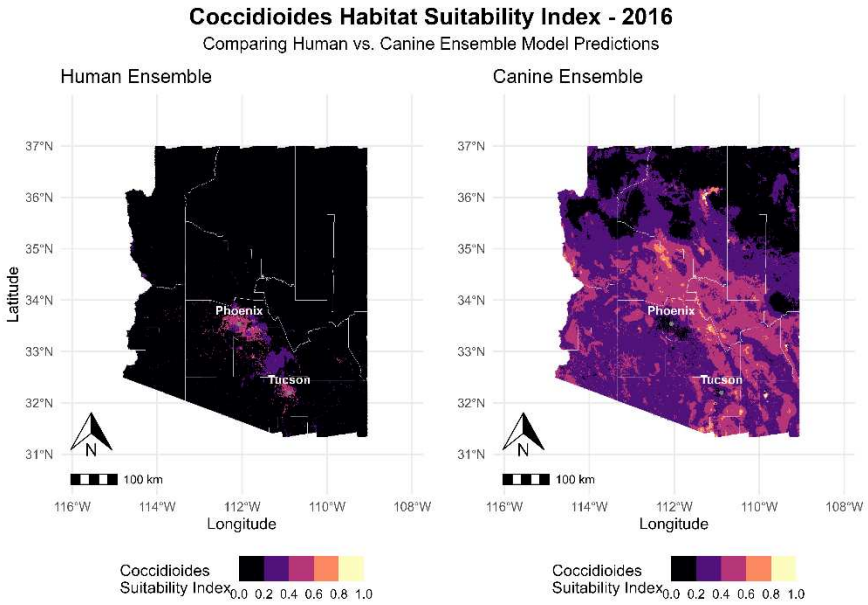

Figure A3.5: Ensemble Coccidioides spp. relative habitat suitability prediction for Arizona in 2016, with human and canine performance compared side by side using AUC scores.

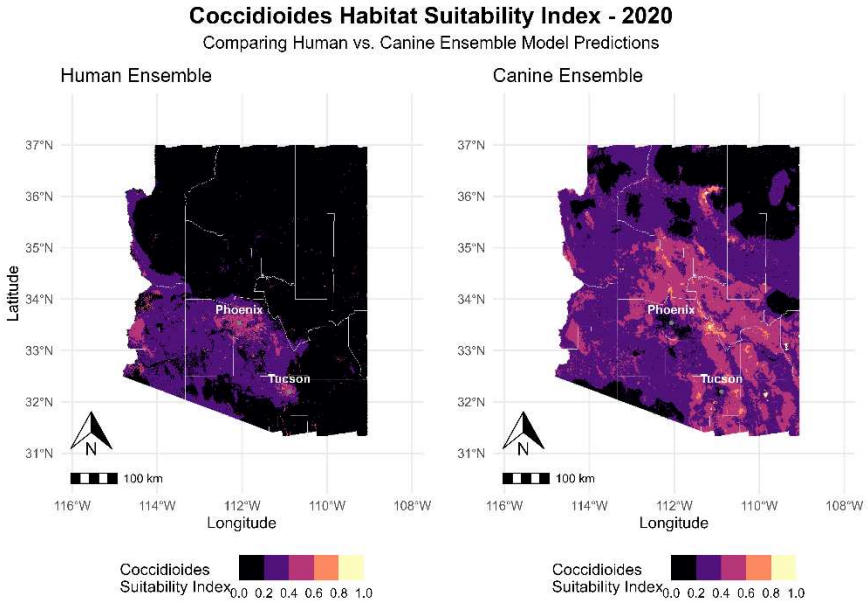

Figure A3.6: Ensemble Coccidioides spp. relative habitat suitability prediction for Arizona in 2020, with human and canine performance compared side by side using AUC scores.

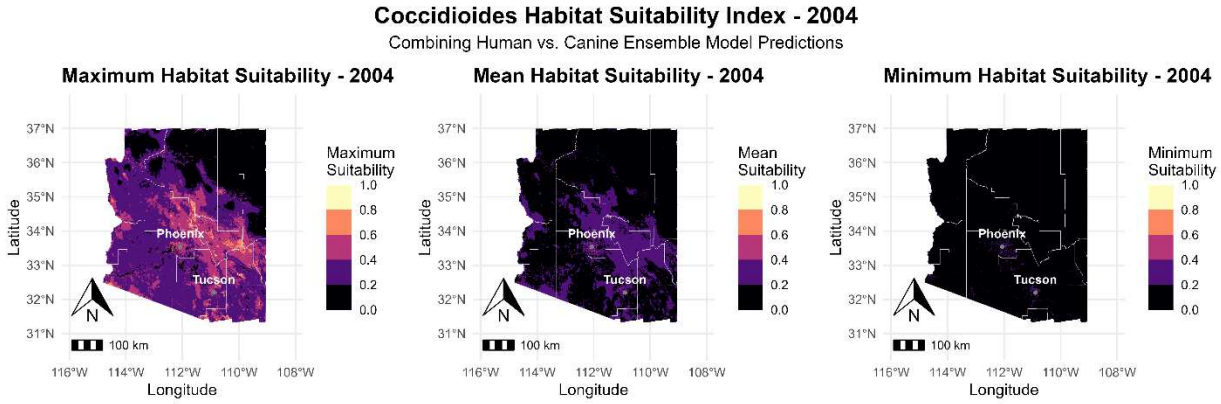

Figure A3.7: Combined model performance when aggregating canine and human models together. From left to right, models were aggregated using maximum values, mean values, and minimum values to show strongest, middle, and weakest performance for the year 2004.

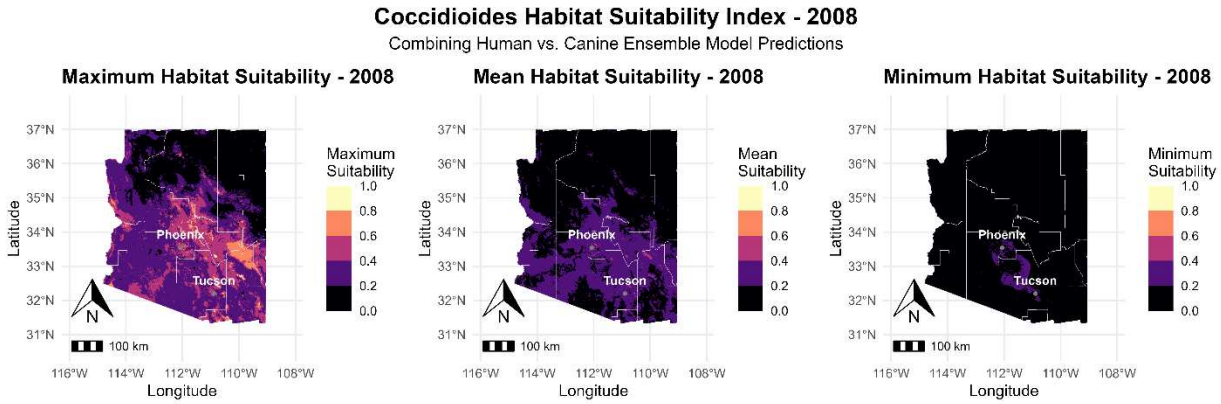

Figure A3.8: Combined model performance when aggregating canine and human models together. From left to right, models were aggregated using maximum values, mean values, and minimum values to show strongest, middle, and weakest performance for the year 2008.

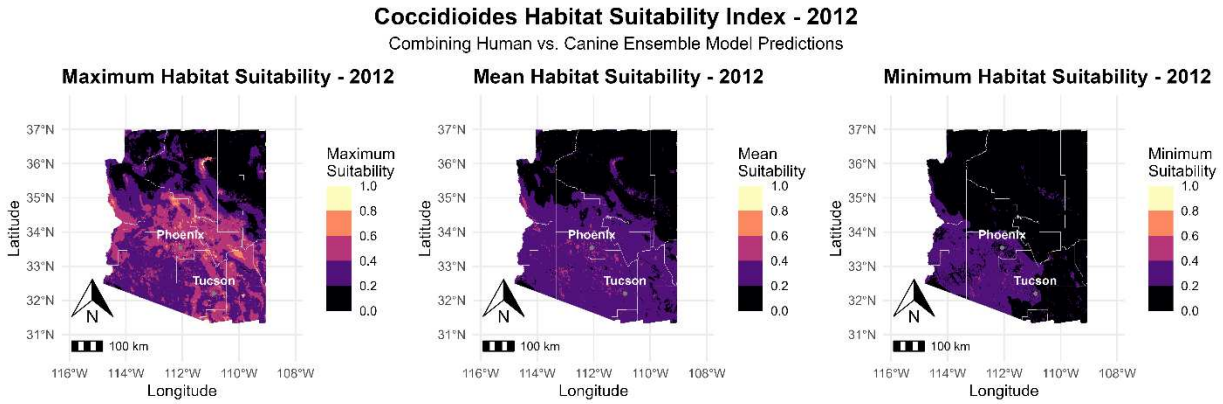

Figure A3.9: Combined model performance when aggregating canine and human models together. From left to right, models were aggregated using maximum values, mean values, and minimum values to show strongest, middle, and weakest performance for the year 2012.

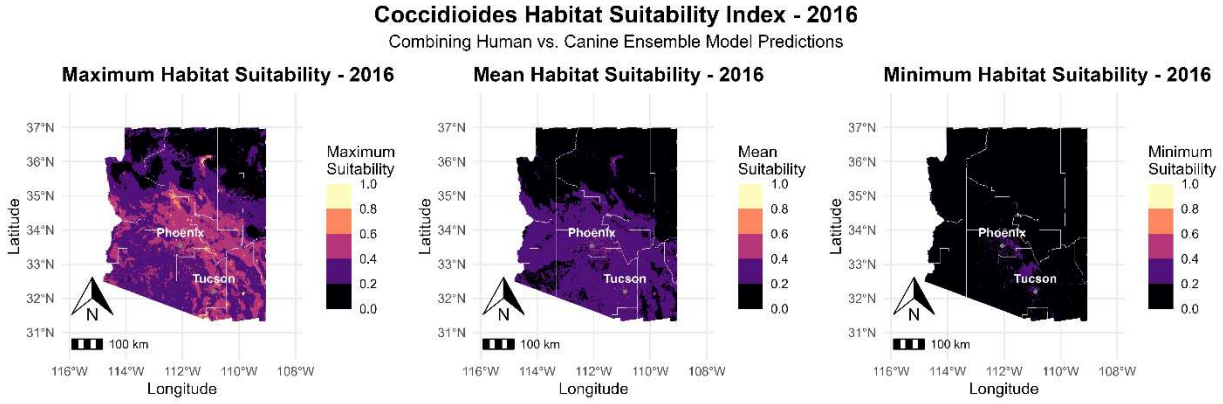

Figure A3.10: Combined model performance when aggregating canine and human models together. From left to right, models were aggregated using maximum values, mean values, and minimum values to show strongest, middle, and weakest performance for the year 2016.

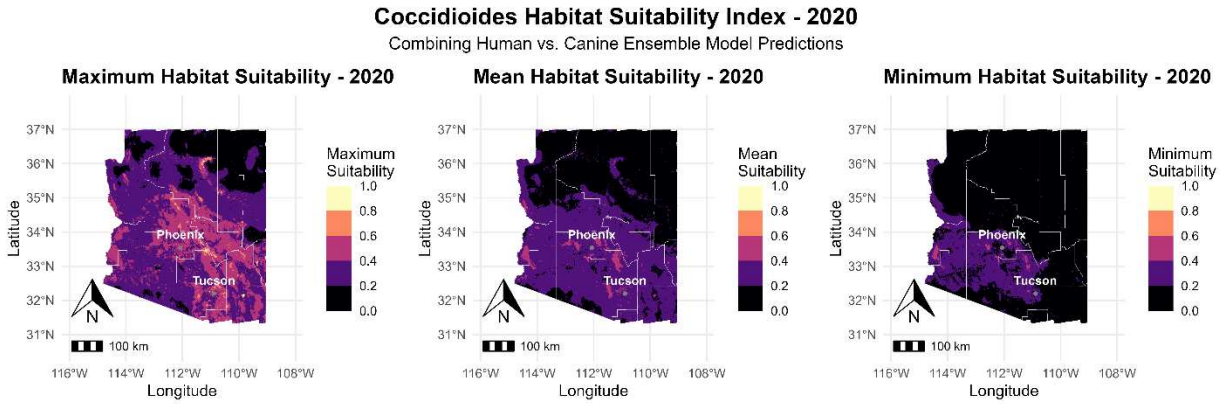

Figure A3.11: Combined model performance when aggregating canine and human models together. From left to right, models were aggregated using maximum values, mean values, and minimum values to show strongest, middle, and weakest performance for the year 2020.

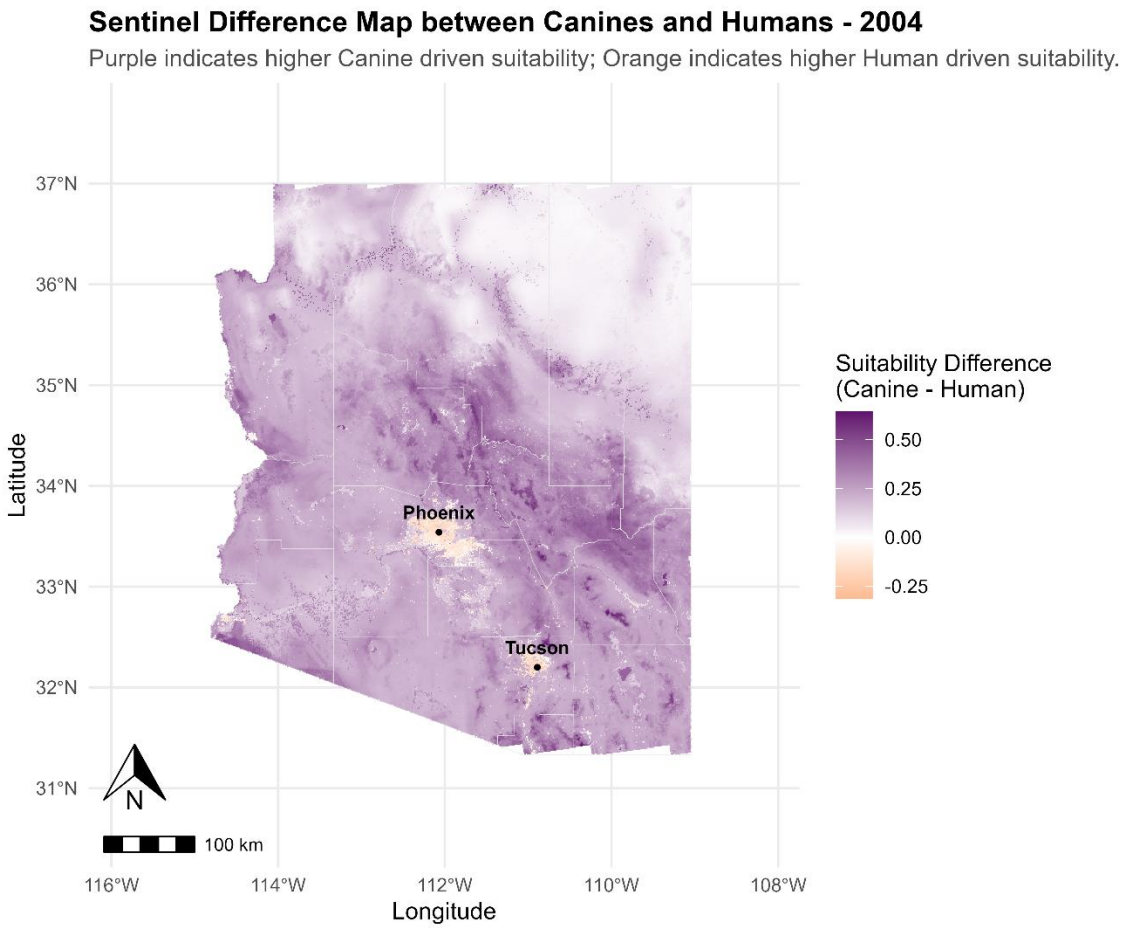

Figure A3.12: Sentinel comparison between canines and humans in 2004. If the color is purple, the canine models are driving suitability prediction, and if the color is orange, the human models are driving suitability. White means both models are predicting suitability evenly. The human models tended to predict more for and near urban centers, while the canine models tended to predict more for non-urban areas.

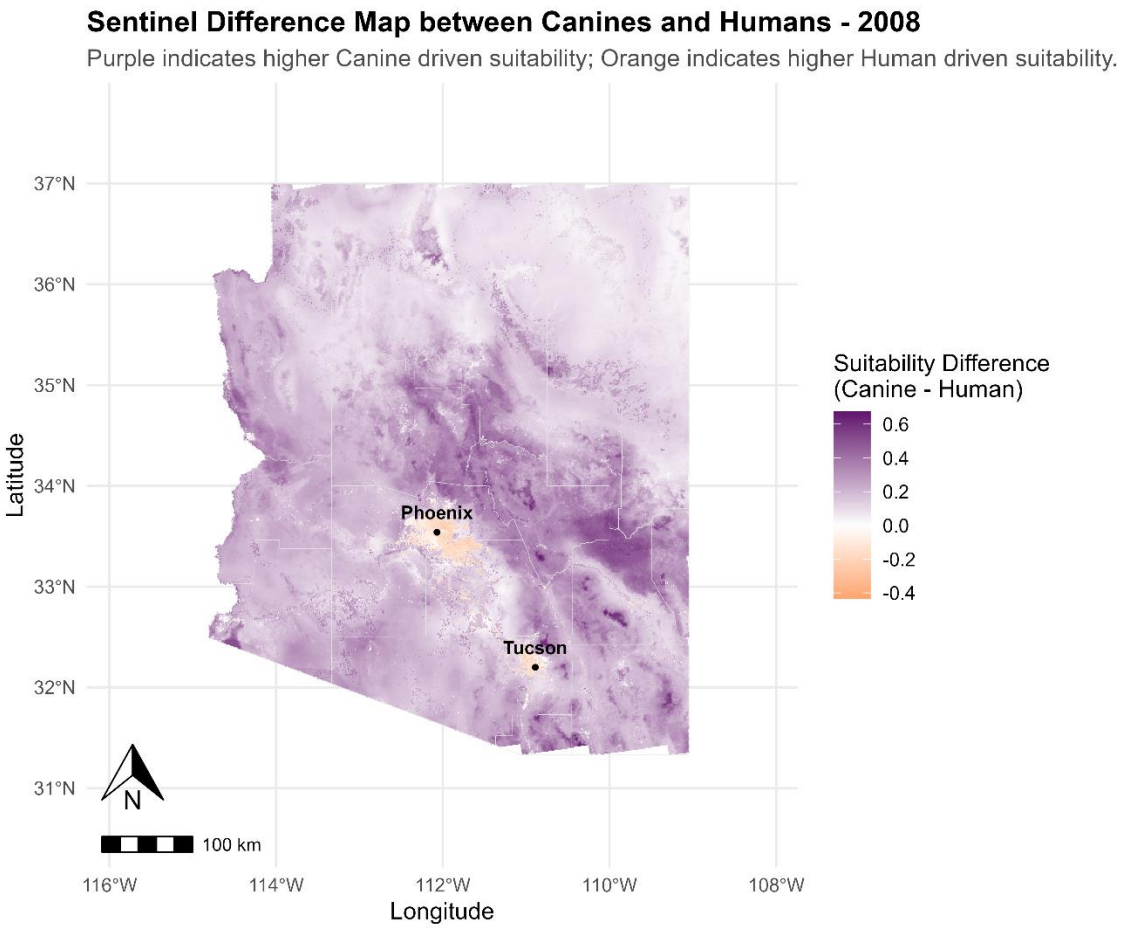

Figure A3.13: Sentinel comparison between canines and humans in 2008. If the color is purple, the canine models are driving suitability prediction, and if the color is orange, the human models are driving suitability. White means both models are predicting suitability evenly. The human models tended to predict more for and near urban centers, while the canine models tended to predict more for non-urban areas.

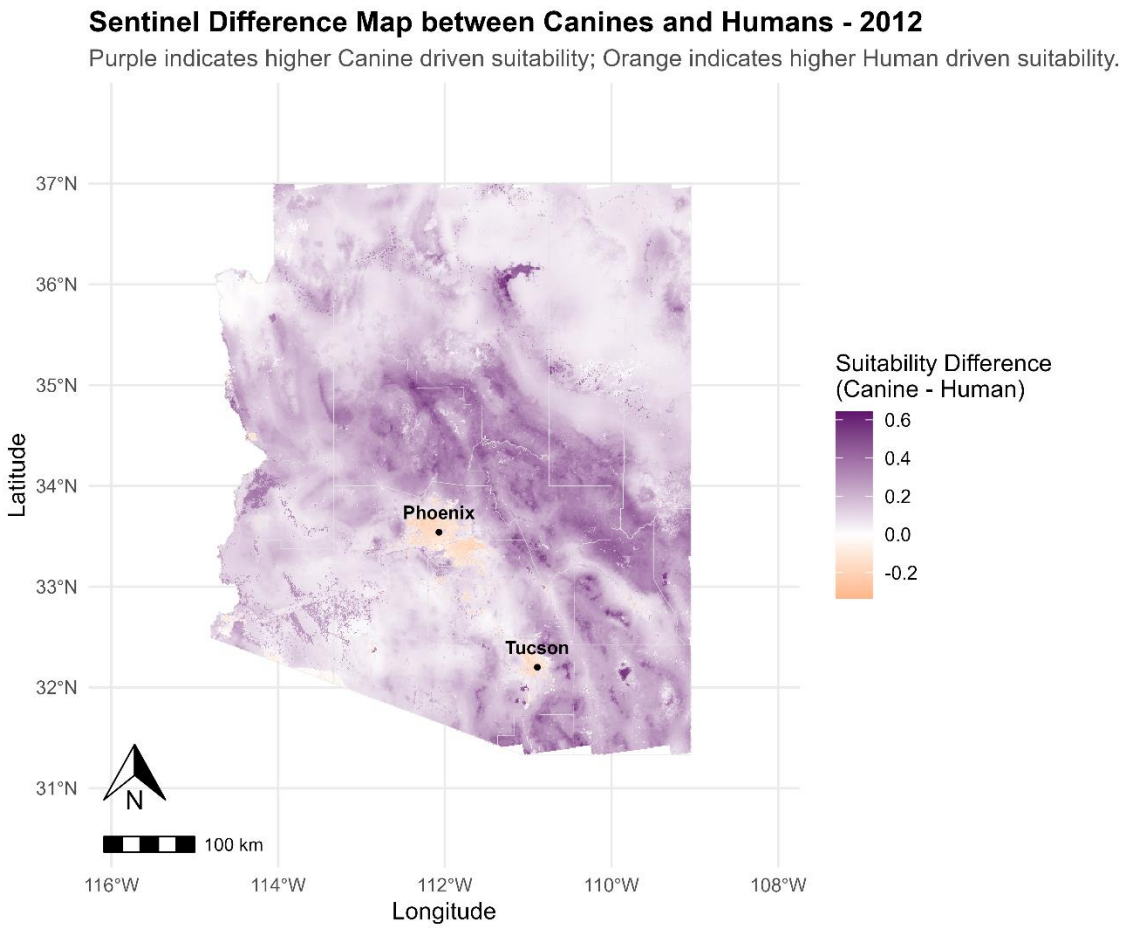

Figure A3.14: Sentinel comparison between canines and humans in 2012. If the color is purple, the canine models are driving suitability prediction, and if the color is orange, the human models are driving suitability. White means both models are predicting suitability evenly. The human models tended to predict more for and near urban centers, while the canine models tended to predict more for non-urban areas.

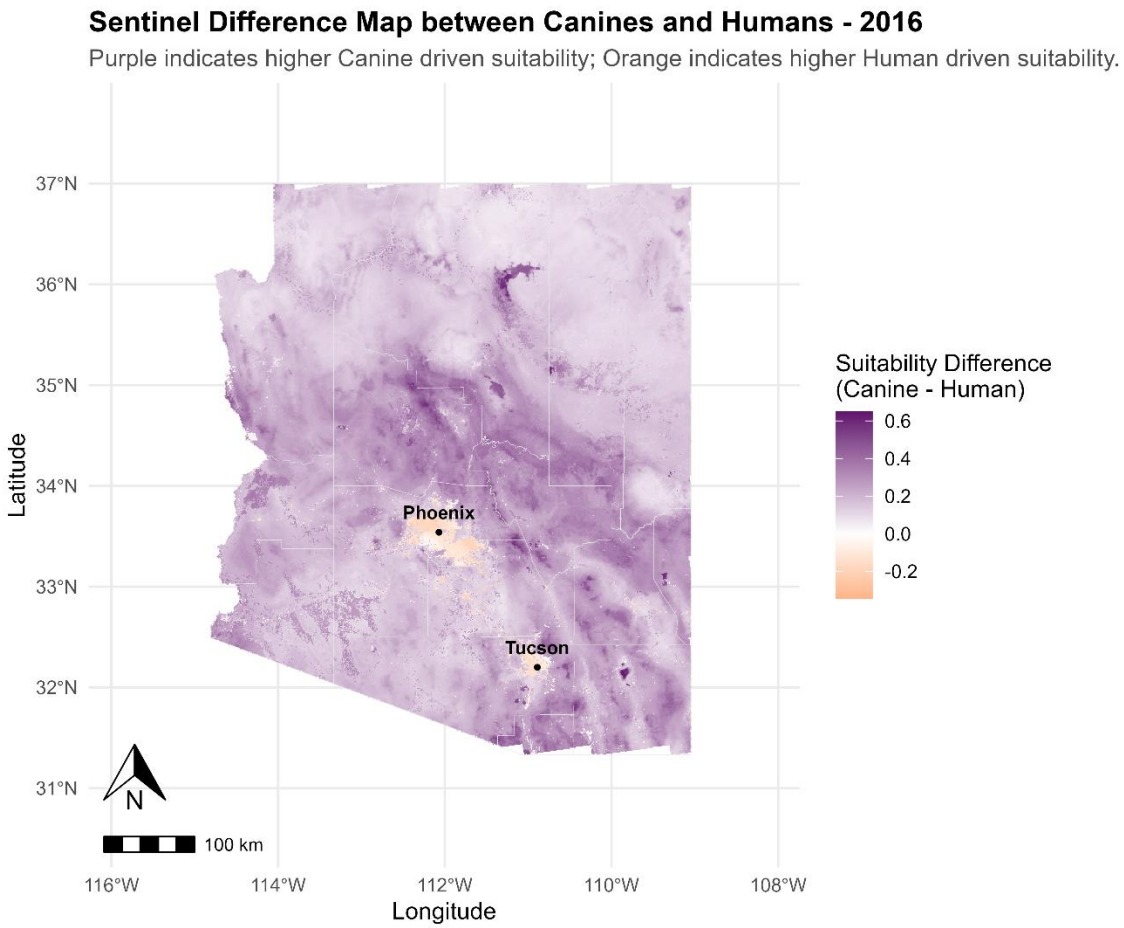

Figure A3.15: Sentinel comparison between canines and humans in 2016. If the color is purple, the canine models are driving suitability prediction, and if the color is orange, the human models are driving suitability. White means both models are predicting suitability evenly. The human models tended to predict more for and near urban centers, while the canine models tended to predict more for non-urban areas.

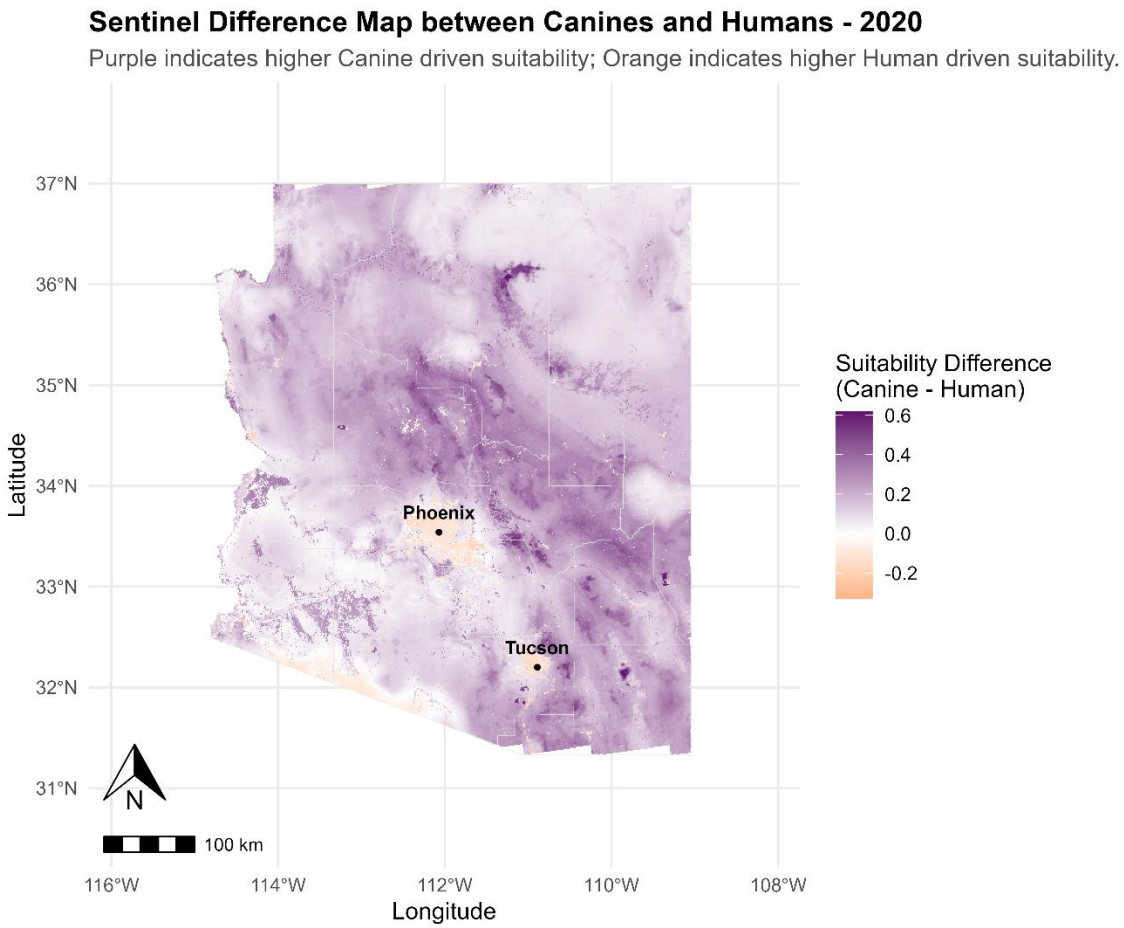

Figure A3.16: Sentinel comparison between canines and humans in 2020. If the color is purple, the canine models are driving suitability prediction, and if the color is orange, the human models are driving suitability. White means both models are predicting suitability evenly. The human models tended to predict more for and near urban centers, while the canine models tended to predict more for non-urban areas.